NATIONAL AND KAPODISTRIAN UNIVERSITY OF ATHENS

FACULTY OF SCIENCES

DEPARTMENT OF CHEMISTRY

POSTGRADUATE DEGREE
«ENVIRONMENTAL CHEMISTRY AND TECHNOLOGY»

MSc THESIS

A lipid biomarker study of the organic matter associated with the indigenous characteristics of the mud matrix and the post-eruptional microbial processes at the Olimpi mud volcano field, Eastern Mediterranean

FRANCESCA PARASCHOS
GEOLOGIST

ATHENS
OCTOBER 2017

MSc THESIS

A lipid biomarker study of the organic matter associated with the indigenous characteristics of the mud matrix and the post-eruptional microbial processes at the Olimpi mud volcano field, Eastern Mediterranean

FRANCESCA PARASCHOS

A.M.: 91509

SUPERVISOR:
Manos Dassenakis, Professor, NKUA

EXAMINATION COMMITTEE

Manos Dassenakis, Professor, NKUA
Alexandra Gogou, Senior Researcher, HCMR
Ariadne Argyraki, Associate Professor, NKUA

DATE OF EXAMINATION
10/11/2017

ΕΡΕΥΝΗΤΙΚΗ ΕΡΓΑΣΙΑ ΔΙΠΛΩΜΑΤΟΣ ΕΙΔΙΚΕΥΣΗΣ

Μελέτη των οργανικών λιπιδιακών βιοδεικτών που σχετίζονται με τα αυτόχθονα χαρακτηριστικά της κύριας μάζας των λασπορροών και με τις μικροβιακές διεργασίες που αναπτύσσονται μετά την εκρηκτική φάση στο πεδίο ηφαιστείων ιλύος Ολίμπι, Ανατολική Μεσόγειο

ΦΡΑΝΤΖΕΣΚΑ ΠΑΡΑΣΧΟΥ

Α.Μ.: 91509

ΕΠΙΒΛΕΠΩΝ ΚΑΘΗΓΗΤΗΣ:
Μάνος Δασενάκης, Καθηγητής, ΕΚΠΑ

ΤΡΙΜΕΛΗΣ ΕΞΕΤΑΣΤΙΚΗ ΕΠΙΤΡΟΠΗ

Μάνος Δασενάκης, Καθηγητής, ΕΚΠΑ
Αλεξάνδρα Γώγου, Κύρια Ερευνήτρια, ΕΛΚΕΘΕ
Αριάδνη Αργυράκη, Αναπληρώτρια Καθηγήτρια, ΕΚΠΑ

ΗΜΕΡΟΜΗΝΙΑ ΕΞΕΤΑΣΗΣ
10/11/2017

ABSTRACT

Mud volcanoes are important structures associated with high seafloor methane fluxes. In these settings sulfide and methane concentrations can be high and unique ecosystems of chemosynthetically based life often dominate. The Olimpi mud volcano field, located in the Mediterranean Ridge accretionary prism, south of Crete, was surveyed during the LEVECO cruise (March-April 2016, R/V AEGAEO) and emphasis was given on the dynamics between the chemosynthetic communities and the dominant biogeochemical processes. An acoustic investigation (swath bathymetry and deep seismic-reflection profiling) of the area along with sediment coring at selected locations on the occurring domes and mudflows was undertaken. Cores were taken from five relatively unexplored mud volcanoes (Gelendzhik, Moscow, Milano, Leipzig and a previously undocumented location).

Lipid biomarkers are used as tools in order to determine organic matter's sources and sinks along with mineralization processes and storage, and to characterize the prokaryotic communities involved. Major diagnostic archaeal and bacterial lipid classes were detected including irregular isoprenoid hydrocarbons (such as PMI and crocetane), isoprenoidaldialkyl glycerol diethers (DGDs) (archaeol and hydroxyarchaeol) and fatty acids. The high abundance of both bacterial and archaeal biomarkers in the sulfate-methane transition zone (SMTZ) indicates increased prokaryotic activity resulting in anaerobic oxidation of methane (AOM). This is commonly observed in such environments and is the result of the symbiotic relationship of sulfate reducing bacteria (SRB) and anaerobic methanotrophs (ANME) which mediate the AOM process. Based on the sn -2-hydroxyarchaeol/archaeol ratio the Archaea were classified as ANME-1 in all cores.

Out of the selected areas studied, Gelendzhik was by far the most 'active' location, exhibiting higher concentrations of methane as well as archaeal and bacterial biomarkers. Ongoing studies on stable carbon isotopic composition of methane, dissolved inorganic/organic carbon in pore waters and phylogenetic characterization will help elucidate the source of methane, the dominant methanogenic and/or methanotrophic processes and the organisms involved in AOM and potentially methanogenesis.

SUBGECT AREA: Lipid biomarkers

KEYWORDS: Olimpi mud volcano field, organic matter, prokaryotic communities, AOM

ΠΕΡΙΛΗΨΗ

Τα ηφαίστεια ιλύος αποτελούν σημαντικές δομές στην Ανατολική Μεσόγειο οι οποίες σχετίζονται με υψηλές υποθαλάσσιες ροές μεθανίου. Σε αυτές τις περιοχές οι συγκεντρώσεις θειικών και μεθανίου μπορεί να είναι υψηλές και συχνά κυριαρχούν μοναδικά οικοσυστήματα που σχετίζονται με χημειοσυνθετικές διεργασίες. Το πεδίο ηφαιστείων ιλύος Olimpi, που βρίσκεται στο πρίσμα προσαύξησης της Μεσογειακής Ράχης, διερευνήθηκε κατά τη διάρκεια της αποστολής LEVECO (Μάρτιος-Απρίλιος 2016, R/V AEGAEO), δίνοντας έμφαση στη δυναμική ανάμεσα στις χημειοσυνθετικές κοινότητες και τις κυρίαρχες βιογεωχημικές διεργασίες. Πραγματοποιήθηκε ακουστική έρευνα (ηχοβολιστική βαθυμετρία, προφίλ σεισμικών ανακλάσεων) της περιοχής, ενώ ταυτόχρονα έγινε συλλογή πυρήνων ιζήματος σε επιλεγμένες περιοχές των ηφαιστειακών δόμων και ροών ιλύος. Οι πυρήνες συλλέχθηκαν από πέντε σχετικά ανεξερεύνητα ηφαίστεια (Gelendzhik, Moscow, Milano, Leipzig και από μία περιοχή που δεν έχει καταγραφεί στο παρελθόν).

Οι λιπιδικοί βιοδείκτες χρησιμοποιούνται ως εργαλεία με στόχο τον καθορισμό των πηγών και δεξαμενών της οργανικής ύλης, των διεργασιών ανοργανοποίησης και αποθήκευσης αλλά και για τον χαρακτηρισμό των εμπλεκομένων προκαρυωτικών κοινοτήτων. Διαγνωστικές κατηγορίες λιπιδίων των Αρχαίων και βακτηρίων ανιχνεύτηκαν και συμπεριλαμβάνουν ισοπρενοειδείς υδρογονάνθρακες (πενταμέθυλο-εικοσένιο (PMI), τετραμέθυλο-δεκαεξάνιο (crocetane)), ισοπρενοειδείς γλυκερο-διαιθέρες (DGDs) (αρχαιόλη, υδροξυαρχαιόλη) και λιπαρά οξέα. Η υψηλή παρουσία βιοδεικτών από βακτήρια και Αρχαία στην ζώνη μετάβασης θειικών-μεθανίου υποδεικνύει αυξημένη προκαρυωτική παρουσία με αποτέλεσμα την αναερόβια οξείδωση του μεθανίου (AOM). Η διεργασία αυτή παρατηρείται σε τέτοια περιβάλλοντα και είναι αποτέλεσμα της συμβιωτικής σχέσης των θειοαναγωγικών βακτηρίων και των αναερόβιων μεθανότροφων αρχαίων τα οποία και την επιτελούν. Με βάση τον λόγο sn-2-υδροξυαρχαιόλη/αρχαιόλη τα Αρχαία κατηγοριοποιούνται ως ANME-1 σε όλους τους πυρήνες.

Από τις μελετημένες περιοχές το Gelendzhik αποτελεί την πιο ‘ενεργή’ τοποθεσία, επιδεικνύοντας μεγαλύτερες συγκεντρώσεις μεθανίου και βιοδεικτών. Οι μελέτες που βρίσκονται σε εξέλιξη για την ισοτοπική σύσταση άνθρακα του μεθανίου, τον διαλυτό ανόργανο/οργανικό άνθρακα στα νερά των πόρων καθώς και για τους φυλογενετικούς χαρακτηρισμούς θα βοηθήσουν στη διερεύνηση των πηγών του μεθανίου, των κυρίαρχων διεργασιών μεθανογένεσης ή κατανάλωσης μεθανίου και των οργανισμών που εμπλέκονται σε αυτές.

ΘΕΜΑΤΙΚΗ ΠΕΡΙΟΧΗ: Λιπιδιακοί βιοδείκτες

ΛΕΞΕΙΣ ΚΛΕΙΔΙΑ: Πεδίο ηφαιστείων ιλύος Olimpi, Οργανική ύλη, προκαρυωτικές κοινότητες, AOM

ACKNOWLEDGMENTS

I would like to thank the following people who in one way or another contributed to the completion of this thesis.

Alexandra Gogou

Grigoris Rousakis, Manos Dassenakis, Ariadne Argyraki, Ioannis Hatzianestis, Panagiotis Michalopoulos, Dimitris Sakellariou, Eleni Kaberi, Stella Psara, Constantine Parinos, Eleni Rousselaki, Stella Chourdaki, Elvira Plakidi, Vicky Paraskevopoulou and Vasilis Lykousis

I would especially like to thank my family, Vasilis Babouris, Maria Fatourou and Chara Albani

TABLE OF CONTENTS

LIST OF FIGURES

LIST OF TABLES

PROLOGUE AND PURPOSE OF THIS STUDY

Extreme marine environments such as the ones presented at the Olimpi Mud Volcano field form unique ecosystems which present high biodiversity. Settings such as these are of great importance since their relationship to gas hydrate reservoirs has been previously proved in other locations around the world. They are also considered to be an energy source for chemosynthetically based life, since gases like sulfide and methane are found in large quantities. The study of such settings is a complex procedure which takes into account various parameters from many fields.

For the purpose of this thesis a molecular-level study was conducted on the organic content of mud flow samples from the Olimpi MV field. More specifically, organic lipid biomarkers of various origins were analysed in order 1) to evaluate the distribution and composition of bacterial and archaeal communities and 2) to evaluate the dynamics between the communities and the biogeochemical processes and finally, 3) to evaluate the indigenous organic characteristics of the mud flows and to try to relate them to the geological background.

This study is part of the multi-disciplinary project titled 'Study of the marine and submarine environment and ecosystem of the Eastern Mediterranean, south of Crete Isl.'. All samples of this study were obtained during the LEVECO cruise, aboard R/V Aegaeo, which took place from the 28th of March 2016 until the 6th of April 2016. All analysis was performed in the organic geochemistry lab at the HCMR under the supervision of Dr. Alexandra Gogou.

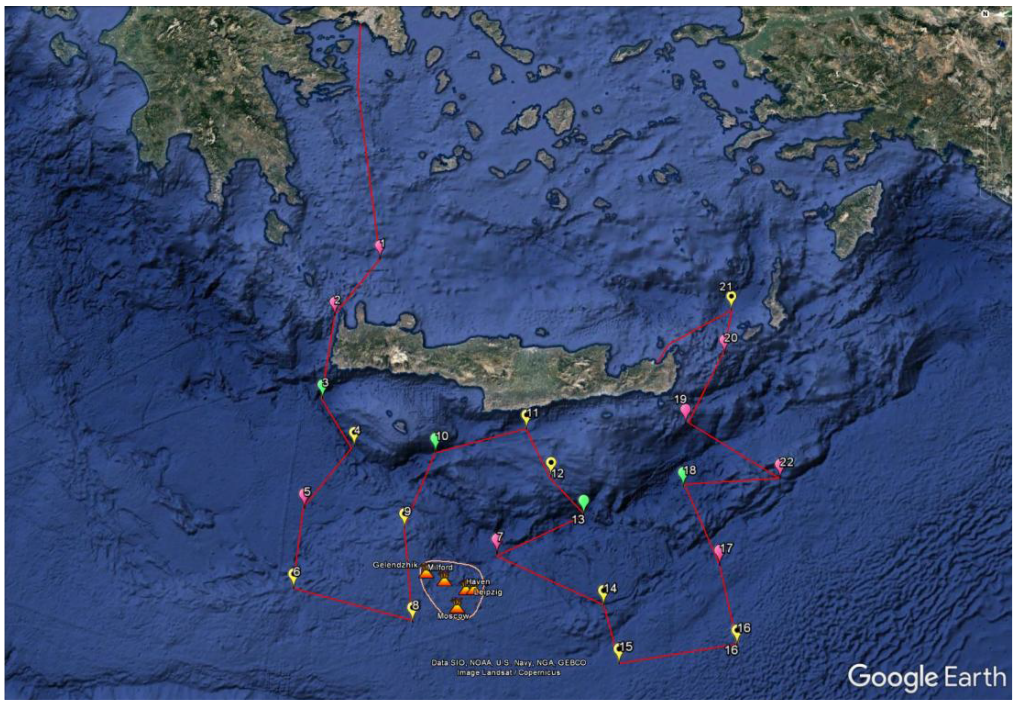

CHAPTER 1 - INTRODUCTION

1.1 MUD VOLCANOES

1.1.1 Definition

Mud volcanism is a phenomenon that has been investigated thoroughly throughout time, since it has been associated with some of the greatest observed oil seep concentrations and gas vents [1].

Simply put, mud volcanoes are geological structures formed by a combination of mud eruption, gas emission and water seepage from the subsurface to the earth's terrestrial surface or seafloor [2–4]. The extruded material forms characteristic isometric to elongated morphological features largely varying both in shape and size, composed by so-called mud breccia sharply contrasting to the surrounding host sediments [1].

Mud volcanoes and cold seeps

Mud volcanoes are often associated with cold seepage, in particular methane seepage, and given the appropriate pressure and temperature conditions, with gas hydrates [2,5]. Cold seeps have become areas of extensive research since they are considered "hotspots" of increased biological activity and have been documented at many seafloor sites worldwide [6].

1.1.2 Driving forces and formation mechanisms of submarine mud volcanoes

The driving forces of mud volcanism are many and can be divided into interrelated geological, tectonic, geochemical and hydrogeological categories [2]. The main driving force for mud volcano formation has been discussed in detail by [1,2,5] and it is thought to be abnormally high pore-fluid pressure caused by a combination of rapid sedimentation, in-situ gas generation and structural or tectonic compression. Specifically, when it comes to submarine mud volcanoes all these driving forces can be summarized into a few key categories which are (1) the high sediment accumulation rate at passive divergent continental margins and in abyssal plains (2) the lateral tectonic compression at active convergent and transform continental margins and (3) a combination of both reasons at specific locations [2].

Over the years there have also been many proposed formation mechanisms of mud volcanoes. They are considered as the result of the destruction of deep gas accumulations by, the piercing of the surface by shale diapirs [7], the rise of fluidized mud along faults by Rakhmanov (1987) and the decomposition of gas hydrates. Examination

of seismic profiles across submarine mud volcanoes has shown that there are two basic formation mechanisms [2].

During the first mechanism (Figure 1.1), a mud volcano forms directly on the top of a seafloor-piercing shale diaper. There are many examples of these volcanoes such as Gelendzhik, Maidstone and Moscow in the Mediterranean Sea [8], the mud volcanoes in the Sorokin Trough (Black Sea), an area in which the diapirs almost reach the seafloor [9] as well as the Buzdag and Elm volcanoes in the Caspian Sea [10]. These structures are usually large (up to 7km in diameter and 200m in height above the seafloor) and can also have several craters out of which mud flows [2]. In the Mediterranean Sea the diapirs rise to the seafloor along fracture zones [11]. In this case, the formation of mud volcanoes depends on fluid migration rates, grain size and consolidation of the diapiric material [5].

During the second mechanism (Figure 1.1), which is the most common, mud volcanoes form as a result of the rise of fluidized mud along faults and fractures. Sediments with a high fluid content reach the seafloor and form the mud volcanic edifice [2]. These volcanoes can be connected to diapirs which form at some depth beneath the seafloor as happens in the Gulf of Mexico [12] and the Black Sea [9]. In many cases though diapiric folds are not observed and the mud channels penetrate directly into the above (source) layers as happens in the deepest parts of the Black Sea, offshore Barbados and the Norwegian Sea. In this mechanism fluid migration plays the primary role and fluids can migrate with mud or independently due to the pressure gradient. When fluids migrate independently brine, water and gas seepages can form before the formation of a mud volcano [2].

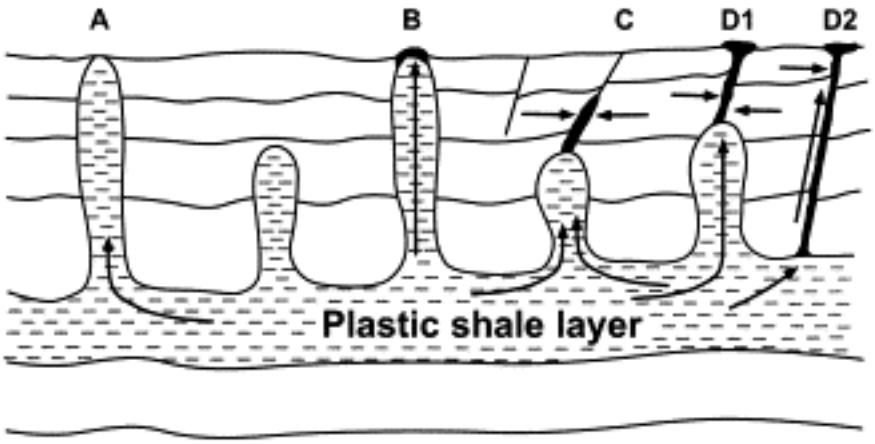

Figure 1.1.Two basic mechanisms of mud volcano formation (A) seafloor-piercing shale diapir without a mud volcano, (B) a mud volcano formed on top of a seafloor-piercing shale diapir; (C) a seafloor seepage; (D1, D2) mud volcanoes formed due to the rise of fluidized sediments along faults [2].

1.1.3 General elements and characteristics

As mentioned earlier mud volcanoes are considered as edifices on land and on the seafloor that result from the emission of argillaceous material, water and gas through various openings or fissures in the crust [1]. Mud volcanoes may erupt violently emitting mud and gas but in most cases, they grow gradually, with progressive outflows of a semi-liquid material called 'mud breccia' [1]

1.1.3.1 Mud breccia

Mud breccia is composed of a clayey and silt-sized matrix, which supports chaotically distributed angular to rounded clasts of terrigenous and biogenic material as well as claystone fragments that are more consolidated than the matrix [13]. The clasts range in diameter from a few millimeters to several meters [14,15] and are derived from the units through which the mud passes on its way to the surface. The matrix usually stems from a specific carrier bed and is characterized by specific geochemical signatures which reflect specific conditions and processes such as clay mineral dehydration and transformation processes.

Young mud volcanoes extrude mud breccia with a very high clast-matrix ratio whereas old mud volcanoes can be virtually clast free with a mud matrix content up to 99% [16,17]. This mud can often be related to the final phases of the eruptive cycle when all loose wall rock has been removed [17].

1.1.3.2 Basic structure

Despite the variations in morphology two main morphological groups can be recognized: (1) an internal feeder system group (2) an external edifice group [1].

Mud breccia is usually extruded through a *central* or *feeder channel* (Figure 1.2) which may be either cylindrical, irregularly shaped, or a slit (i.e., a fracture or a fault) [17]. Near the surface several smaller pipes may split off the main feeder channel. The *main vent* or *central crater* (Figure 1.2) is usually situated on the summit of the volcano and can have many shapes [1]. When the volcano collapses due to an expulsion of a massive amount of material or because the mud has drained through a lower vent, a *caldera* is formed. Craters that are formed on the openings of lateral vents are called *satellite*, *parasite* or *secondary craters* (Figure 1.2) [1]. *Gryphons* (Figure 1.2) which are small secondary vents form around the craters and in many places on the mud volcano body emitting gas, mud and water. They are characterized by a complete absence of solid rock fragments [1]. The body of the volcano is built by the extrusion of mud breccia which spills in thin sheets

forming fan or tongue like shapes. Over time these flows build up forming its body which can cover up to a few tens of square kilometers [1].

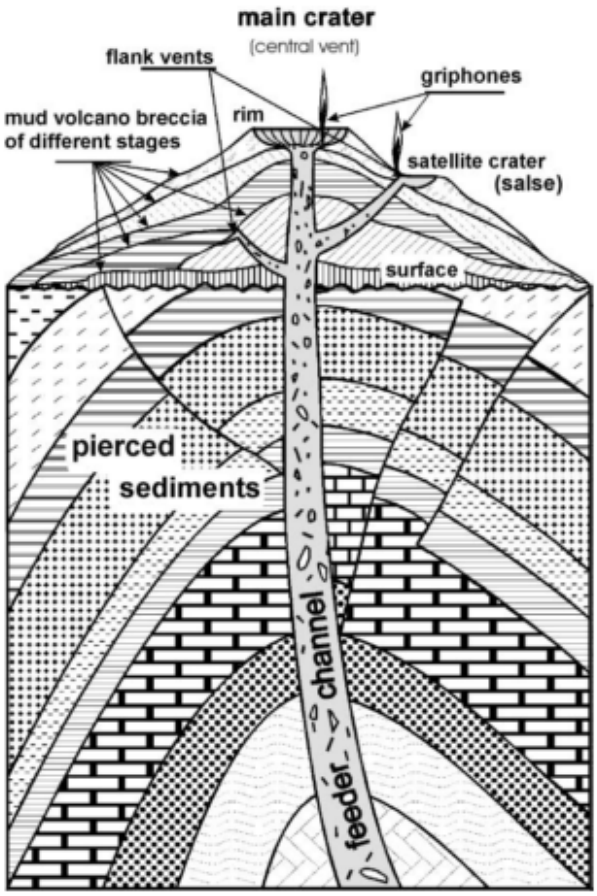

Figure 1.2. Basic structure and elements of a conical mud volcanoes [1].

1.1.4 Global distribution of mud volcanoes

Mud volcanoes are globally distributed (Figure 1.3) and can be found in both marine and terrestrial environments. They have been discovered in 44 onshore [18] and 27 offshore locations [2]. Despite the insufficient survey of oceans, submarine mud volcanoes are thought to be more extensive than the ones found in terrestrial locations. The total number of these formations isn't precisely known and new submarine volcanoes are being discovered ever year (especially during the last two decades) due to continuous investigation of the seafloor with the help of advanced techniques. [2] was the first to make a worldwide estimate of submarine volcanoes and shortly after [1]compiled 270 confirmed and 572 estimated offshore locations. According to [19] 1,100 terrestrial or shallow-water mud volcanoes are known. [20] speculates that the number of large seafloor mud volcanoes could exceed 5,000 whereas [19] states that 150 prominent mud piercing structures are confirmed and nearly 700 submarine mud volcanoes are inferred to occur in deep water. Recently, [21] compiled a worldwide overview of mud volcanoes associated with gas hydrate systems.

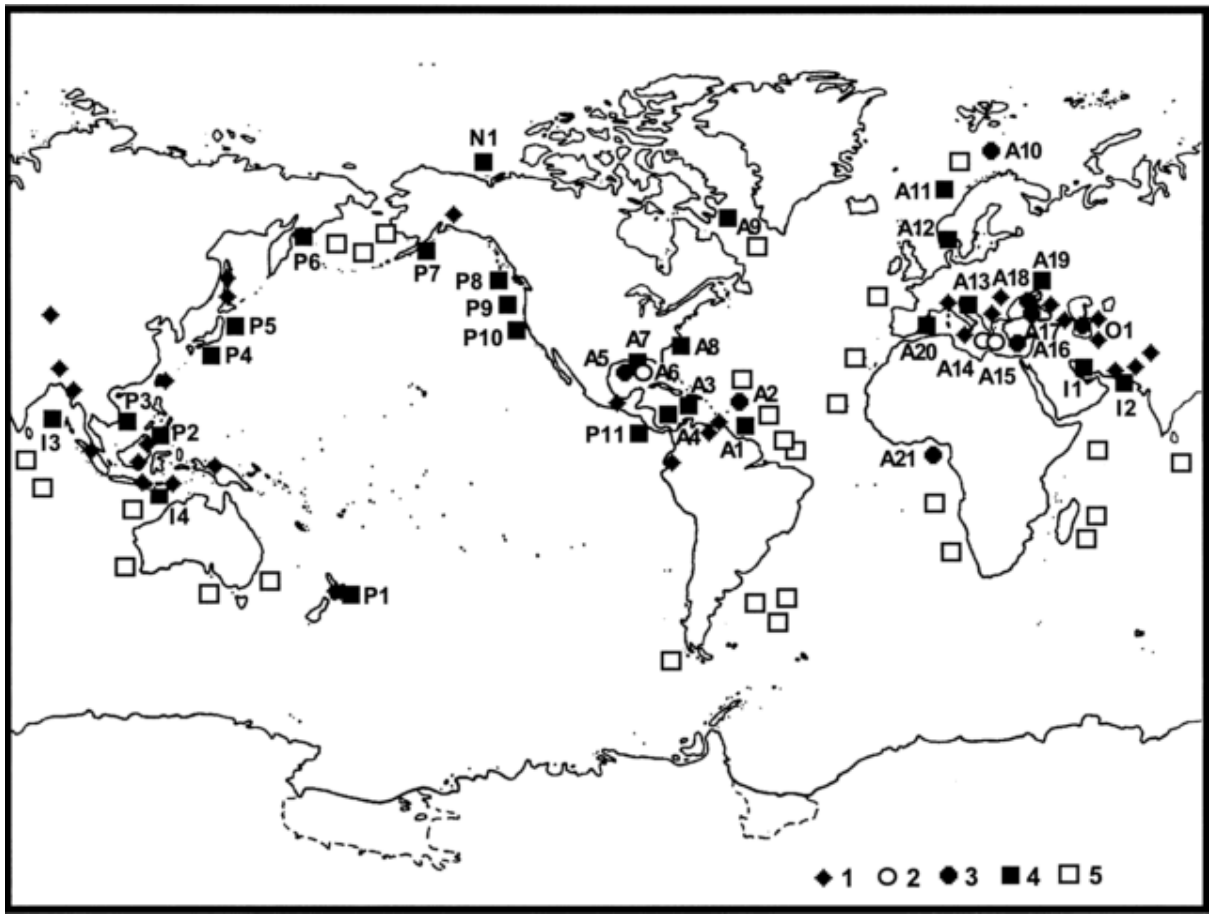

Figure 1.3. Map showing the worldwide locations of onshore (1, after Rakhmanov, 1987, with additions), known (2, without gas hydrates; 3 hydrate bearing), and inferred (4) submarine mud volcanoes. The "possible sediment diapirs" mapped by Lancelot and Embley (1977) are also shown (5) [2].

Since mud volcanoes are formed due to high sedimentation rates and tectonic compression it can be inferred that geological parameters control their geographic distribution. Mud volcanoes are clustered in separate areas forming belts which usually coincide with active areas of plate boundaries and zones of orogenetic structures. These belts are usually confined within compressional zones such as accretionary complexes, thrust and overthrust belts, forelands of Alpine orogenic structures as well as zones of sedimentary basins with enormous sediment thickness which can reach to 15km (Black Sea) or 20km (South Caspian Basin) [19].

Mud volcano groups can also be located outside of these belts in which case they are associated with areas of a high sedimentation rate such as modern fans (including underwater deltas of large rivers) or with areas that present intensive salt diapirism [19]. There have also been reports of mud volcanoes in areas with thin sediments such as the Baltic Sea where the sediment is only 10m thick [22].

The main mud volcano-forming belts around the world include the Alpine-Himalayan belt, the Pacific orogenic belt, and the Atlantic Ocean-Caribbean orogenic belt. Moreover, a

number of mud volcanoes are also situated at some submarine deltaic and fan complexes [1,14,15,23–28].

Alpine-Himalayan belt

More than half of the recorded mud volcanoes are situated within the Alpine-Himalayan belt where there are around 650 terrestrial and at least 470 offshore volcanoes. The belt starts with the Mediterranean Ridge [11] where there are around 110 deep sea volcanoes and the surrounding areas of Sicily, Albania and central and northern Italy where there are around 52 volcanoes documented [29]. It then continues east passing through Romania, the forelands of the Great Caucasus, Azerbaijan, Turkmenistan, through South Caspian Basin, Iran and Pakistan. The belt then passes through the southern Himalayas (India and China) and continues south to the most northeaster part of the Indian Ocean. There are about 150 terrestrial and over 75 offshore volcanoes in this last region [1].

Pacific orogenic belt

The Pacific orogenic belt contains around 150 terrestrial and a large but unknown number of submarine volcanoes [1]. The belt is situated along the eastern and western edges of the ocean. The western part of it is much longer starting at Sakhalin Island in the Sea of Okhotsk running all the way down to Samoa and Australia and then finally ending in the north island of New Zealand. A much smaller number of mud volcanoes are found along the eastern branch of the belt. These volcanoes are mainly situated near Southern Alaska [30], offshore of the Aleutian accretionary complex, offshore California, in the subduction zones off Costa Rica and southern Panama, the Ecuadorean coast, and inland in Peru [19].

Atlantic Ocean – Caribbean orogenic belt

Finally the Atlantic Ocean belts are located in the western and eastern middle parts of the Ocean and in the southern Caribbean Sea [3]. There are nearly 110 active mud volcanoes most of which are located in northern Colombia, northeastern Venezuela, and Trinidad [31]. Many volcanoes are also found in the Barbados accretionary complex [32] and in the southern Caribbean Thrust belts. Mud volcanoes were recently discovered in the eastern Atlantic Ocean in the southern Canary Basin [33], in the Cascadia margin, offshore from Portugal and in the Gulf of Cadiz [34], as well as in the Alboran Basin offshore Morocco [35] where 16 large mud volcanoes were confirmed [19].

Finally, mud volcano clusters which don't belong in these belts are usually connected with submarine deltaic and fan complexes such as the Amazon fan , the Mississippi and Niger deltas [14], the Nile delta, areas of salt diapirism, such as in the Gulf of Mexico [36] and on the Buzachi Peninsula in the northeastern Caspian Sea [37] and also the Hakon Mosby mud volcano on the Bear Island fan, Norwegian Sea [38].

1.1.5 Distribution of mud volcanoes in Mediterranean Sea

In the Mediterranean Sea mud volcanoes form in two main geodynamic settings. The majority of them occur along the various tectono-sedimentary accretionary wedges of the Africa-Eurasia subduction zone, particularly in the central and eastern Mediterranean basins (external Calabrian Arc, Mediterranean Ridge, Florence Rise) and along its westernmost boundary in the Gulf of Cadiz (Figure 1.4). The rest of them occur along parts of the Mesozoic passive continental margins that border Africa from eastern Tunisia to the Levantine coasts (especially off Egypt). Finally, some mud volcanoes also occur within the western Mediterranean back-arc basins [39].

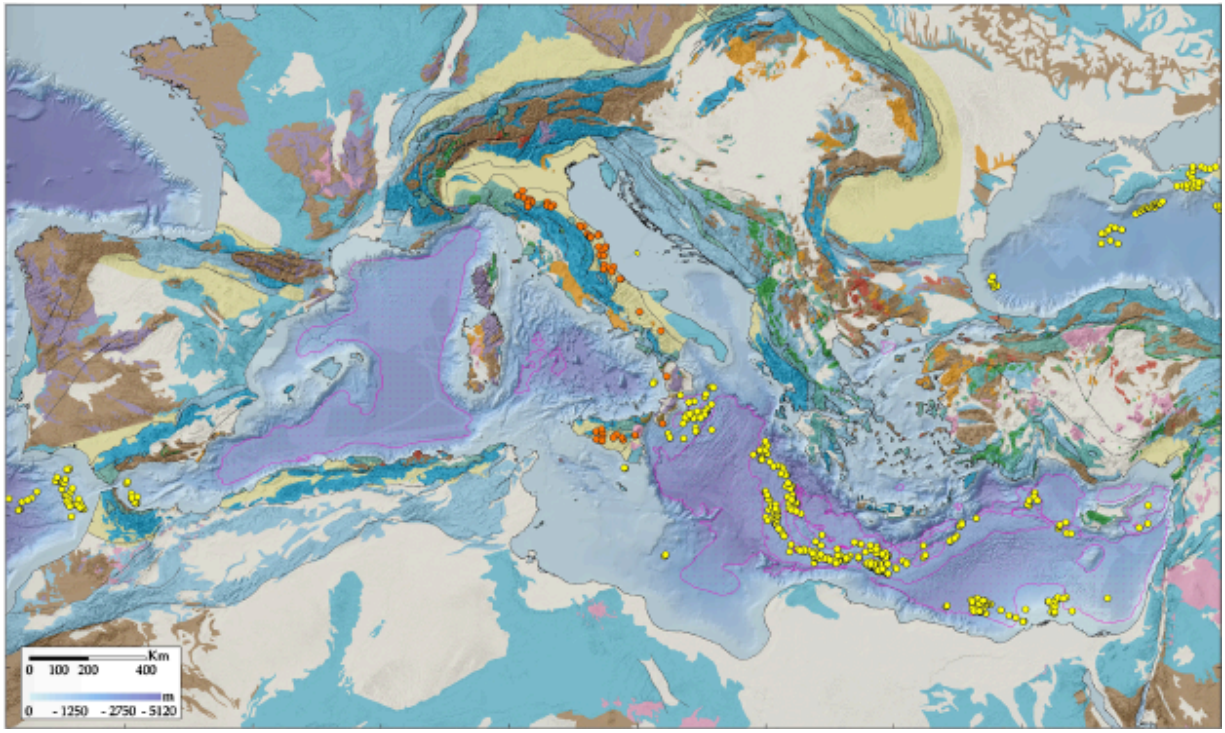

Figure 1.4. Distribution of mud volcanoes (orange and yellow dots) and deep Messinian evaporitic basins (pink lines) in the Mediterranean Sea and Gulf of Cadiz. Most mud volcanoes occur in areas where no thick Messinian evaporate cover exists, with the exception of the north-western Egyptian continental margin [39].

1.1.5.1 Eastern Mediterranean Sea

The eastern Mediterranean is arguably the region with the highest abundance of mud volcanoes and diapirs on Earth [17]. In the last three decades, several features of variable age, geometry and origin have been discovered. The first volcano ever discovered in the Mediterranean Sea is the Prometheus mud breccia dome which was first described by [40] as a mud diapir. The majority of features occur along the accretionary piles and on the North African passive margin within the Nile deep-sea fan [39].

Mud volcano distributions in the eastern Mediterranean can be categorized into four main groups (Figure 1.5):

(1) The mud volcano province in the inner to central Calabrian accretionary prism. This province includes three main features (Madonna, Pythagoras and Sartori mud volcanoes) which are proven by coring [39]. It also contains various other features which are inferred from geophysical data [41].

(2) The numerous formations present in the Mediterranean Ridge and particularly in its western (Ionian) and central parts. Mud volcanoes are organized in two main belts along the inner border of the accretionary wedge and along the main axis of the Ridge. The Olimpi mud volcano cluster belongs in this category. The eastern branch of the Ridge only presents a few inferred volcanoes [39].

(3) A cluster of mud volcanoes in the Anaximander Mountains area. The Anaximander area is considered to be a tectonic relay between the active Mediterranean Ridge and the inactive/less active sedimentary wedge that runs east and northwest of Cyprus [39].

(4) Several large mud volcanoes along the upper continental slope of the passive Nile continental margin. A cluster of small mud cones also occurs in its north western deep corner [39].

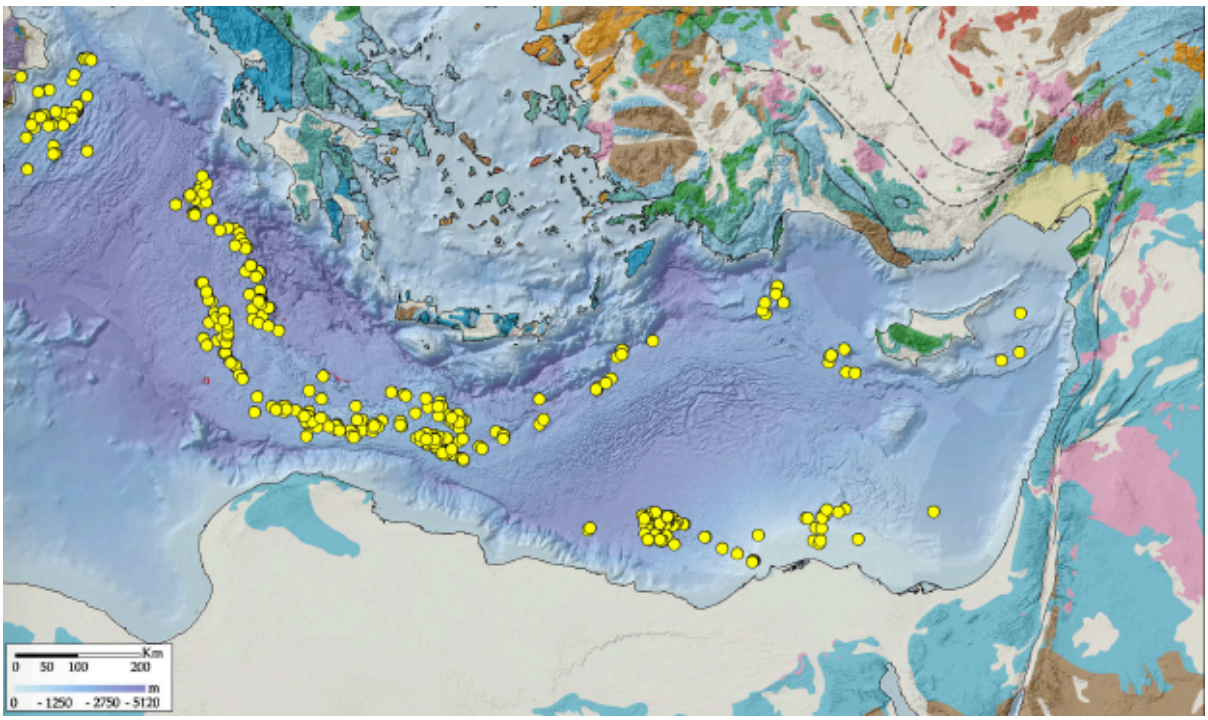

Figure 1.5. Distribution of mud volcanoes and other fluid/mud-releasing structures (yellow dots) in the eastern Mediterranean Sea. Mud volcanoes are widely distributed, particularly within the inner domains of the Calabrian and Mediterranean accretionary prisms, south of Turkey, in the vicinity of the Anaximander Mountains, and on the Egyptian passive continental margin. Extinct mud volcanoes have been detected on the Hecateus Ridge east of Cyprus. Some fluid releasing structures also occur along the Florence Rise [39].

1.1.5.2 Western Mediterranean Sea

In the western Mediterranean, there seem to be two major mud volcano fields (Figure 1.6).

(1) The first one can be detected within the sedimentary of the Gulf of Cadiz. This area consists of a thick pile of deformed sediments which result from the subduction of the central Atlantic oceanic crust beneath the Gibraltar region [39].

(2) The second field is in the western domain of the Alboran Sea. This setting is a back-arc basin where a thick overpressured Early Miocene shale has generated mud diapirism and mud volcanism leading to the formation of several mud volcanoes that continue to seep hydrocarbon rich fluids [42,43].

No other significant mud volcano fields have been described to date within the western Mediterranean basin [39], with the exception of potential deep water mudflows and mud expulsion centers on the western Calabrian margin of the Tyrrhenian Sea within the Marsili back-arc basin [44].

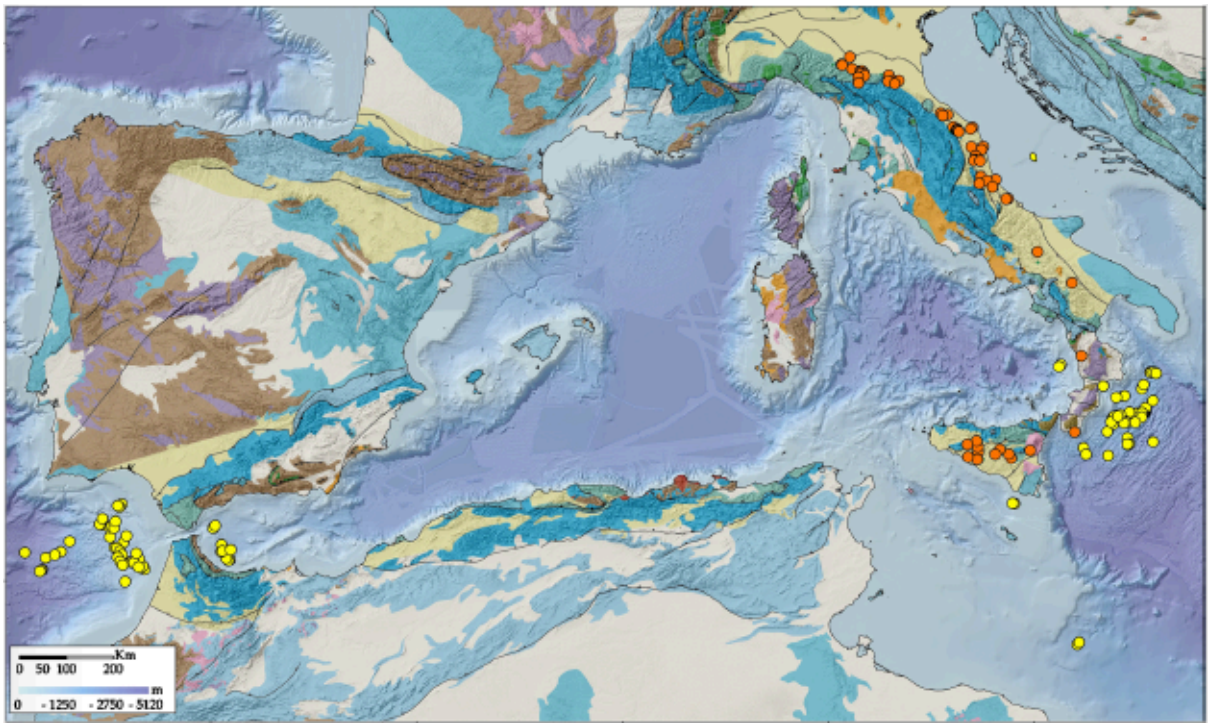

Figure 1.6. Distribution of mud volcanoes and other fluid/mud-releasing structures (yellow dots) in the western Mediterranean Sea and Gulf of Cadiz, including mud volcanoes in the western sector of the Alboran Sea and potentially some areas of the Calabria margin. Red dots depict mud volcanoes known on mainland Italy (based on [45] and taken from [39]).

1.1.6 Significance of mud volcanism

1.1.6.1 Mud volcanoes in petroleum exploration

Mud volcanoes are often associated with petroleum rich basins, examples of which are found in Azerbaijan, the Gulf of Mexico and deep-water Nigeria where thermogenic hydrocarbons enriched in C2+ gases are expelled [46]. As mentioned earlier mud volcanoes eject sediments and rocks that may come from a depth of 2-15km and therefore the study of the ejected material can provide an insight to the deep lithosphere [20]. Consequently, the study of mud volcanoes is especially useful in frontier petroleum exploration areas, for example in the Gulf of Cadiz, where it can indicate an active petroleum system [20].

Mud volcanoes are also often associated with gas hydrates and are considered a potential energy source [47]. Despite this, many mud volcanoes are only likely to provide sub-economic gas hydrate resources due to the insufficient volume of hydrate bound gas [48].

1.1.6.2 Mud volcanoes as a source of methane in the atmosphere and hydrosphere

Mud volcanoes are considered an important geological source of hydrocarbon and non-hydrocarbon gases to the ocean and atmosphere. The most significant emitted gas is methane which is an important greenhouse gas playing a major role in climate change. Mud volcanoes emit gas during both quiescent and eruptive periods but the exact numbers are hard to quantitate.

[19] claims that average volumes of 3.3 to $3.6 \cdot 10^6$ m^3 per year during quiescent periods, and about $12 \cdot 10^6$ m^3 to more than $350 \cdot 10^6$ m^3 per single eruption during eruptive periods are emitted. [25] argue that at least 1–2 Tg/year and as much as 10–20 Tg/year may be emitted from onshore mud volcanoes whereas [17] suggests that all volcanoes on earth (both onshore and offshore) release only 0.08–1.41 Tg/year of gas. [20] has suggested that the volcanoes emit around 6 Tg of methane directly into the atmosphere which represents around 1% of the total concentration.

The gas flux from mud volcanoes to the ocean is much harder to estimate since the number of deep-water volcanoes is unknown. [20] estimated that approximately 27 Tg of gases may escape into the ocean (assuming there are around 5,000 submarine mud volcanoes) on continental slopes every year suggesting that the total hydrocarbon seepage from deep-water areas (currently estimated at 18-50 Tg per year) may be underestimated.

1.2 HYDROCARBONS AND GAS HYDRATES

1.2.1 Hydrocarbon formation

As mentioned above, hydrocarbons and especially methane are released to the oceans and atmosphere through mud volcanoes and cold seep structures in general. Those hydrocarbons are formed in the sediments by thermogenic or biogenic processes. In both processes, buried organic matter mainly produced by marine primary productivity is the base of the reaction.

Thermogenic formation

During thermogenic formation of hydrocarbon gases and oil, temperatures between 60^{o} and 200^{o} are required to induce thermocatalytic cracking of the organic material [49]. The amount of higher hydrocarbons depends on (1) temperature, age and organic matter in the sediments [50], (2) on the source material [51] and (3) on the hydrogen content relative to the available carbon [52].

When there is a high hydrogen to carbon ratio (>>H/C) in the system then oil formation dominates, whereas a low hydrogen to carbon ratio (<H/C) leads to the formation of gas [52]. At the same time methane is more prominent in temperatures higher than 200^{o} whereas oil and higher hydrocarbons are formed in lower temperatures [51].

Biogenic formation

Biogenic methane is produced during microbial methanogenesis, which is the last step in the metabolic carbon pathway. Methanogenesis is performed by anaerobic bacteria via three main processes which are the:

(1) Hydrogenotrophic pathways
(2) Acetate fermentation pathways
(3) Methylotrophic pathways

The hydrogenotrophic and acetate fermentation pathways are the most common ones [53]. This topic will be discussed in greater detail further down.

Origin of hydrocarbons

The origin of hydrocarbons can be inferred through their molecular and isotopic composition (Figure 1.7). During thermogenic formation, higher hydrocarbons (C2+) such as ethane, propane, butane, pentane and hexane are also produced along with methane (C1). A low ratio between C_1/C_{2+} usually suggests a thermogenic origin of these hydrocarbons [54]. Methanogens on the other hand produce pure methane therefore a higher ratio of C_1/C_{2+} (>1000) is more likely to be biogenic.

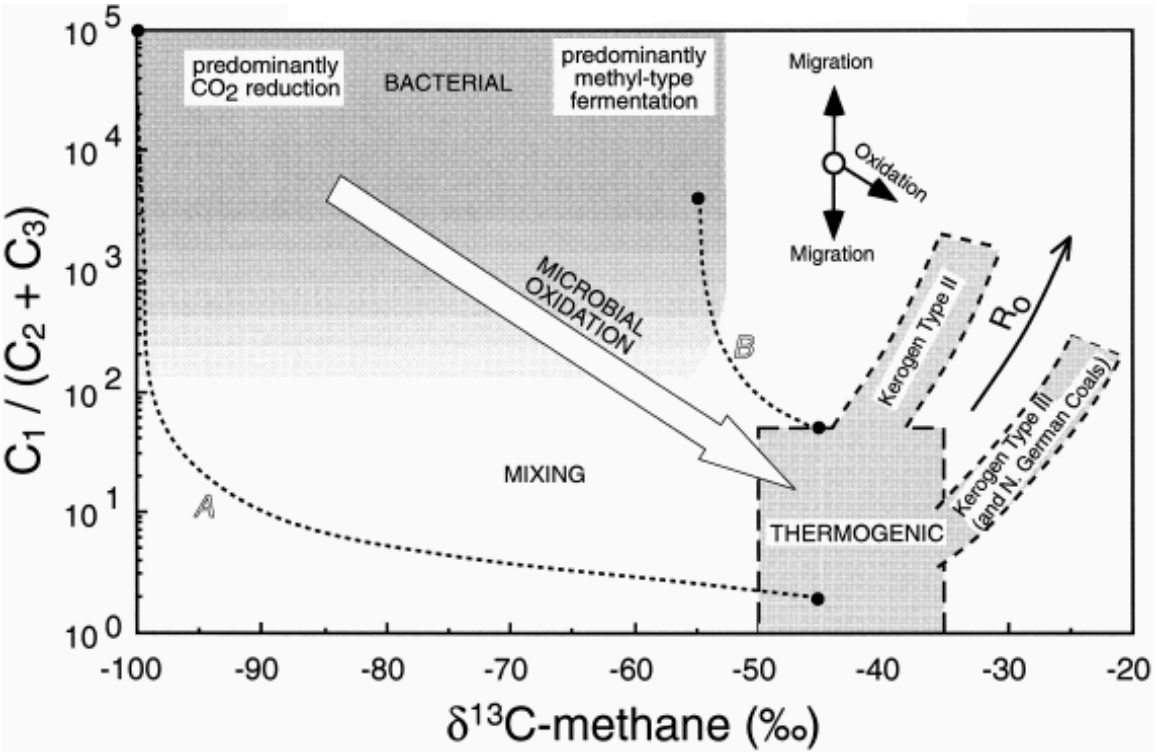

Figure 1.7. The 'Bernard' diagram (after Bernard et al., 1978) which combines molecular and isotope compositional information. The relative compositional effects of migration or oxidation are also indicated [53].

1.2.2. Methane and its isotopic composition

1.2.2.1 General properties

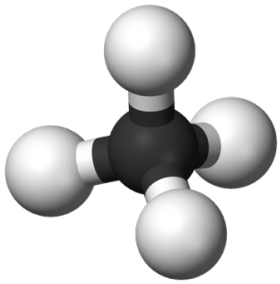

Figure 1.8. The methane molecule

Methane is the simplest organic molecule belonging to the n-alkane series. It is a tetrahedral molecule (Figure 1.8) with four equivalent C-H bonds and it is the most reduced form of carbon. At room temperature and standard pressure, it is a colourless and odourless gas. Methane represents the main component of natural gas, though other hydrocarbons such as ethane, propane and butane can be present. Its solubility in water is rather low (~2,5 mM at 0^{o}C and pressure of 1 atm) and it is negatively affected by temperature [265] and salinity [266]. Pressure on the other hand has a positive effect on its solubility according to Henry's Law.

1.2.2.2 Methane as a greenhouse gas

Methane is an important greenhouse gas due to its ability to absorb and re-emit radiation, trapping the heat 25 times more efficiently than carbon dioxide [55]. The fluctuations (Figure 1.9) between the atmospheric methane concentration and temperature during the glacial-interglacial cycles have been studied by many [56,57].These studies have proved that there is a positive correlation between greenhouse gases and the temperature record that was found in Antarctica during the last four glacial-interglacial cycles.

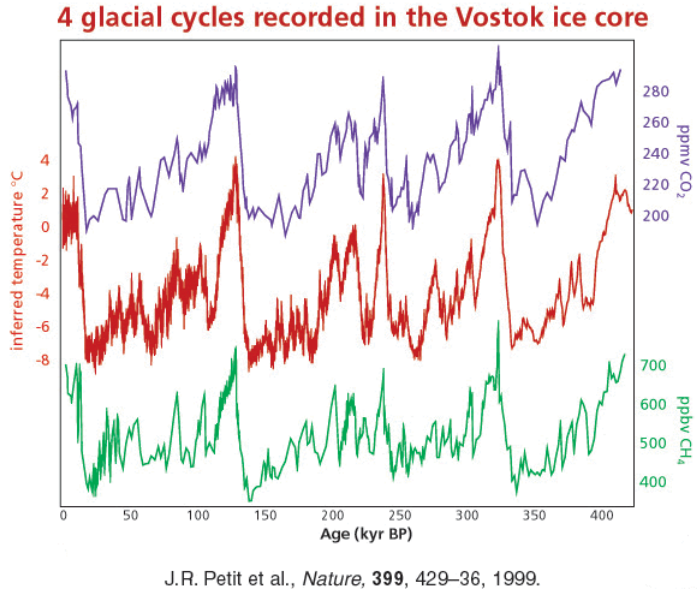

J.R. Petit et al., *Nature*, **399**, 429–36, 1999.

Figure 1.9. The variations of CH4, CO2 and temperature during the last four glacial-interglacial cycles in the Vostok ice core [56].

1.2.2.3 Isotopic composition of methane

Carbon isotopes

Carbon has 15 isotopes from ^{8}C to ^{22}C but only three of them occur naturally, ^{12}C, ^{13}C and ^{14}C. Out of those three ^{12}C and ^{13}C are stable and occur in a natural proportion of about 99:1. ^{14}C is the longest-lived radioisotope with a half-life of 5,700 years and is produced by thermal neutrons from cosmic radiation in the upper atmosphere. It is then transported down to earth and absorbed by living biological material. ^{12}C is the most abundant isotope amounting to 98.93% of the total elemental carbon. As for methane, its isotopic value in nature can be affected by the contribution of different isotopomeres such as ^{12}C,^{13}C and ^{1}H,^{2}H. Lighter isotopes are preferred by living organisms that discriminate against the heavier ^{13}C isotope during the utilization of carbon leading to products enriched in ^{12}C or else products with a lower (more negative) $\delta^{13}C$ value. Since different metabolic pathways discriminate differently against ^{13}C the study of isotopes can be used to infer the origin of the organic compound.

The $\delta^{13}C$ value is expressed as the per mil (‰) deviation from the Vienna Pee Dee Belemnite standard (VPDB) [53] according to the equation:

$$\delta^{13}C = \left[\frac{\left({}^{13}C/{}^{12}C\right)\text{Sample}}{\left({}^{13}C/{}^{12}C\right)\text{Standard}} - 1 \right] 10^{3}$$

Isotopic composition of methane

As mentioned earlier methane sources can be classified as thermogenic or biogenic [53] and references therein). The differences in isotope distribution between thermogenic and biogenic methane are related to several factors which include (1) the precursor compounds, (2) the differences in the type of the kinetic isotope effects (KIE) and (3) the higher temperatures needed for the generation of thermogenic hydrocarbons [53].

Thermogenic methane is generally more enriched in ^{13}C with $\delta^{13}C$ values between -50‰ and -20‰ [53]. Biogenic methane on the other hand is more enriched in ^{12}C and therefore $\delta^{13}C$ values are lower than -50‰ and can even be as low as -100‰ depending on the methane reduction process [50,53]. Methane derived from bacterial sources has carbon isotopic compositions that are dependent on their environment. Marine bacterial methane is generally more depleted in ^{13}C compared to terrestrial bacterial methane which is a result of the dominance of CO2 reduction in the marine environment as opposed to acetoclastic methanogenesis in the terrestrial one. Thermogenic methane that moves upwards from some depth can be mixed with shallow formed biogenic gas and as a result the hydrocarbons sampled from sediments near the surface represent a mixture of both sources. Furthermore, during microbial consumption of methane and the accompanied fractionation processes its isotopic composition is altered, making it harder to distinguish its source [58].

Hydrogen isotope ratios ($^{2}H/^{1}H$) of methane (Figure 1.10) can also be used to classify the origin of the gas but are less useful as an isolated parameter [53]. For thermogenic methane, the δD_{CH4} can range between -100‰ to -275‰ whereas for biogenic/bacterial methane that range is much greater at approximately -150‰ to -450‰ [53]. The problem with δD_{CH4} is that there is a considerable overlap between different thermogenic and bacterial sources (as seen in Figure 1.10) but when used in combination with additional molecular or isotope compositional gas data such as C_2-C_4 , it can be of great use [53].

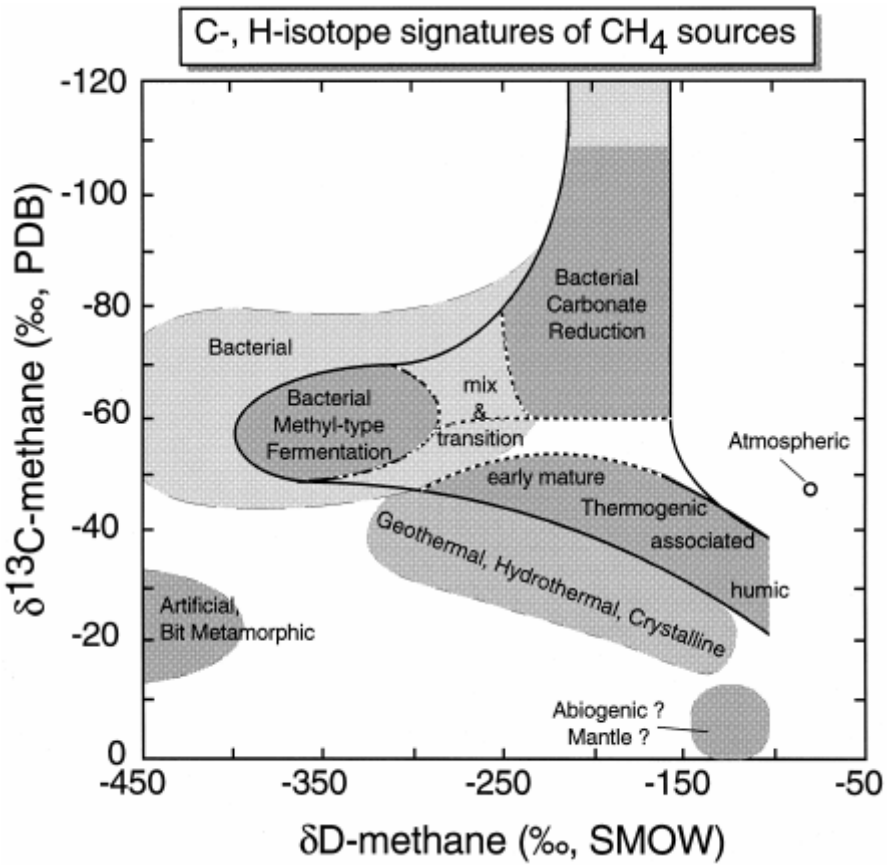

Figure 1.10. CD diagram used for the classification of bacterial/biogenic and thermogenic gas. The diagram combines $\delta^{13}C$ and δD_{CH4} values [53].

1.2.3 Gas hydrates

1.2.3.1 General properties

Gas hydrates had been defined as a 'substance' [59,60] or 'inclusion compound' [61,62] for many years. [63] on the other hand classified them as a mineral. Nowadays gas hydrates are considered as clathrates. Clathrates consist of two dissimilar molecules mechanically intermingled but not chemically bonded. These clathrate compounds are comprised of a host molecule (water) which forms a framework that traps inside the guest molecule (gas). In other words, gas hydrates can be considered as modified ice structures enclosing methane and other hydrocarbons but which have a much higher melting point than ice. Hydrate inclusions usually are white or greyish-white in colour and their content in the sediment varies from about 1-2% to 35% by volume and changes through depth of the mud volcano area [2].

Gas hydrates can contain different types of gas molecules in separate cages, depending on the gas composition in the environment of formation. Biogenic, thermogenic or of a

mixed origin methane is their main component which accumulates in concentric-zonal structures controlled by the flow of ascending warm fluids [2,64,65]. These warm fluids come from the mud volcanic fluid as well as from the surrounding recent sediments [2]. Apart from methane though H_2S, CO_2 and other hydrocarbons can be found in the structure [66].

Up until now gas hydrates have been found to occur in three different crystal structures (Figure 1.11) [67] The first two structures (I and II) crystalize within a cubic system whereas the third structure (structure H) crystallizes within a hexagonal system analogous to water-ice [66].

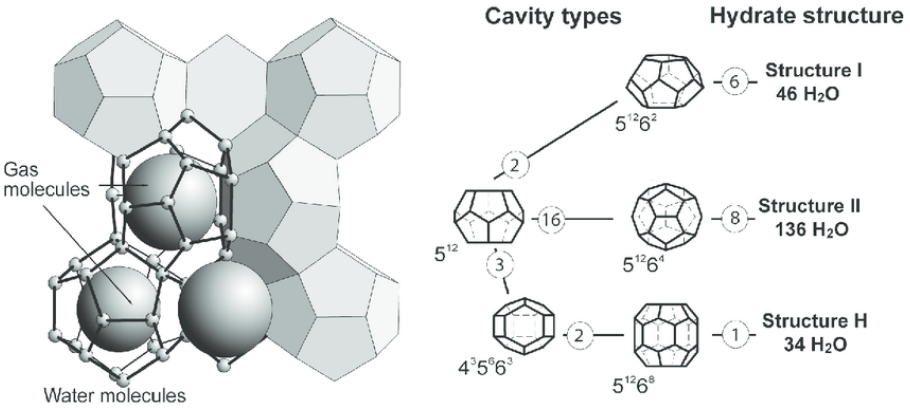

Figure 1.11Gas hydrate structures and cage types. Left: Gas hydrate structure I [66].

1.2.3.2 Formation of gas hydrates

Gas hydrates are restricted to polar (onshore and offshore permafrost) and deep ocean regions on earth due to their formation requirements, and are described as the biggest known methane source on earth [60,68–71]. In 1984, Ginsburg first mentioned the association of gas hydrates with mud volcanoes and ever since this association has been noted in many places around the earth. For gas hydrates to occur some conditions must be met. First of all, thermogenic or biogenic methane must be present in high enough concentrations in order to stabilize the hydrate structure, and secondly thermodynamically favourable conditions must be present [66]. If both those conditions are met then methane will combine with water to form hydrates. [2] proposed a model for gas hydrate formation based on data from the Haakon Mosby mud volcano in the Norwegian Sea, which is characterized by a concentric-zonal distribution of gas hydrates [38,65].

Gas hydrates can occur within the edifice of the volcano as well as in the peripheral marine sediments (Figure 1.12) but do not occur in the center/crater of the volcano due to high temperatures [2]. The rising fluids are warmer by about 15°-20° C than their surrounding sediments at a sub-bottom depth of around 1m and contain gas either as a

solution or as a free phase [2]. When this warm fluid becomes colder as it comes near the seafloor, gas hydrates crystallize due to the decrease in gas solubility [72]. At the peripheral part of the volcano the hydrates form due to gas that comes from the central part of the volcano and is transported in solution by diffusion whereas the water that is needed is local and contained in the host sediment. Sometimes local biochemical gas may also be captured in the hydrates [2]. This process of formation is analogous to the conventional metasomatic process of mineral formation [73].

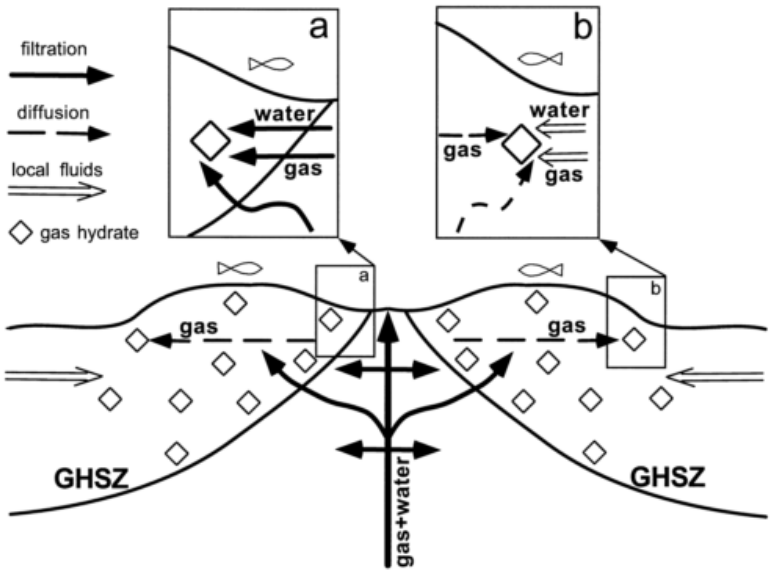

Figure 1.12. The proposed model of formation of gas hydrates within a mud volcano by [2]. B) peripheral formation of gas hydrates analogous to metasomatic processes of mineral formation.

1.2.3.3 Gas hydrate stability zone

The gas hydrate stability zone (GHSZ) refers to a zone and depth below the seafloor in which hydrates exist naturally. As mentioned earlier the occurrence of gas hydrates depends on temperature, pressure and composition [60]. The existence and depth of this hydrate stability zone is often indicated by the presence of the BSR (bottom-simulating-reflector). The BSR is a seismic reflection that is visible due to the different densities between hydrate saturated sediments, normal sediments and those containing free gas [74] and occurs at the base of the GHSZ. In other words, it is a high-amplitude reflector that is associated with a phase reversal that approximately parallels the seafloor [75]. Maximum depth of this stability zone is controlled by the geothermal gradient and in continental margins its thickness is around 500m. In areas of high geothermal heat flow, the maximum depth of the zone will become shallower therefore decreasing its thickness. In contrary, the thickest GHSZ are observed in areas of low geothermal heat flow. In general, the maximum depth at which the GHSZ is observed reaches 2000m.

1.3 LIFE AT COLD SEEPS AND THE PROCESSES INVOLVED

Submarine cold seeps emitting various hydrocarbons are considered to be geologically driven 'hotspots' of increased biological activity. The first discovery of such chemosynthetic communities happened in the deep Gulf of Mexico [76], the subduction zones off Oregon in the eastern Pacific [77], and in the trenches off Japan in the western Pacific [78] and since then they have been documented at various seafloor sites worldwide [6].

Cold seeps are highly diverse habitats in which a wide array of mega-, macro- and meiofauna (symbiotic or not) in addition to an enormous biomass of microbial communities can be found. The seep communities differ from other marine deep-water ecosystems as they are colonized by specific anaerobic microbiota. These microorganisms use hydrocarbons as their energy source [79] and at the same time produce hydrogen sulfide by reducing seawater sulfate [80]. The seeps are characterized by high spatial variability and therefore a patchy occurrence of methane or sulfide dependant biota. This spatial variability depends mainly on the magnitude of fluid flow [81–85].

With low flow rates, sufficient methane is provided in order to fuel near surface biological activity and at the same time downward transport of sulfate and oxygen rich seawater is allowed into the first few sediment centimeters [85]. Much higher flows result in altered pore water composition and elevated sulfide concentrations which migrate all the way up to the seafloor allowing the growth of microbial mats [84,86,87].

1.3.1 Microbial communities

The chemosynthetic microbial communities which inhabit cold seep environments provide the base for growth of the rich and active ecosystems that are decoupled from photosynthesis [88]. These microbial communities depend on the long-term availability of chemically reduced electron donors such as methane and sulfide as well as higher hydrocarbons [89]. In locations where gas hydrates or gas vents are present the anoxic sediments that lay above them have the highest biomass known to occur in marine ecosystems with up to 10^{12} cells per cm^3 [90].

The key functional microbial groups in these systems have distinct metabolic abilities (adapted to the exploitation of reduced compounds) and include methanotrophs, methanogens, hydrocarbon degraders, sulfate reducing and sulfide oxidizing bacteria [80]. Hydrocarbon degradation is usually dominated by sulfate- reducing bacteria of the Deltaproteobacteria [91]. Methanotrophs and methanogens are comprised of Archaea and specifically methanotrophic and methanogenic Euryarchaeota and uncultured

Crenarchaeota [92]. Microbial mats are a key indicator community of active cold seep systems [93]. These mats consist of sulfur-oxidizing bacteria that use up the AOM-derived sulfide fluxes to the seafloor. They are highly diverse and each population has distinct adaptations to enable the use of sulfide, nitrate and oxygen that develop in the methane rich sediments [94].

1.3.1.1 Anaerobic Oxidation of Methane (AOM) and ANaerobic MEthanotrophs (ANME)

Ever since the late 1990s anaerobic oxidation of methane (AOM) and the microorganisms performing it have been the focus of many studies [90,95,96]. Ribosomal RNA investigations revealed that AOM is performed by consortia of Archaea, ANaerobic MEthanotrophs (ANME) which are closely related to the order Methanosarcinales, and sulfate-reducing bacteria (SRB) of the *Desulfosarcina*/ *Desulfococcus* (DSS) order [90,91,97,98].

Anaerobic oxidation of methane (AOM)

Anaerobic oxidation of methane (AOM) (Figure 1.13) is a microbial process which was first recognized in the 1970s in anoxic marine sediments [99–101]. Up until then oxidation of methane was assumed to only take place under oxic conditions but the truth is that aerobic oxidation of methane is very limited in marine sediments due to the rapid utilization of oxygen during organic matter degradation. [102] described AOM as a 'microbial process embedded within a complex network of biogeochemical reactions'. During this process, a consortium of anaerobic methane-oxidizing Archaea and sulfate-reducing Bacteria consume methane (CH4) and sulfate (SO_4^{2-}) and release bicarbonate (HCO3-) and sulfide (HS^-) [90,103–105].

The overall reaction that takes place is:

$$SO_4^{2-} + CH_4 \rightarrow HCO^{3-} + HS^- + H2O$$

[100] proposed sulfate as the most probable electron acceptor in this situation which was later on confirmed by the detection of radioactively labeled products (like CO2 and sulfide) which were formed during the turnover of artificially labeled substrates (like $^{14}CH_4$ and $^{35}SO_4^{2-}$) [106,107].

As biogenic or thermogenic methane migrates upwards and gets consumed by AOM, seawater sulfate slowly diffuses downwards into the sediment pore water where it is reduced either by AOM or by organoclastic sulfate reduction. The zone where both compounds are almost entirely reduced or oxidized is called the sulfate-methane

interface (SMI) [104,108,109]. The methane flux from below controls the depth of the SMI where higher inputs shift the SMI zone towards shallower depths [108,110].

AOM also results in increased alkalinity (or else bicarbonate (HCO_3^-) which is also expressed as dissolved inorganic carbon (DIC)) and therefore authigenic carbonates can form when calcium and other cations are present [111–113].

The carbonates form based on the reaction:

$CH^4 + SO^{2-} + Ca^{2+} \rightarrow CaCO_3^- + HS^- + H_2O$

These authigenic carbonates are mainly aragonites and Mg-rich calcites which can vary in shape and size ranging from small crystals [114] to carbonate chimneys [98]. They are preserved in time and can be detected all the way back to the Carboniferous (around 300my) [115]. Furthermore, sulfide (another product of AOM) forms iron sulfides in the presence of dissolved iron which present themselves as black spots or areas in the sediment.

Other phenomena related to the AOM process include:

(1) Secondary methanogenesis in the lower part of the SMI during which methanogens use the DIC derived from AOM to generate ^{13}C depleted CH_4 (Borowski et al. 1997; Hong et al., 2013; Hong et al. 2014)

$4H_2 + HCO_3^- + H^+ \rightarrow CH_4 + 3H_2O$

(2) AOM back flux, introduced by [119], which is based on a theory that enzyme-catalyzed reactions like AOM are reversible [120]. This back flux occurs in the lower parts of the SMI zone where sulfate is limited. In contrast to methanogenesis no hydrogen is required to form the CH_4. [121] reported a 5% AOM back flux of DIC to CH4.

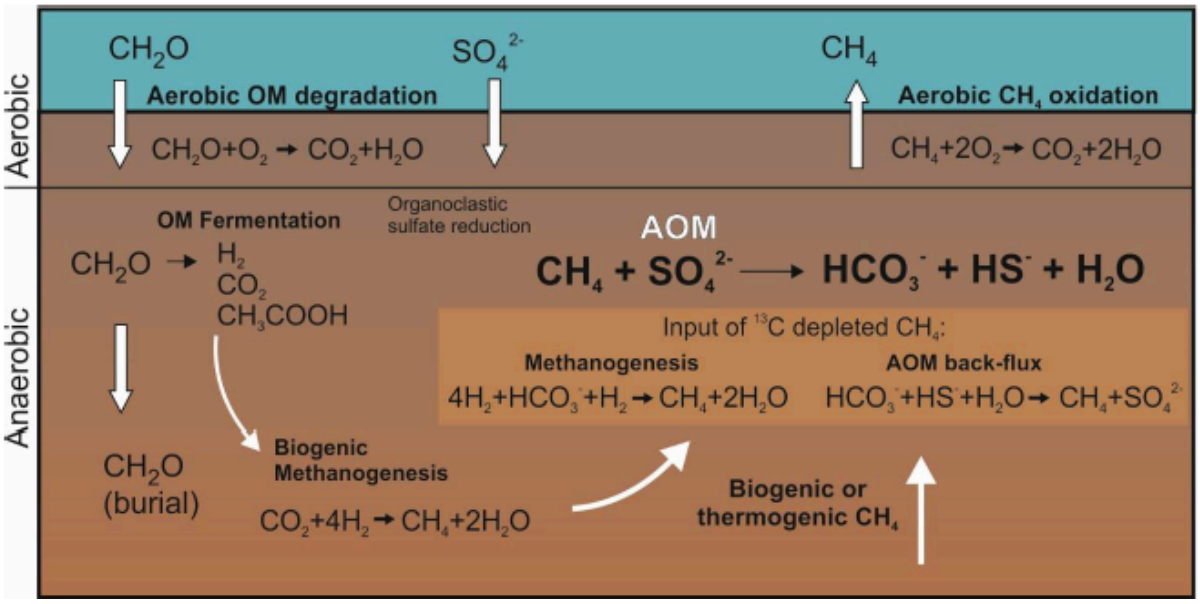

Figure 1.13. Aerobic and anaerobic processes which take place in marine sediments. The figure depicts biogenic and thermogenic methane fluxes, AOM, sulfate reduction, organic matter degradation, secondary methanogenesis and AOM back-flux. Modified after [122] and [119].

ANaerobic MEthanotrophs (ANME)

Up until now, ANaerobic MEthanotrophs have not been successfully isolated and therefore information has been obtained by cultivation-independent techniques. For example, lipid biomarkers and the analysis of 16S rRNA have been used in order to study these anaerobic methanotrophs and have shown that they are divided into three phylogenetic groups: ANME-1, ANME-2 and ANME-3.

ANME-1 Archaea (Figure 1.14) are distantly related to *Methanosarcinales* and *Methanomicrobiales* and occur in association with sulfate-reducing bacteria of the *Desulfosarcina-Desulfococcus* (DSS) group from the δ-proteobacteria [98] [92] in monospecific aggregates or single cells [92,97]. [123] based on in vitro experiments concluded that ANME-1 showed the highest methane dependent sulfate reduction rates between 16^{o} and 24^{o} C. Furthermore, according to study the pH optimum of ANME-1 showed a wide range between 6.8 and 8.1.

ANME-2 Archaea (Figure 1.14) are affiliated with the methanogenic order *Methanosarcinales* and have been observed in physical association with DSS [90,92]. The ANME-2 Archaea are located in the central core of each microbial aggregate and are surrounded by a shell of *Desulfosarcina* spp [124]. These aggregates were first discovered in the surficial sediments above the gas hydrates of Hydrate Ridge [90]. Contrary to ANME-

1, ANME-2 are better adapted to cold temperatures and present higher activity at pH values of 7.4 [123].

Finally, ANME-3 Archaea (Figure 1.14) are affiliated with the methanogenic genera *Methanococcoides* and *Methanolobus* and have been found in syntrophic partnerships with *Desulfobulbus* sp. (DBB) [93,125]. They were recently discovered in sediments from the Haakon Mosby mud volcano [125].

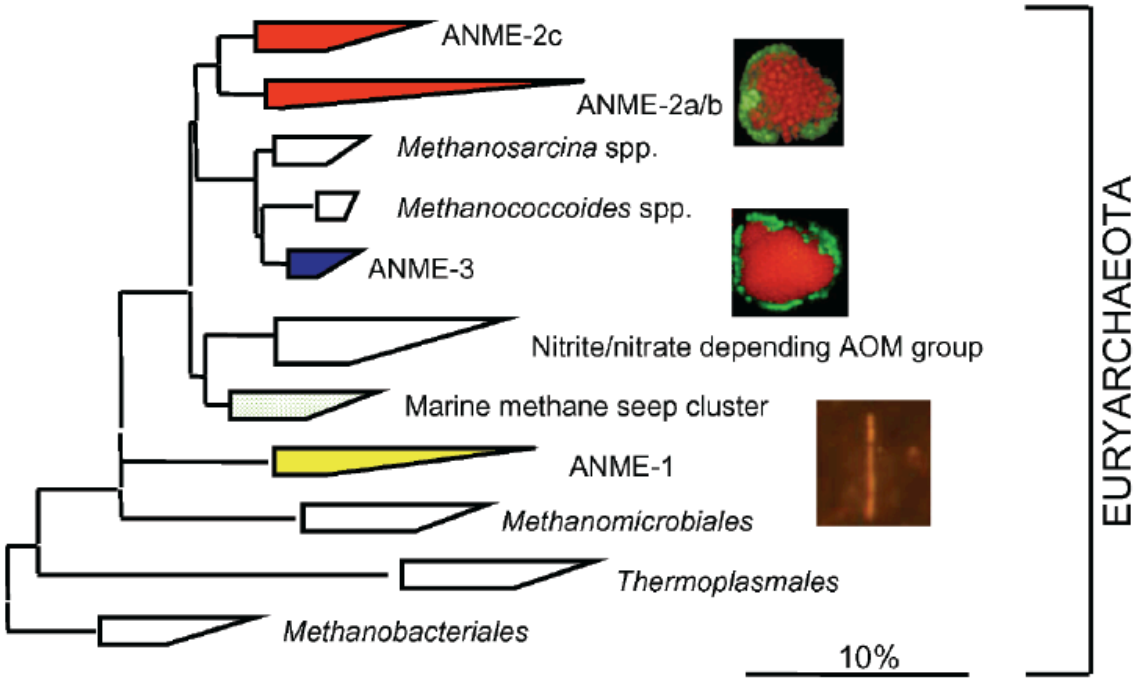

Figure 1.14. Phylogenetic tree of Euryarchaeota, including ANME-1,2,3 and some methanogens [90,92], MUMM project.

1.3.1.2 Microbial methanogenesis and methanogens

Methanogenesis

During the microbial degradation of organic matter macromolecular organic compounds are broken down into smaller molecules through a sequence of redox reactions leading to the formation of methane. Microbial methanogenesis is the last step in the metabolic carbon pathway and is performed by anaerobic Archaea via three main processes: (1) hydrogenotrophic, (2) acetate fermentation and (3) methylotrophic pathways.

Hydrogenotrophic pathway $CO_2 - 8H^+ + 8e^- \rightarrow CH_4 + 2H_2O$

Aceteate fermentation pathway $CH_3COOH \rightarrow CH_4 + CO_2$

During these first two pathways, which are the most common [53] hydrogen (H^+) and acetate (CH_3COOH) are transformed into methane (CH4) and carbon dioxide (CO2). Both hydrogen and acetate though are also required for sulfate reduction and are therefore not available for methanogenesis in the zones where sulfate is present. As a result, these two pathways are restricted to the methanogenic zone [53]. The formation of methane leads to an increase in pore water pressure which drives the produced hydrocarbons upwards to lower pressured sediments.

Other processes for the formation of methane include:

Methanol reduction	$CH_3OH + H_2 \rightarrow CH_4 + H_20$
Disproportionation of formate	$4HCOO^- + 4H^+ \rightarrow CH_4 + 3CO_2 + 2H_2O$
Disproportionation of methylamines	$4CH_3NH_3 + 2H_2O \rightarrow 3CH_4 + CO_2 + 4NH_4^+$

Despite the different pathways of methanogenesis (during which different carbon sources are utilized) all methanogens share the same final step in which the methyl-coenzyme M reductase (mcr) catalyzes the reaction between the methyl-coenzyme M and the coenzyme B therefore promoting the reduction of the methyl group into methane.

Methanogens

Methanogens are strictly anaerobic organisms since the hydrogenase enzyme complex F_{420} they have is not stable in the presence of oxygen, nitrate and nitrite [126]. This coenzyme works as an electron donor during the reduction of CO2 and methanol [127]. Methanogens are represented by five orders of the *Euryarchaeota* which include the (Figure 1.15): *Methanobacteriales, Methanococcales, Methanomicrobiales, Methanosarcinales* and *Methanopyrus*. Different metabolic pathways are used amongst each group. *Methanobacteriacea* utilize CO2, formate or methanol while *Methanococcacea* CO2 or formate. *Methanomicrobiacea* use CO2, formate or alcohols as their substrate whereas *Methanosarcinales* can disproportionate methanol or use acetate, methylamines or other methylated compounds in order to produce methane [127–129].

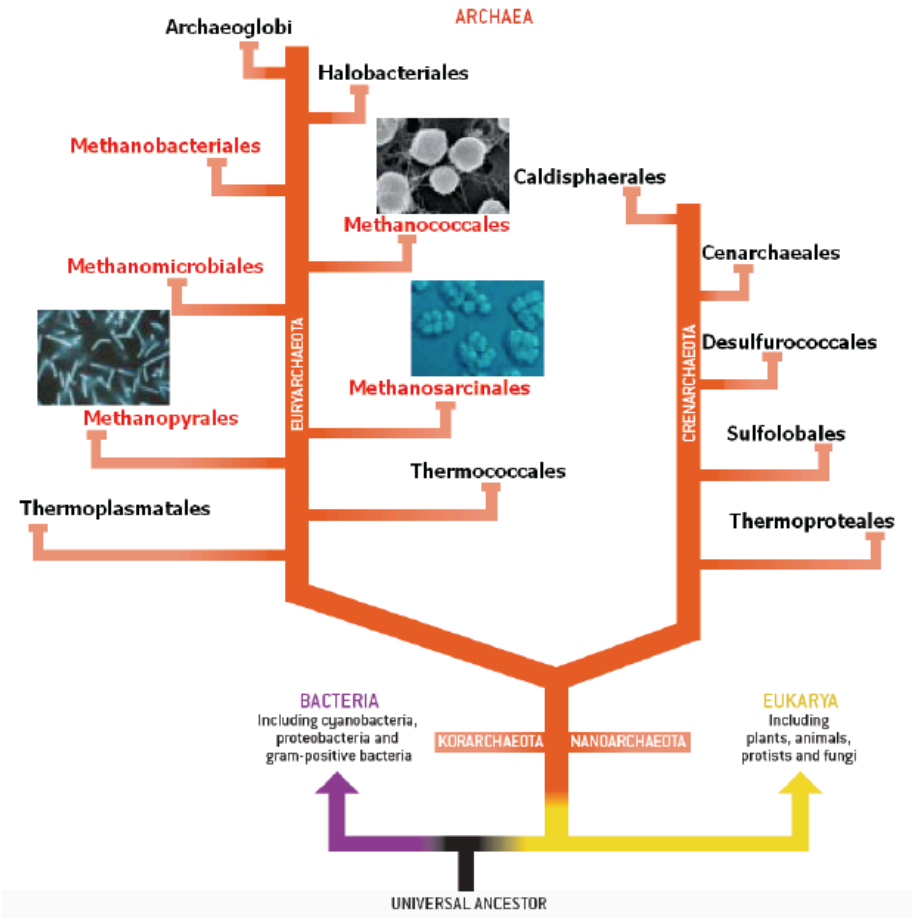

Figure 1.15. Phylogeny of Archaea. Methanogens are displayed in red [130].

1.3.1.3 Sulfate reduction and Sulfate-Reducing Bacteria (SRB)

Sulfate Reduction

As mentioned previously one of the main biogeochemical processes underlying energy flow in cold seep settings is the anaerobic oxidation of methane (AOM) via sulfate reduction (SR) [90,93,98,131]. But the importance of sulfate reduction is more widespread since it is considered to be one of the most important processes for the degradation of organic matter in marine sediments [132]. Sulfate reduction is a form of anaerobic respiration that uses sulfate as the terminal electron acceptor. Along with methanogenesis, sulfate reduction is considered to be an exclusive microbially-mediated reaction [99,133–135].

During this dissimilatory process (Figure 1.16) three steps take place (1) Conversion of sulfate to Adenosine 5'-phosphosulfate (APS), (2) Reduction of APS to sulfite and finally (3) Reduction of sulfite to sulfide.

The general reaction that describes sulfate reduction is [136].

$2CH_2O + SO_4^{2-} \rightarrow 2HCO_3^- + H_2S$

The sulfide that is produced from sulfate reduction can be used by sulfur-oxidizing, chemoautotrophic prokaryotic organisms. Sulfate reduction in marine sediments is limited by the rate of sulfate supply from the seawater and therefore the reduction zone may be relatively shallow in organic rich areas where sulfate is rapidly depleted. In pelagic sediments on the other hand where the organic content is relatively low the reduction zone can occupy several meters.

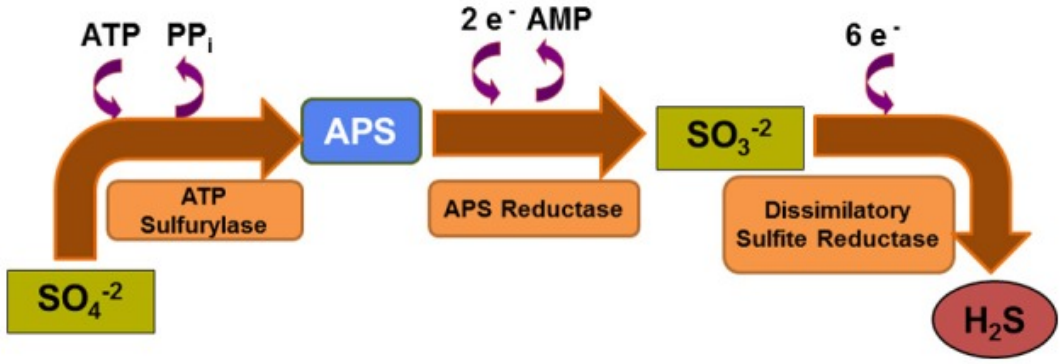

Figure 1.16. Overview of the dissimilatory sulfate reduction pathway [137].

Sulfate Reducing Bacteria (SRB)

Sulfate reducing Bacteria (SRB) play a major role in the anaerobic degradation of organic matter in marine sediments. They are generally obligate anaerobes, mostly belonging to the δ-proteobacteria (*Desulfovibrio, Desulfotomaculum, Desulfobacter, Desulfobulbus)* but there are also members among the Gram-positive eubacteria and the thermophilic archaebacteria (*Thermodeulfobacterium, Thermodesulfovibrio,* Archaeoglobus, Caldivirga). They can tolerate wide ranges of pH, pressure, temperature and salinity. What all sulfate reducers have in common is the ability to use sulfate as the final electron acceptor [138]. Electron donors come from a wide range of low molecular weight compounds derived from the degradation of organic matter. The most important substrate they use is acetate which is completely oxidized to CO2 by the group of SRB that utilize the citric acid cycle (e.g *Desulfobacter*). Other reducers such as *Desulfovibrio* do not have a citric acid cycle and use other substrates such lactate [139].

In cold seep settings sulfate reducers can be grouped into four different categories. These categories include (1) SEEP-SRB1 (which are related to Desulfococcus/Desulfosarcina or DSS group, (2) SEEP-SRB2 (which aren't related), (3) SEEP-SRB3 (related to Desulfobulbus) and finally (4) SEEP-SRB4 (related to Desulforhopalus) [91].

CHAPTER 2 - MOLECULAR BIOMARKERS

2.1 INTRODUCTION

Biomarkers, or else biological markers, were first described in the 1960s [140,141] as 'molecular fossils' or 'chemical fossils', which basically means that these compounds originated from formerly living organisms. The 'chemical fossil' term eventually evolved to 'biological marker' [49] which was then contracted to the current term of 'biomarker'. Their significance mainly derives from the fact that in the course of time their structure shows little to no change from their parent organic molecules in living organisms.

In comparison to other organic molecules, biomarkers can generally reveal more information concerning the origin of the organic matter as well as the transformation/diagenetic mechanisms that take place through time. The basic characteristics responsible for their distinction amongst compounds are (1) their structure which is composed of repeating subunits, clearly indicating that their precursors were components of living organisms, (2) their main identifying structural characteristics which are chemically stable during sedimentation and early burial and finally (3) the fact that each parent biomarker is common in specific organisms.

Molecular biomarkers and the three domains of life

The organisms which contribute to the carbon cycle on Earth can be divided into three categories or else- three domains of life. These domains include the (1) Archaea and (2) Bacteria, which are both prokaryotes [142] and the (3) Eukarya, which are eukaryotes or higher organisms. There are various morphological differences between them which also reflect fundamental differences in their biochemical composition. Some of these differences also control the types of biomarkers which originate from the groups.

Higher plants for example, are characterized by the presence of waxes as protective coatings on the leaves. The major components of these waxes are saturated straight-chain fatty acids with >22C atoms as well as components derived from these acids such as straight-chain alcohols (n-alkanols) and alkanes (n-alkanes). Microorganisms and multicellular algae on the other hand are composed of straight-chain fatty acids and their biosynthetically related n-alkanes and n-alkanols which generally have <22C atoms.

Prokaryotes, which are the main focus of this study, are mainly distinguished by their diverse biochemistry and the habitats in which they grow [143] and therefore the study of the related biomarkers can provide a lot of information. Unlike eukaryotes who use steroids in their cell membranes, bacteria do not appear to contain any sterols and use

hopanoids (which are rare in other organisms) as cell membrane rigidifiers. Archaea on the other hand contain phospholipid ethers.

2.2 LIPID BIOMARKERS AND CELL MEMBRANES

Lipids represent one of the most important components of organic biomarker molecules which are stable under geologic conditions. Lipids can generally be defined as all substances produced by living organisms, which are insoluble in water and can only be extracted by organic solvents such as hexane, acetone, toluene, methanol etc. Lipids can include simple organic compounds such as alkanes, alcohols, aliphatic carboxylic acids but most of them exist as combinations of these simple molecules with one another. These combinations include wax esters, triglycerides, steryl esters, phospholipids as well as glycolipids and glycoproteins which are combinations of lipids with carbohydrates and proteins respectively.

Cell membranes

Cell membranes (Figure 2.1) are usually composed of a bi-layer of amphipathic compounds which are molecules that contain both hydrophobic and hydrophilic surfaces at opposite ends. In these bilayers, the polar end of one set of lipids faces the aqueous interior while the polar end of the other set of lipids faces the external environment. The non-polar portion of both sets of lipids forms a hydrophobic zone within the membrane bilayer.

Membrane lipids

The main membrane lipids of bacteria and eukarya are glycolipids and phospholipids which are basically composed of fatty acids connected to a polar head. The fatty acid chains typically have 12-24 carbon atoms and may be saturated or have one or more double bonds. Short chain C12, C14, C16 n-alkanoic acids are produced by all plants but dominate the lipids in algae [144]. Longer chain n-alkanoic acids such as C24, C26 and C28 are major components in the epicuticular waxes of land plants. Attached to the fatty acids are various moieties such as phosphates and sugars. Membrane lipids of Archaea differ from bacteria and eukarya since they are characterized by isoprenoid hydrocarbons linked together with ether bonds. They can either have a single polar head with isoprenoid side chains ranging from 15-25 carbons or may have two polar heads joined by C40 biphytanyl isoprenoids.

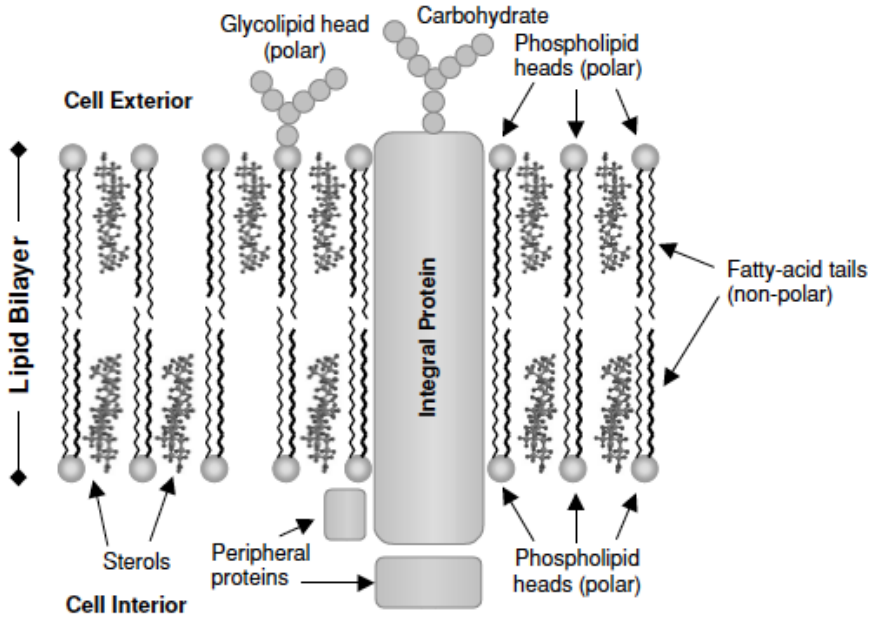

Figure 2.1. Schematic of an eukaryotic lipid cell membrane. Phospolipids and glycolipids are composed of two fatty acids bound to a polar head. These lipids form a bilayer with a hydrophobic interior and a hydrophilic exterior (taken from The Biomarker guide, Vol. 1).

The remainder of the cell membrane is mainly composed of proteins and some carbohydrates which are either attached to enzymes or the polar heads of lipids and always face the exterior of the membrane.

Table 2.1. Comparison of lipids from the three domains of life [145].

Lipid class	Archaea	Eubacteria	Eukarya
Glycerolipids	+	+	+
Hydrocarbon chain	Isoprenoid	Fatty acid	Fatty acid
Carbons in compound	C_{15-25}/C_{40}	C_{12-24}	C_{12-24}
Hydrocarbon bonding type	Ether	Ester	Ester
Position in glycerol	*sn*-2,3	*sn*-1,2	*sn*-1,2
Phospholipids	+	+	+
Glycolipids	+	+	+
Phosphoglycolipids	+	+	+
Sulfoglycolipids	+	−	+
Phosphosulfogylcolipids	+	−	−
Sulfolipids	−	−/(+)	+
Sphingolipids	−	−/(+)	+
Hopanoids	−	+	−/(+)
Steroids	−	−/(+)	+

+, present in all or some species; −, absent; −/(+), absent in most species.

Some of the most important lipid classes used in this study are briefly mentioned below whereas specific biomarkers are analysed in greater detail in the next chapter:

1.Glycerides

Glycerides are esters of the alcohol glycerol. Glycerol molecules contain three hydroxyl groups and therefore can react with up to three carboxylic acid molecules forming mono-, di- and triglycerides. Fats and phospholipids are amongst the most important glycerides.

A. Fats are triglycerides formed from straight-chain carboxylic acids called fatty acids, each fatty acid in a triglyceride molecule can be different. **Fatty acids** usually have a chain length of C12-C36 and are predominantly saturated (alkanoic acids) in animals whereas in plants they are usually unsaturated (alkenoic acids) and polyunsaturated. In plants specifically, the major fatty acids are the C18 mono-, di- and triunsaturated forms and polyunsaturated forms are more common in algae than higher plants.

Biosynthesis of fatty acids

Fatty acids are formed from acetyl (C2) units which are derived from glucose in the presence of various enzymes, coenzymes and proteins and as a result have predominantly even numbers of carbon atoms. During their biosynthesis, the first step is the formation of acetyl coenzyme A (acetyl-CoA). A succession of steps (Figure 2.2) such as addition, decarboxylation dehydration and reduction follows in order to produce palmitate (C16). Higher acids are built from palmitate with the use of different enzymes. Finally, unsaturated products result from the enzymatic desaturation (dehydrogenation) of these acids.

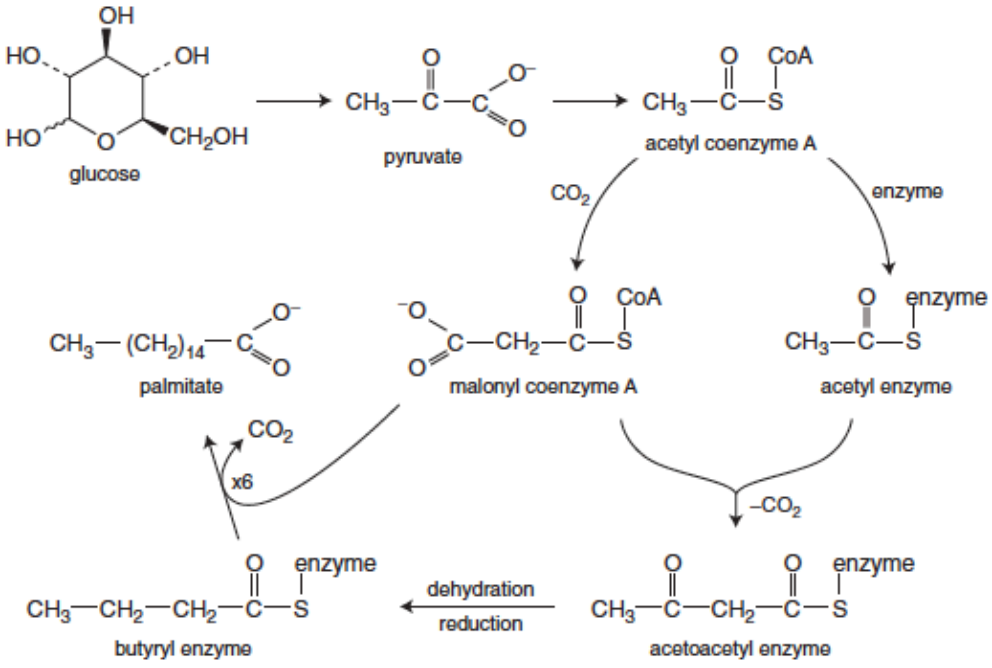

Figure 2.2. Biosynthesis of saturated fatty acids in plants and animals. Palmitate is formed by successive additions of malonyl coenzyme A to the enzyme-bound chain, with CO2 being lost at each addition. This results in chain elongation by a (CH2)2 unit at each step. Details of the formation of butyryl (C4) from acetyl (C2) are shown, while the subsequent six further additions, terminating in palmitate, proceed similarly (Killops and Killops, 2005).

B.Phospholipids (Figure 2.4) are also triglycerides which contain one phosphoric acid and two fatty acid units. These lipids are arranged in a bilayer with the non-polar (hydrophobic) alkyl chains of the fatty acids directed towards the interior of the layer whereas the polar (hydrophobic) phosphate ends are placed on the surface of the membrane (Figure 2.3). Phospholipids are the main type of cell membrane lipids and account up to 65% in plant cells [146].

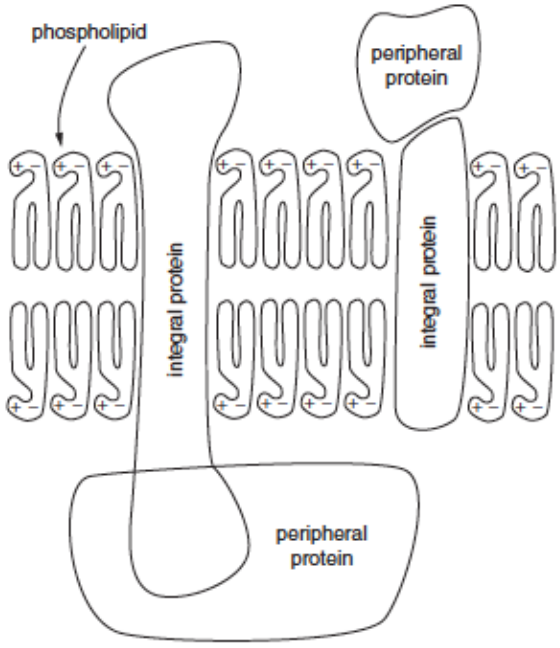

Figure 2.3. Phospholipid arrangements in cell membranes (Killops and Killops, 2005).

C.Glycolipids (Figure 2.4) can be described as any compound in which lipids and carbohydrates are combined. Glycolipids (with a sugar instead of a phosphate head) are found in plant cell membranes and can account for up to 20% of membrane lipids. They are also important components of the cell membranes of Gram-positive bacteria as well as major components of the cell membranes which surround chloroplasts in higher plants, algae and cyanobacteria.

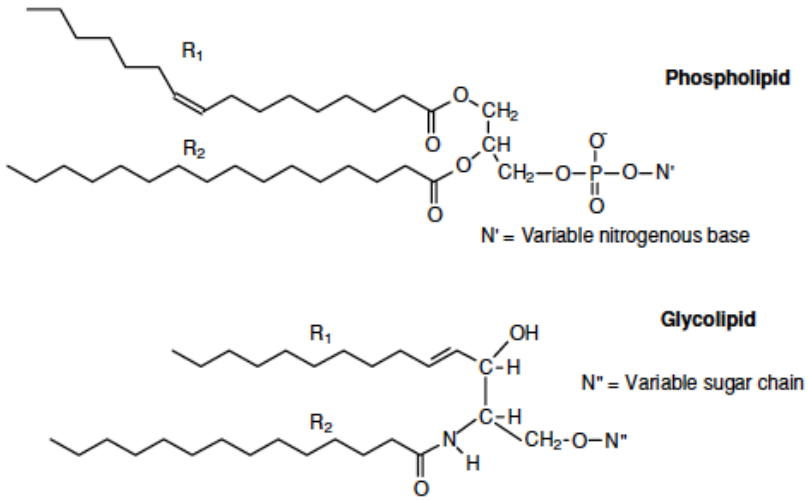

Figure 2.4. Examples of phospholipids and glycolipids which are the main constituents of eukarya and bacteria. The non-polar side chains R1, R2 originate from fatty acids that typically have 12-24 carbon atoms and may be saturated or contain one or more double bonds (taken from The Biomarker Guide, Vol. 1).

D.Ether lipids are also glycerides which are formed by fatty alcohols (n-alkanols) instead of fatty acids and therefore form ether instead of ester linkages. Cell membranes of anaerobic bacteria contain large amounts of plasmalogens, which have both ester and ether linkages. An important example of ether lipids can be found in the cell membranes of Archaea, which only contain phytanyl chains (formed from the saturated counterpart of the alcohol phytol).

2.Waxes

Waxes, such as the ones found on leaf cuticles, mainly function as protective coatings. They are mixtures of many components with high melting points, the most important being esters of fatty acids with straight-chain saturated alcohols (fatty alcohols). The fatty acids and alcohols found in these wax esters (alkyl esters) have similar chain lengths in the range of C24-C28 with a predominance of even carbon numbers. Steryl esters are another category of wax esters in which the alcohol joined to the fatty acid is a sterol. Hydrocarbons are also present in waxes, and mainly long chain n-alkanes, containing mostly odd numbers of carbon atoms in the range of C23-C35 (C27, C29, C31 being the predominant ones). Most bacteria on the other hand do not contain waxes.

3.Terpenoids

Terpenoids occur in all living organisms and are described as a class of lipids which displays great diversity of structures and functions. Their unifying theme is that they are

all constructed from C5 isoprene units, the number of which is used to classify them, but they do not necessarily contain exact multiples of five carbons. Naturally occurring terpenoids contain oxygen, found in alcohol, aldehyde, ketone and carboxylic acid groups. Many terpenoids form cyclic systems, but there are also many non-cyclic ones called **acyclic isoprenoids**.

Biosynthesis of terpenoids

Terpenoids are biosynthesized from acetate units ($C_2H_3O_2^-$) which derive from the primary metabolism of fatty acids, carbohydrates and some amino acids. The mevalonate pathway is thought to be the major route for terpenoid biosynthesis during which Acetyl-CoA is involved in the generation of the C6 mevalonate unit. The fundamental isoprenoid unit (isopentenyl pyrophosphate, IPP) is subsequently produced during decarboxylation (via phosphorylation) of the mevalonate unit in the presence of ATP. Subsequently, terpenoids are synthesized from this fundamental unit by enzymatic condensation reactions.

The most important classes of terpenoids include:

Monoterpenoids, which contain 2 isoprene units and are particularly abundant in higher plants and algae.

Sesquiterpenoids, which contain 3 isoprene units and can function as essential oils in plants or as fungal antibiotics. Mono- and dicyclic sesquiterpenoids are common in plants.

Diterpenoids, which contain 4 isoprene units and are usually di- and tricyclic compounds. Most of these diterpenoids are abundant in higher plants. Phytol is the most important acyclic diterpenoid and it forms part of the chlorophyll-a molecule. Phytanol or dihydrophytol which is the saturated analogue of phytol is present in many bacterial glyceride ether lipids.

Triterpenoids, which contain 6 isoprene units and appear to have derived from the acyclic isoprenoid squalene (C30H50). Most triterpenoids are tetracyclic or pentacyclic and the tetracyclic ones belong primarily to the class of **steroids**. On the other hand, pentacyclic C30 triterpenoids can have a six-membered E ring involving compounds (oleanoid, ursanoid, lupanoid series) which usually have a higher plant origin, or a five-membered E ring such as the **hopanoids**. Hopanoids are also called bacteriohopanoids since they are common components of bacterial cell membranes, major examples being diploptene, diplopterol, bacteriohopanetetrol and aminobacteriohopanetriol [147,148].

1.Steroids

Steroids are the tetracyclic triterpenoids formed by the enzymatic oxidation of squalene which is then followed by cyclization (Figure 2.5). This process produces either cycloartenol, the precursor of most plant steroids, or lanosterol, the precursor of animal, fungal steroids and some plant steroids. Lanosterol (C30) is then converted into cholesterol (C27), by enzymatic oxidation and carboxylation, which is the precursor of all other animal steroids. The term sterol is commonly used to denote saturated or unsaturated steroidal alcohols. More specifically, saturated alcohols are called stanols, whereas unsaturated ones stenols. Most of the cholesterol and related plant sterols is bound in cell membranes and in lipoproteins.

In eukaryotic cell membranes sterols are inserted between adjacent fatty acid chains in the phospholipid structures (Figure 2.7). The rings of these compounds are rigid, which in turn restricts the movement of the fatty-acid chains which are closest to the polar head groups. Sterols are generally absent or rare in heterotrophic bacteria and their limited occurrence can be due to ingestion rather than bacterial synthesis. The main sterols in photosynthetic organisms are referred to as phytosterols and include the higher plant stigmasterol and β-sitosterol.

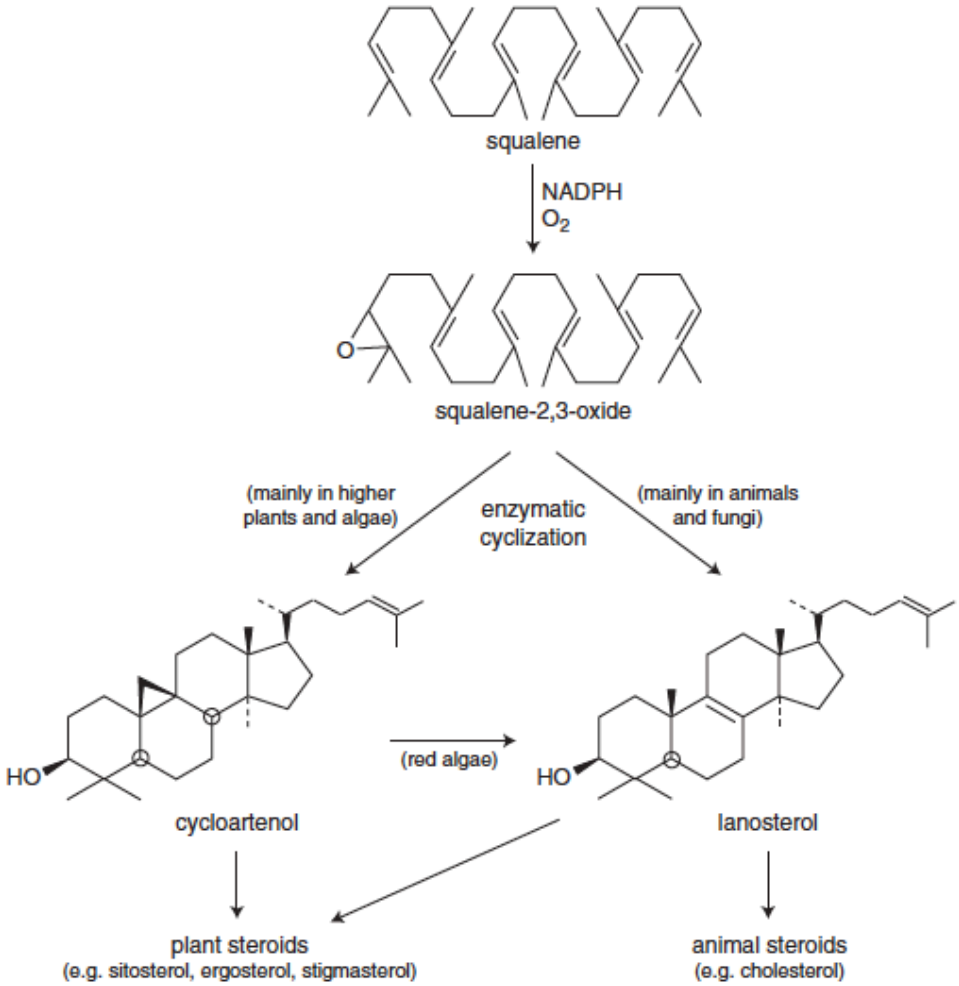

Figure 2.5. Steroid biosynthesis from squalene [149].

2.Hopanoids

Hopanoids are pentacyclic C30 triterpenoids with a five-membered E ring largely confined to bacteria [147]. They are abundant and widespread in the environment and geosphere [147,148,150] and their ubiquity is not only due to the wide range of bacteria that synthesize them [150,151] but also due to the relative stability of the hopanoid hydrocarbon skeleton. Just like sterols they are biosynthesized by the cyclization of squalene to hopene by the squalene-hopene cyclase (Figure 2.6) followed by elongation reactions [152].

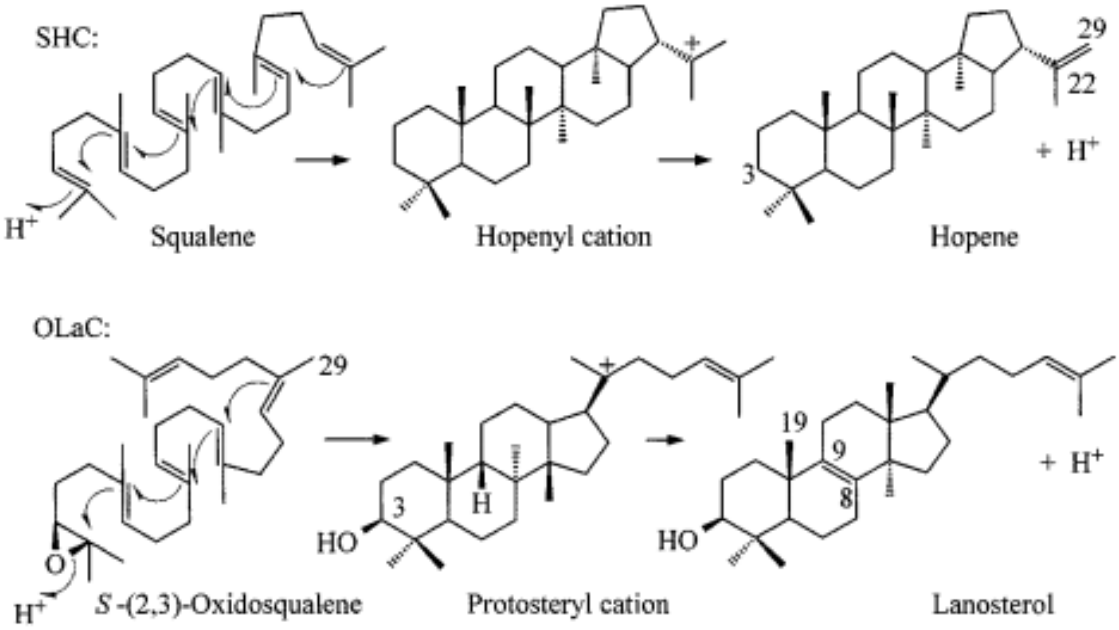

Figure 2.6. Reactions of squalene-hopene cyclase (SHC) and (S)-2,3-oxidosqualene-lanosterol cyclase (OLaC) [152].

They are produced by both Gram-positive and Gram-negative bacteria and are relatively abundant in cyanobacteria, methanotrophic bacteria and members of the α-proteobacteria, especially the nitrogen-fixing ones [152]. Structurally, they are similar to sterols [153] and their percentage in bacterial cells is similar to that of sterols in eubacterial cells at around 0.1–5 mg/g dry cell weight. Functionally, they have been described as prokaryotic sterol analogues regulating membrane fluidity and inducing order in the phospholipid matrix of membranes (Figure 2.7) [152]. Hopanoids may also be produced extracellularly as parts of barriers with selective permeability to water and oxygen [154].

So far, hopanoids have not been detected in Archaea or most eukaryotic organisms, however small amounts have been detected in some ferns, mosses and fungi [155]. Hopanoids found in plants have two characteristic structural features, (1) the absence of a side chain and (2) an oxygen group at C-3 thus indicating that they originate from oxidosqualene instead of squalene. Plant hopanoids have no known specific functions

apart from being components in waxes and resins and are therefore considered secondary metabolites [152].

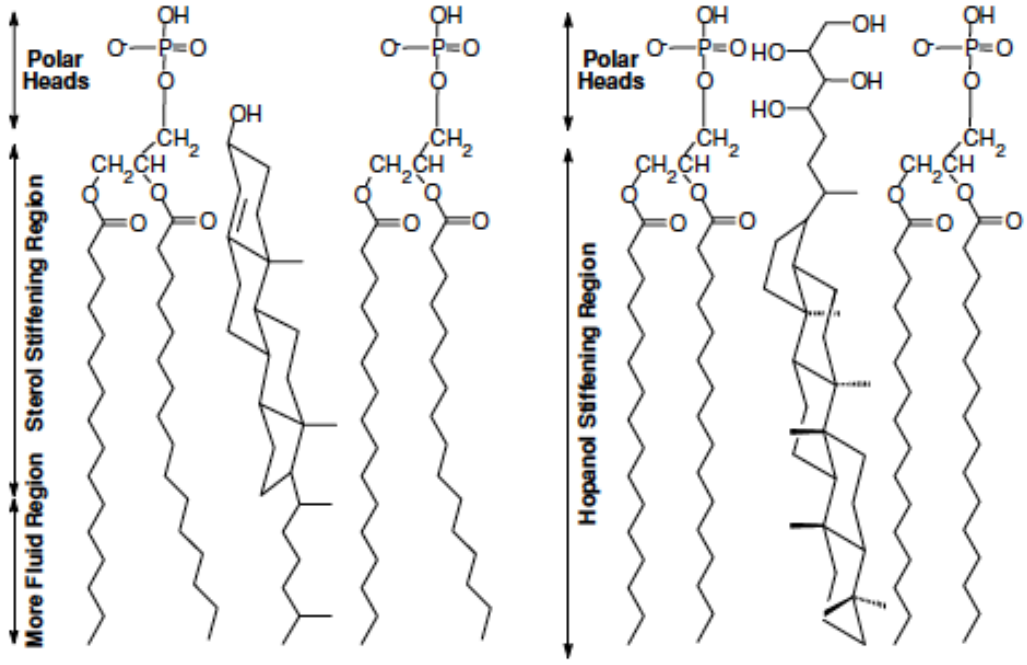

Figure 2.7. Insertion into the lipid membranes of sterols in eukarya and hopanols in bacteria in order to provide rigidity and stability (taken from The Biomarker Guide, Vol. 1).

2.3 BIOMARKERS AND DIAGENESIS

In an organic geochemistry context diagenesis is described as the microbial process affecting the products of primary production during deposition and the early stages of burial. During these diagenetic transformations, the rates at which various compound classes are degraded differ but in the end the original biological macromolecules (lipids, proteins, polysaccharides, lignin) comprise around 20% of the total organic matter.

In general, proteins degrade faster than other major organic compound classes, whereas carbohydrates are only slightly less readily degraded. Both classes though are not necessarily completely degraded since traces of them have been found in Precambrian sediments (M.H Engel). Lipids on the other hand appear to be a bit more resistant and can survive diagenesis with only minor alterations, although lipids that can be recycled (e.g. fatty acids) also do exist. The preservation of these compounds increases when they are associated with resistant structures. Lipids for example can be furtherly protected

when they are incorporated in resistant coatings, such as pollen and leaf cuticles [156]. Microbial degradation products can also be used during the formation of new macromolecular material which happens via condensation reactions. This condensed insoluble organic residue, or geopolymer, is also known as kerogen in lacustrine and marine sediments.

Lipid biomarkers, as noted previously, preserve their basic skeleton form throughout diagenesis and much of catagenesis. During diagenesis, they undergo the same types of reactions as other organic compounds, (1) defunctionalization, (2) aromatization and (3) isomerization. The diagenetic products are generally hydrocarbons (saturated or aromatic), although other groups (such as fatty acids) can also survive the process to a lesser extent. Unsaturated non-aromatic compounds can form at first (for example sterenes from stenols) but they are reactive and either become reduced (hydrogenated), therefore resulting in the formation of aliphatic hydrocarbons such as steranes and hopanes, or undergo aromatization. Finally, during diagenesis and catagenesis biomarkers can also undergo isomerization, which is the interconversion of isomers.

The major groups of diagenetic compounds which were used extensively in this study are briefly discussed below.

1.Hopanes

Hopanes are composed of three stereoisomeric series, namely 17α,21β-, 17β,21β-, and 17β,21α(H)-hopanes. Their main precursor in source rocks include hopanoids such as bacteriohopanetetrol and related bacteriohopanes (Figure 2.8) which have a biological 17β,21β(H)-stereochemistry. Bacteriohopanetetrol is an aphipathic molecule since it has both polar and non-polar ends therefore making it suitable for the lipid membrane structure [150]. This stereochemical arrangement though is thermodynamically unstable and as a result during diagenesis and catagenesis the 17β,21β(H) precursors are transformed into the 17α,21β(H)-hopanes and 17β,21α(H)-moretanes. At the same time the biological 22R configuration converts to a mixture of 22S and 22R αβ-homohopanes.

Hopanes with more than 30 carbon atoms are called homohopanes. These homohopanes have a side chain with an asymmetric center at C-22, resulting in two peaks for each homolog (22S and 22R).

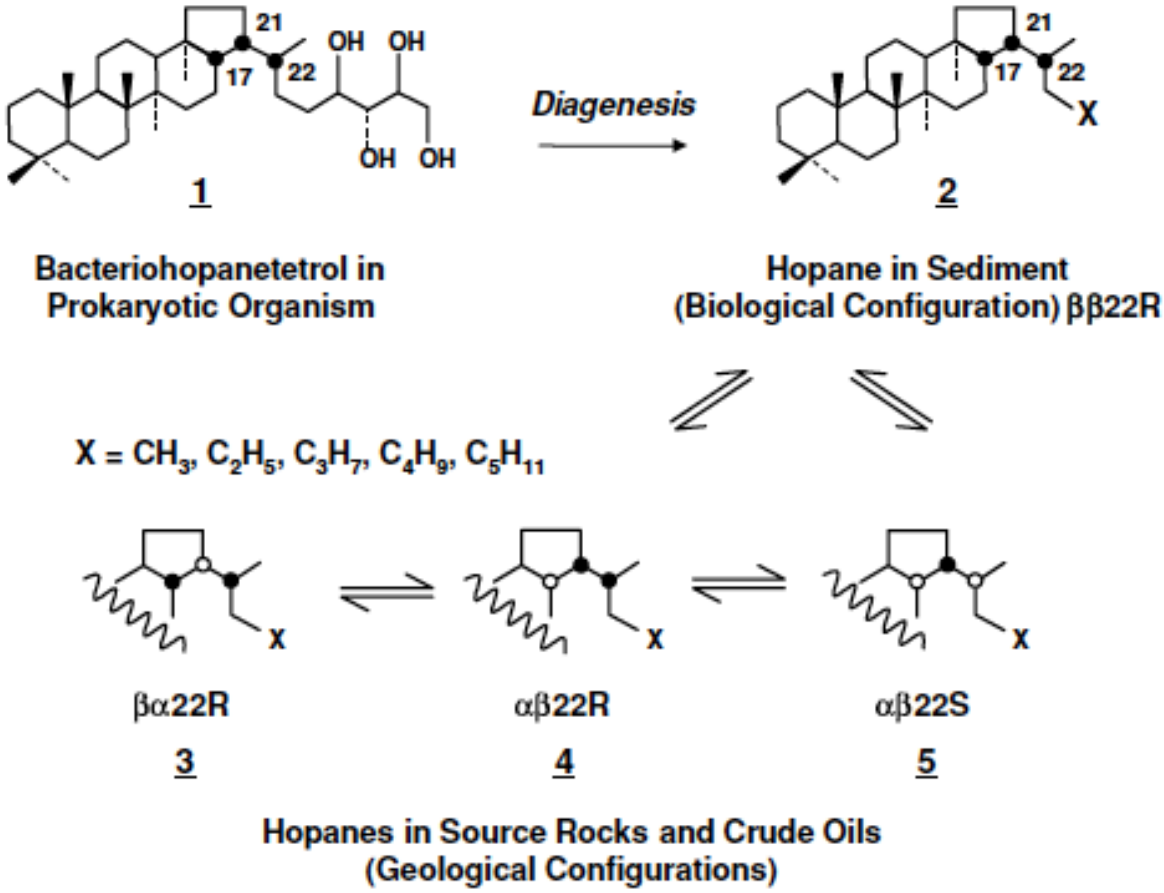

Figure 2.8. Hopanes originating from bacteriohopanetetrol which is found in the lipid membranes of prokaryotic organisms (Ourisson et al., 1984). The biological configuration [17β,21β(H)-22R] of bacteriohopanetetrol (1) and its immediate saturated product (2) is unstable during catagenesis and undergoes isomerization to geological configurations (e.g. 3, 4, 5). The 17β,21α(H)-hopanes (e.g. 3) are called moretanes, while all others are hopanes (e.g. 2, 4, 5) (taken from The Biomarker Guide, Vol. 1).

2.Steranes

Steranes are an important class of steroidal biomarkers that are formed from sterols found in eukaryotic organisms [157,158] during diagenesis and catagenesis (Figure 2.9). Just like bacteriohopanetetrol, sterols are amphipathic and present the 8β,9α,10β(CH3),13β(CH3),14α,17α(H) 20R configuration in living organisms. All sterols in living organisms appear to only show the 20R configuration but during catagenesis and thermal maturation the biologically derived 20R isomer converts to a nearly equal mixture of 20R and 20S. In addition to that, the 14α,17α(H)-stereochemistry in the sterol is lost in favor of the thermodynamically more stable 14β,17β(H) form. More specifically, the 5α,14α,17α(H) 20R configuration (ααα*R*) inherited from living organisms undergoes isomerization which results in increasing amounts of the other possible stereoisomers until the equilibrium ratio for ααα*R*, ααα*S*, αββ*R*, and αββ*S* is around 1 : 1 : 3 : 3.

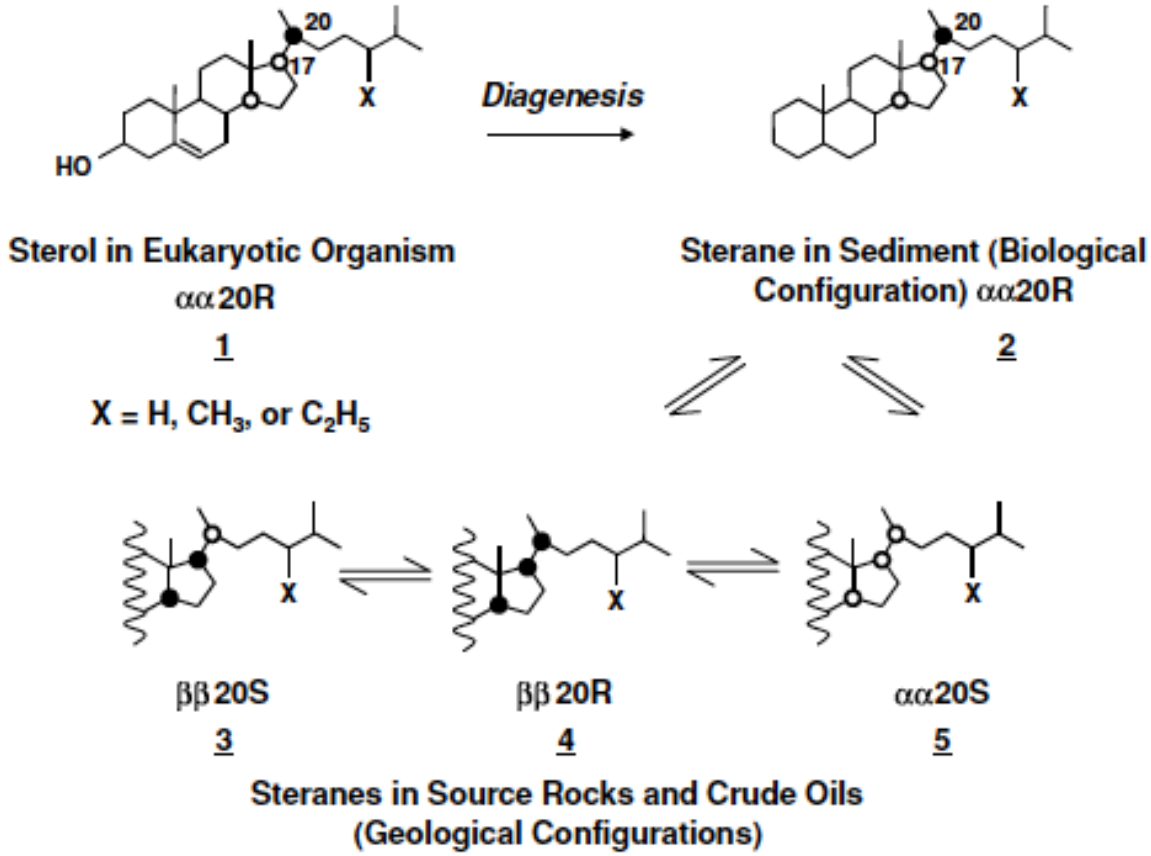

Figure 2.9. Steranes originating from sterols found in the lipid membranes of eukaryotic organisms. The biological configuration [14α,17α(H)-20R] of the sterol precursor (1) as well as in its immediate saturated product (2), is unstable doing catagenesis and undergoes isomerization to geological configurations (3,4,5) (taken from The Biomarker Guide, Vol. 1).

3.Acyclic isoprenoids pristane (C19) and phytane (C20)

The acyclic isoprenoids pristane (C19) and phytane (C20) have been assumed to be diagenetic products of the phytyl side chain of chlorophyll (Figure 2.10) even though other sources of their precursors have been suggested such as bacteriochlorophyll a and b in purple sulfur bacteria [159].

During the early stage of diagenesis, the isoprenoid alcohol, phytol, is released by hydrolysis from chlorophyll and is considered to be the starting point of many defunctionalisation reactions. In 1969, Brooks suggested that variations in the Pr/Ph ratio may reflect variations in the oxidation state during the early diagenesis of chlorophyll and therefore the ratio of these compounds has been used as a palaeonvironmental indicator.

Anoxic (or reducing) conditions promote the cleavage of the phytyl side chain to phytol which then undergoes reduction to dihydrophytol and then phytane. On the other hand, oxic conditions promote the oxidation of phytol to phytenic acid which then undergoes decarboxylation to pristine and then reduction to pristane.

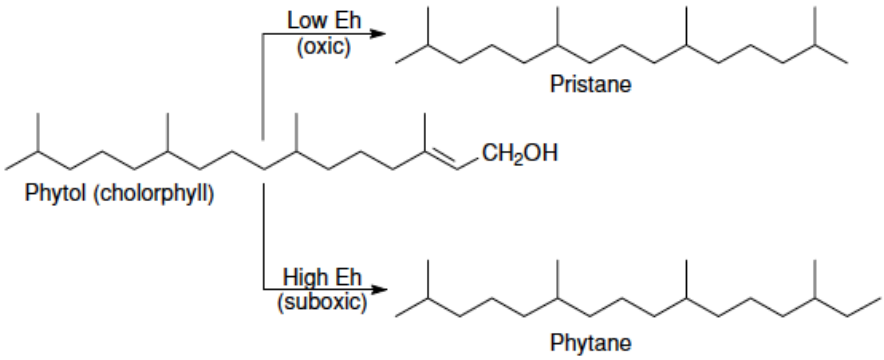

Figure 2.10. Diagenetic origin of pristane and phytane from phytol (derived from the side chain of chlorophyll a) (taken from The Biomarker Guide, Vol. 2).

2.4 LIPID BIOMARKERS IN THE STUDY OF PROKARYOTIC COMMUNITIES

As mentioned previously one of the characteristic differences between Archaea, bacteria and eukarya is the structure of their membrane lipids and therefore their study proves to be an important tool during the analysis of microbial communities and the processes related to them [160,161].

When it comes to prokaryotic communities such as the ones involved in the Anaerobic Oxidation of Methane (AOM), these lipid biomarkers can usually provide information up until the kingdom and in some cases the order of the microorganism. The first biomarker related to AOM was the irregular isoprenoid crocetane (2,6,11,15-tetramethylhexadecane) which was observed in the SMTZ of sediments in the Kattegat [162,163] in 1994. Crocetane, a C20 isoprenoid hydrocarbon, was then suggested to be a biomarker of anaerobic methanotrophic Archaea due to its strong depletion in 13C relative to the assimilated methane. Subsequent studies provided a series of other biomarkers related to AOM which are all characterized by very low δ13C values as a consequence of methane utilization.

2.3.1 Archaeal biomarkers

The membrane lipids of Archaea are unique and easily distinguished by the membrane lipids of bacteria and eukaryotes. They are composed of di- and tetra- ether lipids of glycerol as well as C20, C25 and C40 isoprenoid alcohols [164].

Several diagnostic biomarkers have been attributed to different AOM communities, and specifically to Archaea. The first strong evidence of Archaea mediating AOM was the presence of archaeol and sn-2-hydroxyarchaeol with δ13C values < -100‰, which were found in methane rich sediments from the Eel River Basin [105]. Since then subsequent studies have provided a series of archaeal biomarkers which all show very low δ13C values as a result of methane utilization. Characteristic examples of archaeal biomarkers are briefly discussed below.

1.Isoprenoidal dialkyl glycerol diethers (DGDs)

Isoprenoidal dialkyl glycerol diethers (DGDs), which are glycerol ether lipids containing phytanyl chains of C20, C25 or C40 isoprenoids, are mainly represented by archaeol (or else diphytanylglycerol) and sn-2-hydroxyarchaeol (Figure 2.11). Unlike archaeol, which has been found in a wide variety of Archaea, hydroxyarchaeols in general have only been detected in certain strains of the order Methanosarcinales, Methanopyrales, Thermoplasmatales and Sulfolobales [165–168]. An extended version of sn-2-hydroxyarchaeol, the rather uncommon C20,25 sn-2, C-7 hydroxy isoprenoid glycerol diether, has also been identified in methane-related carbonates from areas with active cold seepage within the Eastern Mediterranean, in the Gulf of Cadiz (NE Atlantic), and within the Costa Rica accretionary prism (Eastern Pacific) [169].

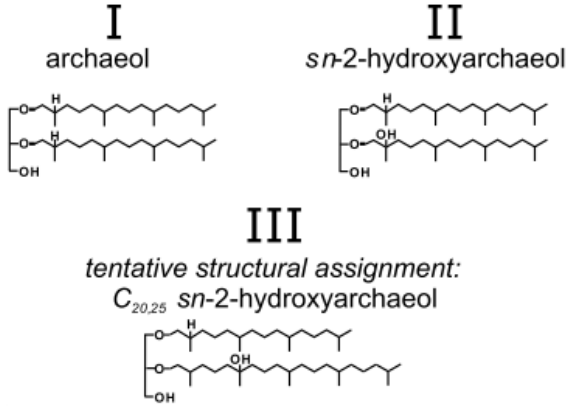

Figure 2.11. Archaeol, sn-2-hydroxyarchaeol and the extended C20,25 version [169].

2.Glycerol dialkyl glycerol tetraethers (GDGTs)

Glycerol dialkyl glycerol tetraethers (GDGTs) contain two glycerol head groups linked by ether bonds with two biphytanyl moieties which can have up to 4 cyclopentane rings (Figure 2.12). Tetraether lipids and specifically GDGTs are only known to occur in the membranes of thermophilic and methanogenic archaea and non-thermophilic Crenarchaeota [170]. These polar lipids are ubiquitous in sediments (including low maturity bitumens and oils) but aren't reported as often since they require special analysis. In the absence of this analysis, GDGT contents can be inferred from their decomposition products, the acyclic and cyclic biphytanes [171–173].

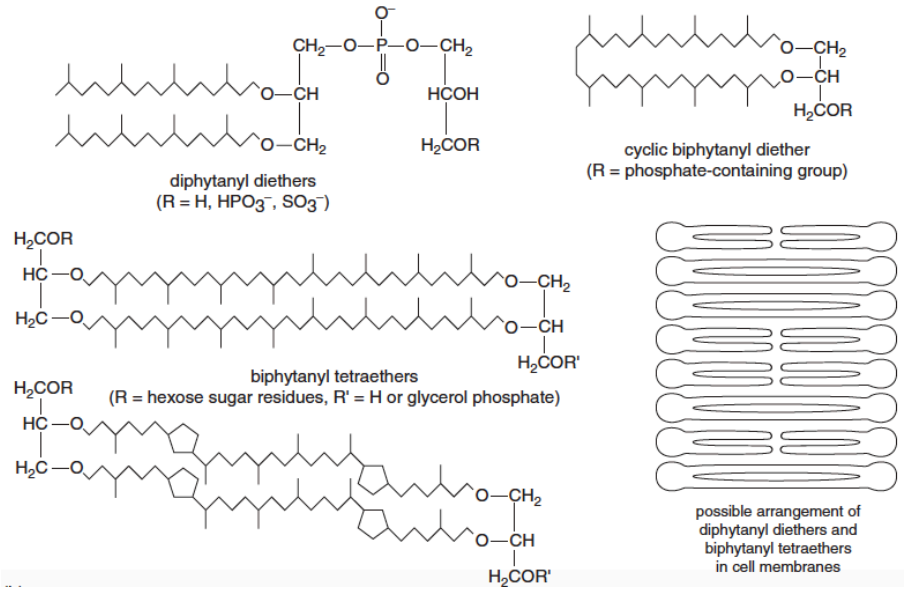

Figure 2.12. Diphytanyl diethers, biphytanyl tetraethers and their possible arrangement in cell membranes (taken from Killops and Killops, 2005).

3.Isoprenoidal hydrocarbons

As mentioned above, the first biomarker found related to AOM was the irregular isoprenoid crocetane (2,6,11,15-tetramethylhexadecane, C20H42) which was highly depleted in 13C. Crocetane is a tail-to-tail linked isoprenoid hydrocarbon diagnostic for methanogenic and methanotrophic Archaea which is diagnostic of most habitats dominated by ANME-2 consortia (Niemann, 2008). Another tail-to-tail linked isoprenoid hydrocarbon found in such environments is PMI (2,6,10,15,19 pentamethylicosane, C25H52) which is found in virtually all studied AOM settings and can be used to distinguish between the ANME communities [174].

2.3.2 Bacterial biomarkers

Bacterial compounds belonging to the sulfate reducing bacteria have also been found to present a strong depletion of ^{13}C. These ^{13}C depleted bacterial lipids are surprisingly diverse [175–177] and can be used to distinguish the possibly different eco-types of the same SRB species [174].

The most important compounds when studying the sulfate reducing AOM partners are fatty acid glycerol esters of which the fatty acid (FA) moieties are analyzed as fatty acid methyl esters (FAME). Other important compounds derived from SRBs are the non-isoprenoidal mono and dialkyl glycerol ethers (MAGEs and DAGEs) [175,176]. Even though these compounds have been associated with the sulfate reducing bacteria that mediate AOM, none of these compounds are exclusive to a particular SRB group [178]. Both of these important lipid classes are briefly discussed below.

1. Fatty acids

Free fatty acids can be distinguished into four different series which include 1) the saturated n-alkanoic acids, 2) the unsaturated n-alkenoic acids which are divided into the monounsaturated fatty acids (MUFA) and polyunsaturated fatty acids (PUFA), 3) the branched fatty acids (Br-FA), and 4) the ω-oxo-carboxylic and α,ω-dicarboxylic acids.
Sulfate reducing bacteria have been found to contain abundant iso- and anteiso-branched C15:0 fatty acids, the ratio of which can also be used to distinguish between ANME-1/ Seep-SRB1 and ANME-2 Seep-SRB1 communities [174]. The C16:1ω5 is another characteristic FA which is dominant in ANME-2/Seep-SRB1 systems [172,177]. Finally, the unusual cyC17:0ω5,6 has been found to be restricted to the ANME-2/Seep-SRB1 community [177] whereas the sulfate reducing partners associated with ANME-3 were found to have high amounts of the specific C17:1ω6 FA [93].

2. Alkyl glycerol ethers

Mono and dialkyl glycerol ethers (MAGEs and DAGEs) have been observed in many AOM environments and are considered to be SRB biomarkers due to their similarity with the co-occurring fatty acids [175,179]. MAGEs appear to be more abundant in the ANME-2/Seep-SRB1 and ANME-3 communities whereas DAGEs are more common when the prevailing community is the ANME-1/Seep-SRB1 [174].

CHAPTER 3 - STUDY AREA

The Olimpi Mud Volcano field (OMV)

3.1 INTRODUCTION

The Olimpi Mud Volcano field (OMV) is located within the Central Mediterranean Ridge (Figure 3.1) , south of Crete [180–182]. The field covers a surface area of more than 6,000 km^2 and is the largest known mud volcano field in the Mediterranean [183]. During the last two decades, it has received a lot of attention and has been investigated with side-scan sonar techniques [184], coring [40,185], and shallow drilling during ODP Leg 160 [186]. Mud volcanism in this area is generally related to buoyancy (density inversion) and is triggered by the collision of the African and Eurasia plates, forcing undercompacted clayey sediments to extrude along parts of the central and hinterlandward parts of the prism [23].

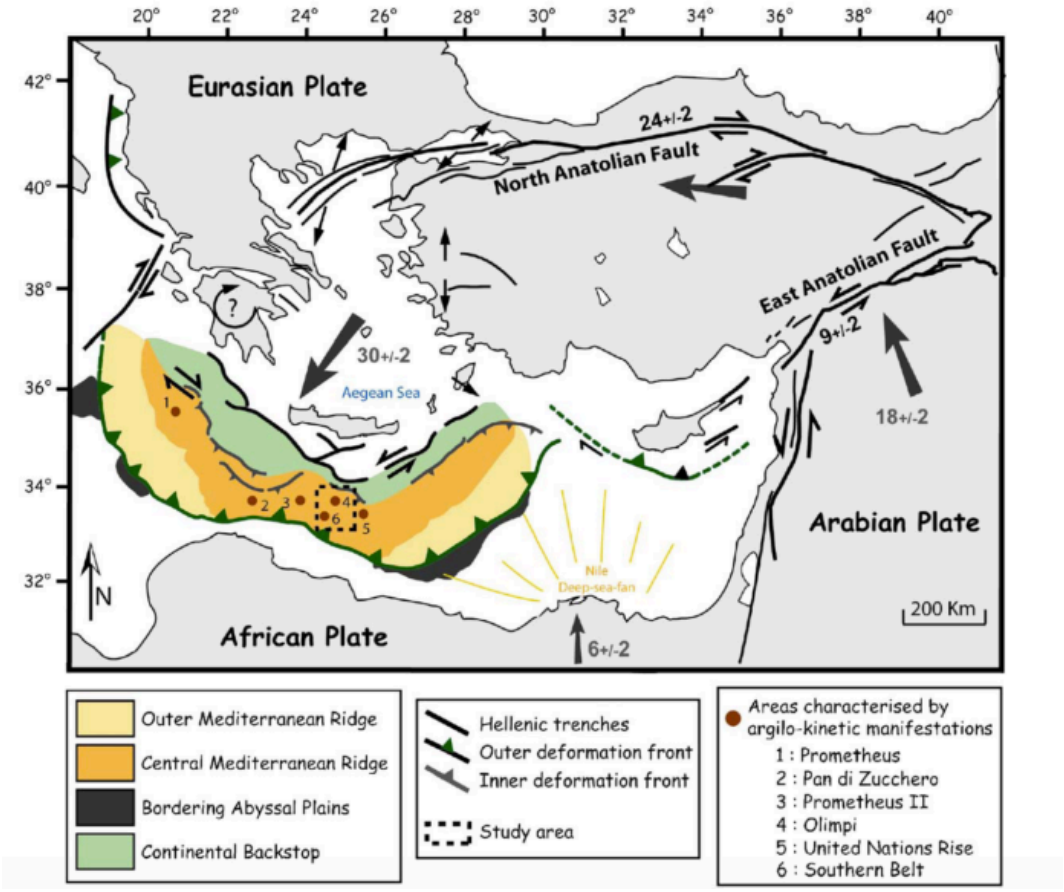

Figure 3.1. General kinematic and tectonic context in the Eastern Mediterranean, main domains identified across the Mediterranean Ridge and location of the five main mud fields known including the Olimpi Mud Volcano field [183].

3.2 TECTONIC FRAMEWORK – THE MEDITERRANEAN RIDGE (MR)

As mentioned above the Olimpi field is located in the Mediterranean Ridge. The Mediterranean Ridge accretionary complex is up to 250km wide and approximately 2000km long [187] and is situated between the converging plates of Africa and Eurasia. The Ridge extends from the Ionian deep basin to the west, to the Levantine basin to the east and is located between the Hellenic trenches to the north and various narrow remnants of abyssal plains to the south. Morphologically, there are two distinct areas forming the accretionary prism which are (1) the actual thrust wedge, and (2) the Inner-Ridge which is believed to represent the paleo Mediterranean Ridge and which presently acts as a backstop to the modern wedge [188].

Numerous geophysical surveys (which have gone as deep as 6km) have observed that the whole wedge suffers considerable deformation between Crete and Libya, with reverse and back thrust faulting in the central part and its distal portion [23]. This deformation is a result of the geometry of the converging African plate, namely the Cyrenaica Peninsula indenting the Mediterranean Ridge [23]. The prism is thrust onto the Libyan margin to the south and backthrust over the Cretan margin to the north [182].

The most prominent structural features observed in the central zone are backthrusts which have caused the formation of a topographic escarpment separating the central domain from the Inner Ridge [23].

In this central zone two separate areas (Figure 3.2) are associated with mud extrusion: (1) the first one is observed near the deformation front where small mud volcanoes form an 'outer belt' probably as a result of tectonic dewatering of the toe of the accretionary prism (volcanoes are <1km in diameter) and (2) the second forms in the 'inner belt', around 150km north of the deformation front, where a series of bigger volcanoes (up to 5km in diameter) form as a result of overpressured mud from deep within [23]. The Olimpi mud volcano field belongs to the second category [180,189] in the 'inner belt'. According to [182] it is located just where the backstop extends farther to the south suggesting that there is a regional increase of mud and fluids being forced upward as a consequence of increasing internal pressure within the Mediterranean Ridge.

Acoustic imaging also suggests that some volcanoes such as the ones delineating a north-south trend along the 24^{o}E longitude may be formed by mechanisms other than backthrusting, such as transcurrent faulting [182]. Bathymetrically, these volcanoes aren't seen as cones but as irregular and subdued hills. In acoustic imagery, they are seen as irregular patches of high but also variable backscatter [182]. The backscatter variability is

caused by the presence of various successive mud flows with the highest backscatter belonging to the latest flow [182,190].

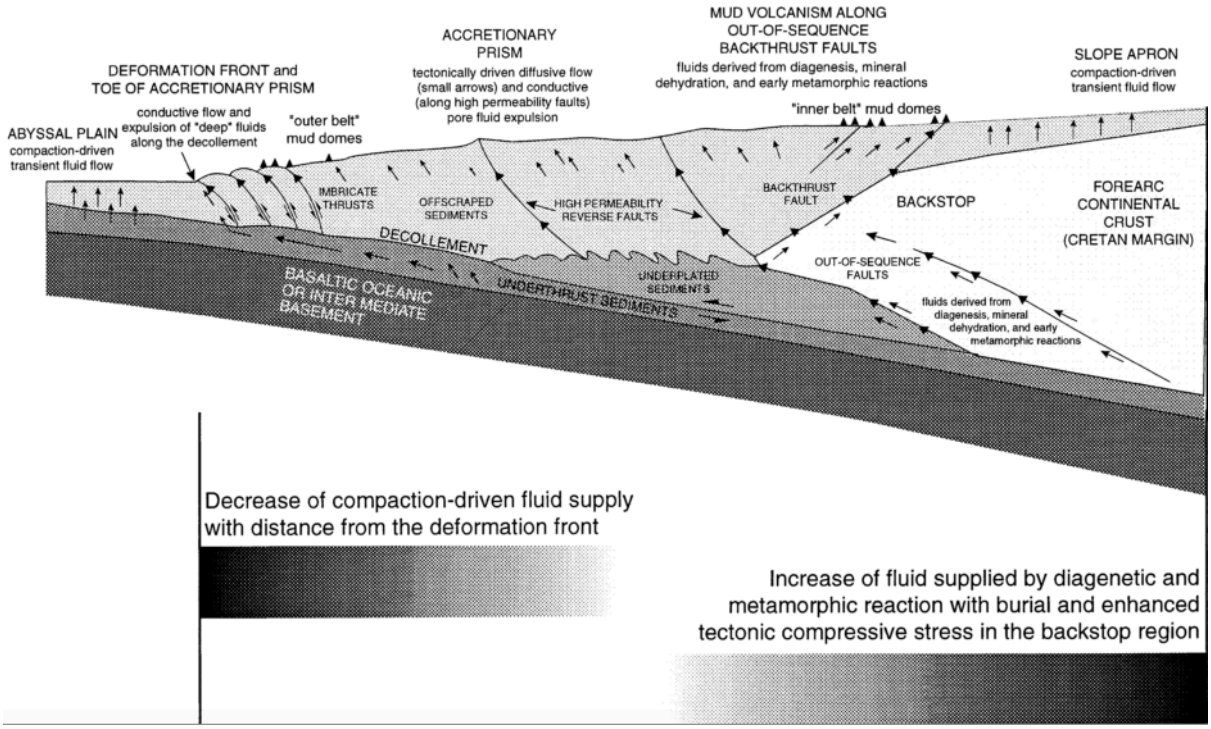

Figure 3.2. Schematic cross section of the forearc which illustrates the two main areas associated with fluid flow. On the left (outer belt volcanoes), fluid loss at the toe of the prism is predominantly due to pore water escape from lateral and vertical compaction of undercompacted sediments. On the right (inner belt volcanoes-hinterland), tectonic stress and deeper burial of accreted units lead to diagenetic reactions, mineral dehydration and metamorphic processes (modified from [191]).

According to [192] and the research performed during the Ocean Drilling Program Leg 160 in 1995 the main mechanism of mud volcanism within the accretionary prism is subduction. The dip angle of the subduction zone below the Mediterranean Ridge therefore controls the source of the mud volcano materials.[193–196] all conclude that the angle of subduction is unusually shallow i.e. $<5^{o}$. In this shallow-dip subduction model the extruded material could have derived from relatively shallow depths of 5-7km. This is in accordance with the findings of [189] which state that petrographic and clay mineralogical studies didn't reveal evidence of deep burial diagenesis or metamorphism of either the clasts or mud matrix. Furthermore, the age of the clasts is consistent with a relatively shallow, partly Miocene succession from beneath.

3.3 GEOLOGIC SETTING AND CONTROLS

3.3.1 Geological setting of the area

The underlying geology of the area plays a significant role when it comes to mud volcanic systems and their extruded materials. The Olimpi field is situated within the eastern basin of the Mediterranean Sea which is a remnant of an old Mesozoic oceanic basin bounded to the south by passive continental margins. It contains thick sedimentary piles of Mesozoic age, as well as several layers of organic rich mater. This setting favours the preservation and maturation of the organic matter therefore leading to potential reservoirs.

Messinian evaporitic series

One of the reasons the Mediterranean Ridge is characterized by such complex internal deformation [197] is the presence of an underlying thick evaporitic series. The Messinian salinity crisis resulted in the deposition of massive salt layers (sometimes over 1km thick) in the deep parts of the western and eastern Mediterranean basins. This event however did not have the same imprint on both domains. The western deep Mediterranean basin may be covered in a salt-rich layer of more than 1km thick which therefore prevents major or any fluid leekages. On the other hand, in the eastern Mediterranean (where the Olimpi mud volcano field is located) there is a discontinuous pattern of evaporitic basins which vary in thickness [39]. This lack of a continuous evaporitic series facilitates the migration of fluids and general seepage.

In terms of the evaporitic series within the Central Mediterranean Ridge the evaporites are well imaged on seismic profiles across the outer part of the Ridge [197]. To the north, the ductile evaporites where deposited in basins bordering the fore-arc (Figure 3.3). Those basins lay on stretched fragments of the Aegean continental crust. Up until now [198], most mud volcano fields have been found in the inner belt of the Mediterranean Ridge where no significantly thick evaporites have been found on seismic data [182,197,199]. Through the cross correlation of MV distributions and the main deep Messinian evaporitic basins [39] also concluded that the MV provinces in the eastern Mediterranean Sea occur where evaporites are thin or even absent. This is a well know phenomenon in the oil industry since it is thought that thick evaporate covers act as traps for deep fluids preventing leakage to the seafloor.

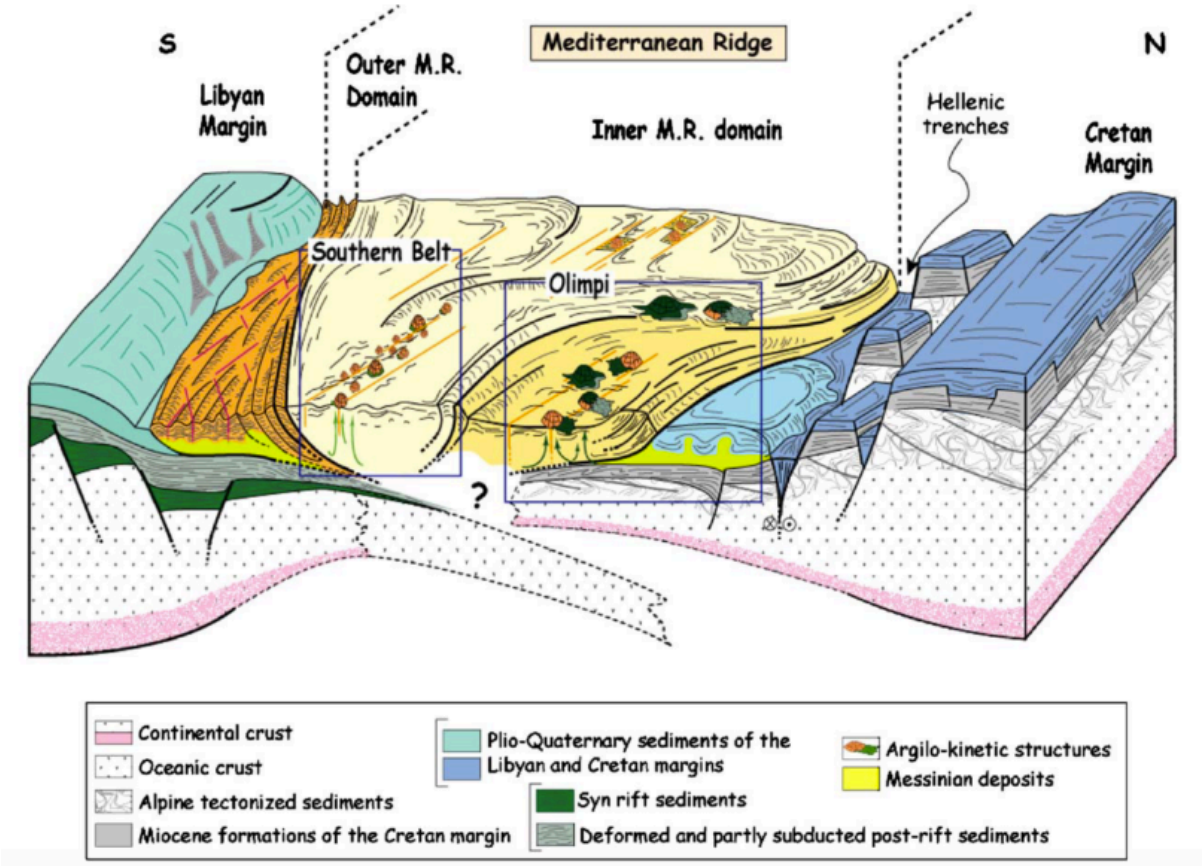

Figure 3.3. 3D tectonic sketch of the Central Mediterranean Ridge with the Olimpi and Southern Belt mud fields. The Olimpi field is related to relatively shallow mud formations with high fluid content [183].

3.3.2 Extruded material

3.3.2.1 Mud Breccia

Mud Breccia Composition

"Mud breccia" was first described by [40] as a clayey matrix containing rock fragments of variable size and composition. Basically, it is a very complex mixture of material which comes from the sedimentary successions through which the mud volcanoes erupted [13]. It contains fragments of rocks that were deposited up to millions of years ago, subsequently buried and are now situated at depths up to a few kilometers [180]. As a result, its study provides important information concerning the composition and genesis of the deep-seated formations of the Mediterranean Ridge [200].

Mud breccia consists of a (1) matrix which is usually clayey and silt-sized, (2) various coarser clasts of terrigenous and biogenic material and (3) claystone fragments that are more consolidated than the matrix [13].

3.3.2.1.1 Mud breccia clasts

Clast composition

Extensive research on the clast compositions of the Olimpi field mud breccia was performed during the TTR-3 Cruise with the R/V Gelendzhik in 1993 and the Ocean Drilling Program Leg 160 in 1995. The studies resulted in the categorization of clasts into three groups, depending on their nature. The groups consist of the (1) lithoclasts, which are fragments of different rocks, (2) crystallocasts, which are grains of minerals, and (3) bioclasts, which mainly consist of foraminifers and shell fragments [13].

Lithoclasts are usually dominated by fragments of mudstones which are tabular or bladed, relatively soft and very thinly laminated. Even though they are the largest group of rocks they don't display a wide range of textures and structures and are usually considered to be structureless. Bioturbidation may also be present in some cases. The colour of mudstones varies from grey to greyish-brown and olive. These clasts consist of smectite, illite and kaolinite in various abundances. Siltstones, another component of the lithoclast fraction, can vary in size between 2-10 cm and are grey, dark grey or brownish grey in colour. They are mostly structureless but some samples can show low-angle lamination. Quartz grains, feldspar grains, globigerina and their shell fragments as well as minor volcanic glass grains can all be part of them [200]. Fine-grained sandstones with a clayey matrix and fine-grained sandstones with a calcite cement are also a part of the lithoclast fraction. They are usually structureless, angular and form a variety of shapes with their size also ranging from 2-10cm [200]. Fragments of micritic limestones are also abundant and they appear as structureless, rounded and sometimes clay rich and organic matter rich clasts [13].

Crystalloclats can consist of polycrystalline aggregates of calcite which are usually structureless, angular and of various sizes. Calcite also appears in fragments of calcite veins which originate from carbonate rocks that got crushed during the formation of the mud breccia. Quartz grains are also prevalent and can vary in shape, size and roundness. On the other hand, plagioclase and potassium-feldspar grains are less abundant and are usually found in sizes smaller than 0.1mm. [13] also found monocrystals of calcite, rare muscovite and glauconite grains.

Bioclasts are usually represented by planktonic foraminifers or fragments of other shells usually filled by spar calcite [13].

Clast age

Based on the calcareous nannofossil assemblages [184] reported that the clasts found in all sampled mud volcanoes are of mixed Pleistocene, Pliocene, Miocene, and Late Oligocene age. Further studies [192,199,200] also mention that the clasts sampled within this area are of Middle Miocene age. There has been some evidence of Cretaceous [185] to Oligocene or Pliocene fauna but there have been concerns about those ages (especially the Cretaceous ones) since it is rather difficult to explain non-compaction of fine grained sediments from the Cretaceous [23].

3.3.2.1.2 Mud breccia matrix

Matrix composition

The mud breccia matrix consists of clay minerals with an admixture of fine, silt-sized grains of quartz, calcite and feldspar [13]. During the Leg 160 of the ODP detailed X-ray studies were performed on the matrix of the recovered mud breccia samples. The results of that study indicate that the matrix is mainly composed of smectite which is usually the predominant component, kaolinite and illite [13]. These results correspond to the ones from the study carried out in 1993 during the TTR-3 Cruise.

Matrix age

The nannofossil and foraminiferal assemblages indicated mostly Early-Middle Miocene age for the mud breccia matrix [184]. [192,200] also presume that the matrix is of a Middle Miocene age and [201] mention the inclusion of some Aptian-Albian components.

The age and depth of this matrix source level remains relatively hypothetical and there have been many proposed hypotheses such as the Aptian “argille scagliose” by [201] to Messinian formations by [186,202,203].

3.3.2.2 Fluid phase

The eruption of fluidized mud in mud volcanic systems is facilitated by the presence of overpressured fluids, the nature of which is closely related to (1) the position of the volcanic system within the Mediterranean prism (which is near the backstop for the Olimpi field) and (2) the depth of the mud source level [183].

More specifically, fluids may have multiple sources (Figure 3.4) and can (1) originate from deep-seated faults thus allowing upward migration of hydrothermal waters [204], but may also be (2) freshened waters from mineral dehydration or gas hydrate dissociation [205], (3) brines [189] or even (4) lateral meteoric water influx.

The geochemically mature fluids usually originate from (Figure 3.4) (1) hydrothermal fluids, (2) the migration of fluids along deep seated thrusts or (3) from lateral fluid fluxes through stratigraphic horizons [17]. 'Fresher' fluids on the other hand result from (1) the expulsion of pore fluid during compaction, (2) the dehydration of minerals (opal, smectite), (3) the expulsion of fluids from internal deformation within the diapiric intrusion and (4) the dissociation of gas hydrates [17].

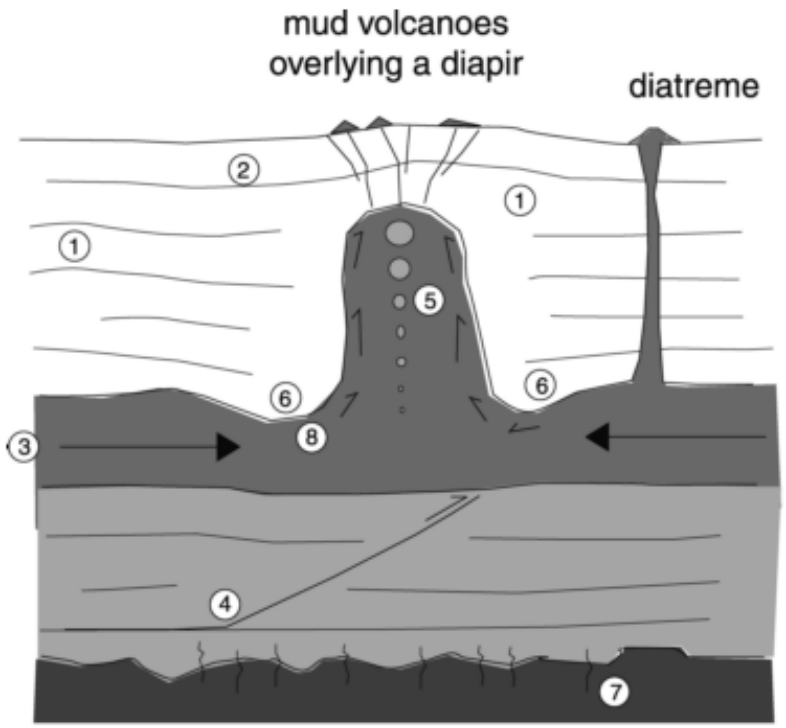

Figure 3.4. Diagram of a mud diapir, mud volcanoes as well as possible fluid sources. Geochemically mature fluids are found in categories 3,4 and 7 whereas 'freshened' fluids can be related to dissociated gas hydrates and the categories 1,6 and 8 [17].

3.3.3 Origin and formation of the mud breccia and fluids

3.3.3.1 Introduction

Mud volcanoes are considered as an important 'tectonic window' into the underlying strata since both the parent bed and some overlying rock fragments are transported to the surface [17]. Within a mud volcanic field the origin as well as the role of each component of the volcanic system can differ substantially. For example, fluid phases often originate from much deeper levels than the position of the parent bed [17] therefore, each phase should be characterized independently.

The mud breccia matrix is usually considered as the parent bed in a study area and can be related to the regional geology and to the lithologies found at depth. However, it can be extremely difficult to do so along accretionary margins such as our study area since the type of sediment that enters the subduction zone may be unknown. In order to gain information about this matrix/parent bed, various marker particles should be used as an indication of the degree of thermal maturation, diagenetic alteration or age [17]. As for the mud breccia clasts, determining their origin should involve the study of both clasts and matrix. These clasts could have either been collected during an upward migration or could also be part of the parent bed/matrix [17].

When it comes to the Olimpi field, trying to relate the mud breccia to the regional geology [40] is a difficult task since there are no matching deposits nearby. Although there were many studies and hypotheses concerning the origin and age of the mud breccia [180,185,206] sufficient understanding of the Olimpi mud volcanism only occurred after the ODP drilling at Napoli and Milano [192,207].

3.3.3.2 Depositional environments of the Mediterranean Ridge formations

The clasts in mud breccia generally represent fragments of rocks which were deposited millions of years ago and are now situated at depths of a few kilometers. Genetic features of these clasts can provide important information concerning the depositional environments of the deep-seated formations of the Mediterranean Ridge [200]. Based on the lithological data from the clasts extruded at the Olimpi field [180] concluded that they had been formed in deep-sea environments at a distance from the continental slope. Hemipelagic and biogenic sedimentation prevailed whereas terrigenous material was supplied periodically by turbidity currents from the continental shelfs.

3.3.3.3 Mud breccia origin and formation

Mud breccia is believed to originate at the depth of the sedimentary source sequence. During its formation a plastic, clayey, overpressured sedimentary series is forced upwards, mechanically assimilating fragments of rocks from the overlying deposits [200].

During the ODP sampling, the oldest clast found was of Burdigalian age (Miocene) [207] and its position within the accretionary prism could have been above underthrust Messinian muds. [199,200,208,209] have also concluded that most of the clasts or of Middle to Late Miocene age and this fact is in good agreement with the relatively low maturity of organic matter in mud breccia [188]. The Messinian age of the muds, which also form the matrix of the breccia, is shown by fauna assemblages [202] and halite microclasts [210].

There has been a lot of debate regarding the origin and mobilization depth of the mud [188] but it is accepted that it has always been part of the upper plate [23].
Various studies have shown that its source may be located at a moderate depth, within slices of Messinian evaporites or older argillaceous material [17]. With the use of the Lopatin method on clasts and matrix from the Milano MV[188] concluded that there is a shallower origin than what was previously thought by [202]. Vitrinite reflectance was low, making it unlikely that the component had experienced elevated temperature or deep burial [188]. These findings were in agreement with another theoretical study based on quasistatic modelling of the mud ascent [211]. The study estimated a mobilization depth of 1.7km which in its turn is in agreement with the 1-2km depth of burial from the maturity data [188].

3.3.3.4 Origin of fluids

At the same time the origin of fluids has also been subject of discussion since their discovery at the Mediterranean Ridge [40,185,207]. The abundance of mud volcanoes within the Ridge can support the presence of petroleum systems at depth but the truth is that there are no reliable data on the nature, ages and depths of the layers from which the fluids originate [39]. A considerable amount of the fluid expelled is probably a product of mineral dehydration reactions [23]. Specifically, smectite dehydration is the most probable reaction since smectite-rich mudstones are the dominant lithology of this part of the accretionary prism [210]. Diluted pore waters of the breccia was originally proposed by [205] to be due to gas hydrate dissociation, but the lack of a BSR and the relatively high temperatures of Mediterranean bottom waters make this hypothesis unlikely [17].

3.3.3.5 Mud mobilization

There have been several hypotheses made in order to explain the mobilization and ascend of mud through the overlying sedimentary cover. These include (1) a density inversion due to sediment undercompation below evaporite layers [188,212,213], (2) triggering of mud mobilization along major faults due to fluid circulations from overpressured deep horizons [186,188,192] and (3) tectonic stresses and overpressuring of the mobile material [2,40,180,182,186,192].

Generally described, mud volcanoes form as a response to overpressure of deep fluids such as hydrocarbons. The process of mud volcanism is driven by the fraction of fluid that rises to liquefy mud-rich units incorporating on its way up solid clasts and shallow biogenic gasses and fluids [1,4,15,214,215].

3.3.3.6 An 'extrusive' emplacement

[198] proposed a hypothesis of two different ascent processes to explain the different mud constructions of the Central Mediterranean Ridge. According to this hypothesis the Olimpi field volcanoes are characterized as an 'extrusive' emplacement and they are related to a relatively shallow and fluid-rich mud source. Both the shallow origin of the mud and its abundance in fluids have been attested by previous studies of clay mineralogy [203], maturity of the organic matter [188] and numerical modelling [211]. This shallow source is located above a southern prolongation of the Cretan thinned continental crust, below the Mediterranean Ridge [183]. Huguen's volcanic-type model had already been proposed [180,186] and partly confirmed during the drilling of the ODP Leg 160 at Napoli and Milano [188,210,216].

3.4 GENERAL DESCRIPTION OF THE OLIMPI MUD VOLCANOES

Previous to this study the Olimpi mud volcano field had been investigated successively with side-scan sonar techniques [184], coring [40,185], and shallow drilling during ODP Leg 160 [207] amongst others. The field includes a large number of dome-shaped features which are surrounded by irregular mud flows and in some instances, such as in the Napoli and Maidstone MVs, by circular depressions [183].

A short general description of the six Olimpi mud volcanoes (Figure 3.5) studied during the Leveco project is presented below.

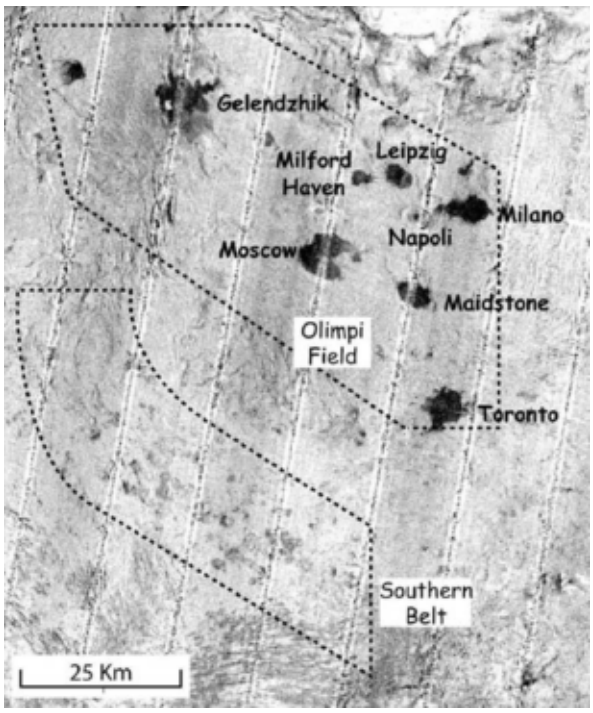

Figure 3.5. Backscatter data showing morphological characteristics of the Herodotus mud fields (Olimpi, UNR, Southern Belt) [198].

1. **Milano**. The Milano MV appears as a 50-60m high flat-topped and highly reflective structure [183] and is located along a major backthrust fault, at the boundary between the sedimentary wedge and its backstop (Rousakis et al, Leveco Report). Mud flows extend over distances of more than 6km towards the northeast and southwest. Seismic tomography performed during the Leveco cruise (Rousakis et al., Leveco Report) revealed that the summit of Milano has a "Christmas tree" like structure below the edifice, which has been created from the inter-layering of multiple mud flows with hemipelagic sediments throughout time. This geometry as well as the pie-shaped summit and extensive mud flows imply long-termed eruptive activity with the extruded material being of low viscosity and coming out from a wide central conduit. The sediment found varies from a flat hemipelagic mud to a bumpy older mud flow. The top of the dome is covered by soft sediments as well as scattered carbonate crusts and fluid seeps locally associated with white bacterial mats [183]. These observations support the fact that Milano represents an active area with active fluid seepage already found by [217] and [218]. Furthermore, large fields of dead bivalve shells and tubeworms are observed which are both occurrences related to fluid venting [219,220].
2. **Moscow.** The Moscow mud plateau is an 8km elongated ridge, trending along an N140 regional fracture [198] and appears rather "atypical" when compared to the sub-circular mud volcanoes of the Olimpi field. A narrow reflection-free strip following the northeastern base of Moscow may indicate the presence of brines, which are often characterized by a weak backscatter signature [221]. It is characterized by collapsed features and extensive mud flows, while it trends along

a regional strike-slip deformation running 140^{o} north. Moscow's proximity to fault zones provides an indication that it has experienced successive violent eruptions at the past (Rousakis et al., Leveco Report).

3. **Gelendzhik and Nice.** Gelendzhik and Nice (Figure 3.6) are considered to be complicated mud volcanoes of irregular shape, located very close to the main tectonic discontinuity-escarpment of the study area. They are more or less located along the longitude 24^{o}10E trend, which separates two regions of significantly different depths [182,199]. In both volcanoes, lateral mud flows are observed over a distance of 8-10km and the bottom reflectivity reveals backscattering strength variations which depend on the age of the flow [198].
4. **Leipzig.** Leipzig is situated around 9km north of Napoli and is associated with mud flows of a NW-SE direction. It is a typical cone-shaped dome with a sharp top and broad spreading mud breccia around the edifice. From this information, it can be inferred that violent expulsions of low porosity muddy material take place during its active phase (Rousakis et al., Leveco Report).

Two types of mud volcanoes within the Olimpi field

Data obtained from the Prismed 2 Cruise enabled the distinction of at least two main types of volcanoes within the Olimpi field. The first type (1) corresponds to subcircular or elongated positive reliefs whose diameter or lateral extent varies from about 1-6km whereas the second type (2) is mainly observed on the western border of the Olimpi field and is associated with bathymetric steps. These volcanoes are irregularly shaped with highly reflective patches. Gelendzhik and Nice are the main examples of this category [198].

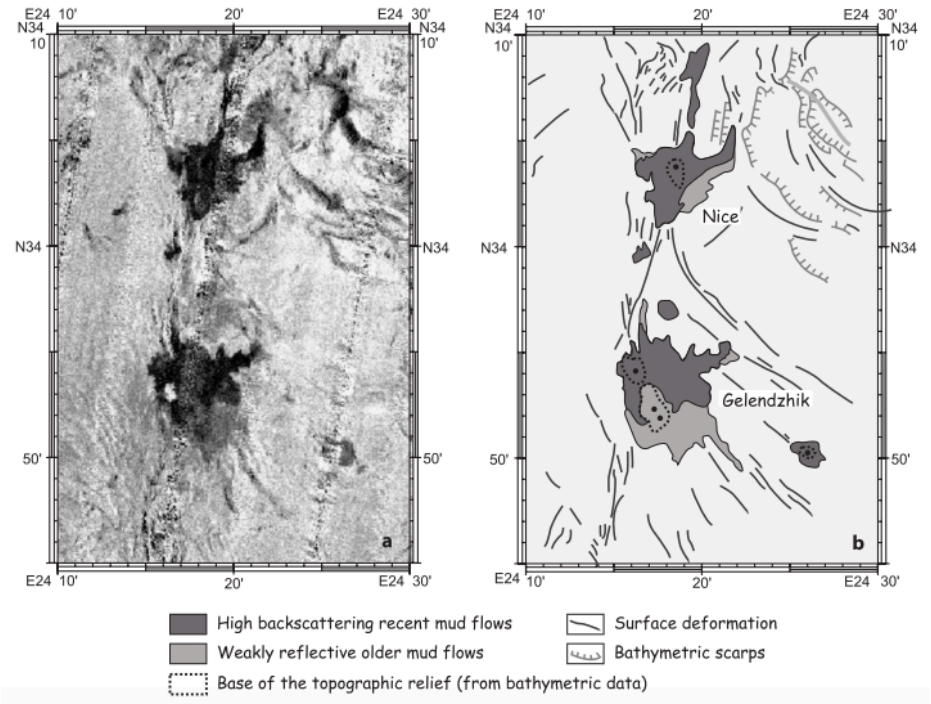

Figure 3.6. Processed (left) and interpreted (right) backscatter data of Gelendzhik and Nice MVs [198].

CHAPTER 4 - MATERIALS AND METHODS

4.1 SAMPLING PROCEDURE

During the LEVECO cruise (Leg 1, 28/03/2016-06/04/2016) aboard the R/V Aegaeo, sediment cores were collected from six mud volcanoes located in the Olimpi mud volcano field (Figure 4.1). Sediment coring was performed at various mud domes and mud breccia matrices with a benthos-type gravity corer, using core barrels (3 or 5 meters long), and a multi corer. In total, there were 8 gravity cores (Figure 4.2, Table 4.1) and 10 multi cores (Figure 4.3, Table 4.2) collected from the six volcanoes, summing up to 300 samples for the analysis of organic biomarkers.

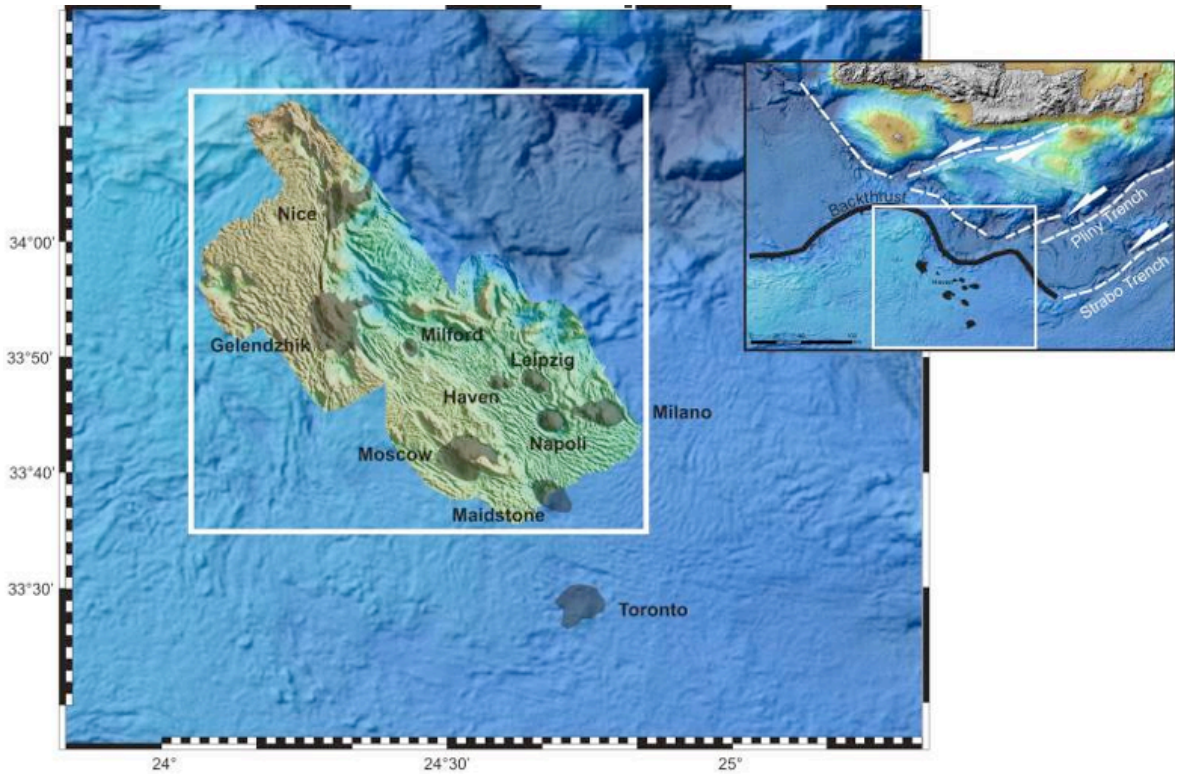

Figure 4.1. Map of the Olimpi mud volcano field and its location within the Mediterranean Ridge (taken from Rousakis et al., Leveco Report).

For the analysis of lipid biomarkers, all samples were collected on-board and immediately sectioned into 1 or 2 cm intervals. The first 10 cm of each core was sectioned into 1cm intervals whereas the rest of the core (>10cm) into 2cm. All samples were immediately stored at -20^{o}C in pre-combusted aluminium foils until further laboratory analysis.

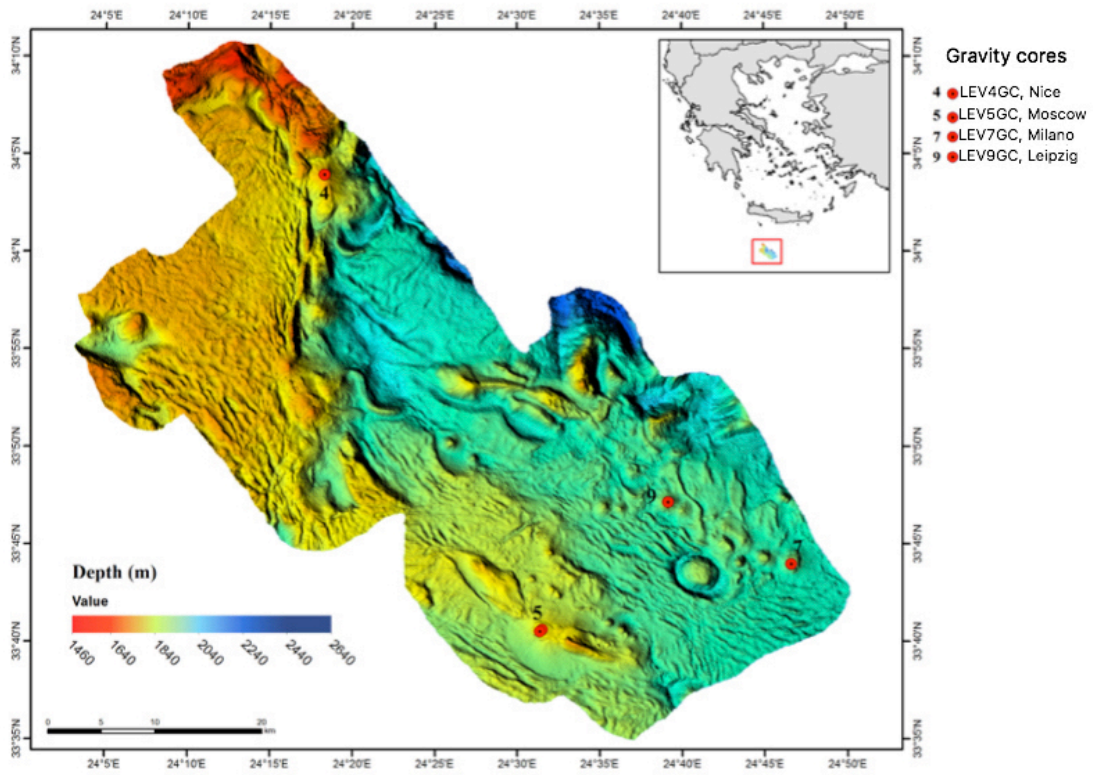

Figure 4.2. Locations of the 4 gravity cores (Nice, Moscow, Milano and Leipzig) superimposed on a bathymetric map of the Olimpi field.

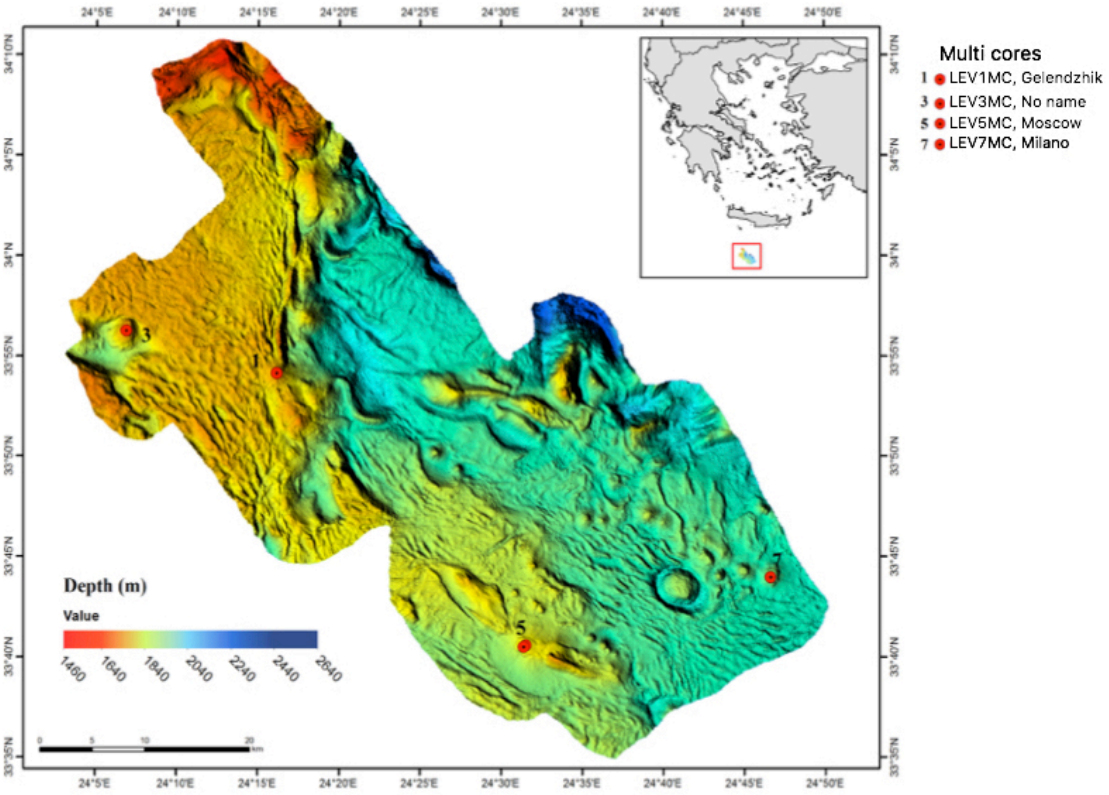

Figure 4.3. Locations of the 4 multicores (Gelendzhik, No name, Moscow and Milano) superimposed on a bathymetric map of the Olimpi field.

Table 4.1. Gravity-Cores. List of stations, coordinates and samples taken during the Leveco cruise.

Station	Location Name	Coordinates	Water Depth	Samples
LEV 1 GC	**Gelendzhik**	33º54’1600 |24º16’1338	1700 m	0-3 cm 15-17 cm 26-28 cm 42-44 cm 62-64 cm
LEV 3 GC	**No Name**	33º56’2664 |24º06’8419	1722 m	5-7 cm 12-15 cm 20-23 cm 30-32 cm 50-52 cm 62-64 cm
LEV 5 GC	**Moscow**	33º40’6297 |24º31’5253	1838 m	0-2 cm 10-12 cm 39-41 cm 100-102 cm 120-123 cm
LEV 7 GC	**Milano**	33º43’9944 |24º46’5713	1950 m	0-3 cm 40-42 cm 60-62 cm 90-92 cm
LEV 9 GC	**Leipzig**	33º47’1512 |24º39’1622	1912 m	10-12 cm 20-22 cm 40-42 cm 70-72 cm 90-92 cm 110-112 cm

Table 4.2. Multi-Cores. List of stations, coordinates and samples taken during the Leveco cruise.

Station	Location Name	Coordinates	Water Depth	Samples
LEV 1 MC	**Gelendzhik**	33º54'1606|24º16'1338	1700 m	0-1 cm
				5-6 cm
				10-12 cm
				14-16 cm
				16-18 cm
				18-20 cm
				20-22 cm
				22-24 cm
				30-32 cm
				38-39.5 cm
LEV 3 MC	**No Name**	33º56'2670|24º06'8457	1722 m	0-1 cm
				5-6 cm
				10-12 cm
				18-20 cm
				20-22 cm
				22-24 cm
				24-26 cm
				26-28 cm
				28-30 cm
				30-32 cm
LEV 5 MC	**Moscow**	33º40'6178|24º31'5417	1833 m	0-1 cm
				5-6 cm
				10-12 cm
				20-22 cm
				30-32 cm
				34-36 cm
				36-38 cm
				38-40 cm
LEV 7 MC	**Milano**	33º43'9852|24º46'6365	1950 m	0-1 cm
				5-6 cm
				10-12 cm
				20-22 cm
				24-26 cm
				26-28 cm

4.2 SAMPLE ANALYSIS

Analytical procedures

4.2.1 Elemental and stable isotopic analysis of organic carbon and nitrogen

For the determination of the organic carbon (OC) and total nitrogen (TN) content as well as the stable isotopic composition of OC ($\delta^{13}C$) and TN ($\delta^{15}N$) sediment sub-samples were oven-dried at 40°C, ground and homogenized. For the removal of inorganic carbon in the form of carbonates, 10-15mg of each sample was weighed in silver capsules and then de-carbonated with the use of HCl (25% v/v). The addition of HCl was repeated five times and between each HCl addition the samples were dried at 60°C for 1.5 hours. After the 5th and final addition the samples were left at 60°C overnight until no effervescent was observed.

Samples were sent for analysis to UC Davis in California were an elemental analyzer interfaced to a continuous flow isotope ratio mass spectrometer (IRMS) was used. More specifically, sediments were analyzed for ^{13}C and ^{15}N isotopes using an Elementar Vario EL Cube or Micro Cube elemental analyzer (Elementar Analysensysteme GmbH, Hanau, Germany) interfaced to a PDZ Europa 20-20 isotope ratio mass spectrometer (Sercon Ltd., Cheshire, UK). Samples are combusted at 1080°C in a reactor packed with copper oxide and tungsten (VI) oxide. Following combustion, oxides are removed in a reduction reactor (reduced copper at 650°C). The helium carrier then flows through a water trap (magnesium perchlorate). N_2 and CO_2 are separated using a molecular sieve adsorption trap before entering the IRMS.

A sample's preliminary isotope ratio is measured relative to reference gases analyzed with each sample. These preliminary values are finalized by correcting the values for the entire batch based on the known values of the included laboratory standards. The final delta values are expressed relative to international standards VPDB (Vienna PeeDee Belemnite) and Air for carbon and nitrogen, respectively.

4.2.2 Lipid biomarker analysis

Total organic extract

Lipid biomarkers were analysed following a modified analytical procedure of [222–224]. Briefly, 10gr of an oven-dried (at 40°C) ground and homogenized sediment was used from each sample. The total organic extract was obtained after the sediment was solvent-extracted three times by sonification with a dichloromethane: methanol mixture (4:1, v/v). After the extraction, a rotary evaporator was used in order to reduce volume to about

15ml. Finally, sulfur content was removed by the addition of activated copper and the sample was left in the fridge overnight.

Fractionation of the total extract

This total extract was subsequently separated into different compound classes by column chromatography with the use of silica gel that had been activated for 1 h at 150°C. During column chromatography compound classes are eluted in order of increasing polarity. The following (Table 4.3) solvent systems were used to elute different compound classes.

Table 4.3. Table of compound classes, their solvents used for elution and their Internal Standards.

Fraction	Solvents	Compound Classes	Internal Standard (IS)
F1	n-hexane	Aliphatic hydrocarbons	C24d50
F2	n-hexane: toluol (9:1)	PAHs	PAH + C24d50 mixture
F3	ethyl acetate: n-hexane (5:10)	alcohols, sterols, hopanols	5α-androstan-3β- ol + C21OH
F4	methanol: formic acid (24:1)	Free fatty acids	Tricosanoic acid

Silylation of alcohols

Hydroxyl-bearing compounds (such as n-Alkanols and steroidal alcohols) in fraction F3 were derivatized to the corresponding trimethylsilyl (TMS) ethers prior to GC-MS analysis with the use of N, O-bis-(trimethylsilyl)-trifluoroacetamide (BSTFA). Silylation is the most widely used derivatization procedure for GC analysis. BSTFA specifically, reacts with a range of polar organic compounds, replacing active hydrogens with a –Si(CH3)3 (trimethylsilyl) group. Generally, in silylation an active hydrogen is replaced by an alkylsilyl group, most often trimethylsilyl (TMS). Compared to their parent compounds, silyl derivatives generally are more volatile, less polar, and more thermally stable. Silyl derivatives are formed by the displacement of the active proton in –OH, –COOH, =NH, –NH2, and –SH groups.

Briefly, 100μl of BSTFA was added to the evaporated (dry) F3 fraction of each sample which was subsequently heated for 1 h at 90°C. After that the fraction was once again evaporated to dryness under a gentle nitrogen stream prior to its analysis via GC-MS.

Methylation of free fatty acids

Free fatty acids within the final fraction F4 were methylated to the corresponding fatty acid methyl esters (FAME) with the use of boron trifluoride in methanol (BF3/MeOH, 14% w/v in methanol). During methylation, a methyl group (CH3) from the methanol is transferred to the acyl chain of the fatty acid producing the fatty acid methyl ester. BF3/MeOH is one of the most popular catalysts for transesterification and is used as a rapid means of esterifying free fatty acids.

Briefly, during this procedure 100μl of BF3/MeOH and a drop of toluol were added to the evaporated (dry) F4 fraction of each sample which was subsequently heated for 45min at 90^{o}C. After that the sample was left to reach room temperature and 0.5ml of extracted (x3 with hexane) distilled water was added in order to stop the ongoing reaction. The aqueous layer was washed out with 2ml of hexane (x4) in order to extract the methyl esters. The organic extract was eluted through extracted anhydrous Na_2SO_4 in order to remove any residual water. Both pipette and the Na_2SO_4 were washed through with DCM in order to obtain any of the remaining organic extract. Finally, the extract was dried in a rotary evaporator prior to analysis via GC-MS.

GC-MS analysis and Quantification

The analysis of all fractions and qualitative/quantitative determination of lipid biomarkers was performed via gas chromatography/mass spectrometry (GC-MS) on an Agilent 7890 GC, equipped with an HP-5MS capillary column (30m×0.25mmi.d.×0.25μm phase film), coupled to an Agilent 5975C MSD. For the analysis of the PAH fraction, a selected ion monitoring (SIM) acquisition program was used, whereas for the rest of the fractions (F1, F3, F4) the MSD operated in full scan mode.

Individual lipids were identified by a combination of (1) comparing GC-retention times of authentic standards to retention times of our samples and (2) comparing mass spectral data of each peak to mass spectral data found in literature. Quantification of each peak was based on the GC-MS response and a comparison of peak areas to a known quantity of an internal standard which was added to the sample prior to the organic compound extraction. In order to test for various sources of contamination procedural blanks were processed in parallel to the samples during each step of the analytical method.

CHAPTER 5 - RESULTS AND DISCUSSION

Studied parameters

The studied parameters and therefore results of this study can be grouped into two major categories which include (1) the indigenous characteristics of the mud matrix and (2) the post-eruptional, in situ produced microbial biomarkers.

1.Indigenous characteristics of the mud matrix

The organic matter associated with the mud matrix can provide valuable information about the underlying formations of the area. More specifically, information about the eruptional events as well as the origin and depth of the ascending mud was inferred through the study of n-alkane, hopane, sterane and PAH distributions. The thermal maturity of the organic matter is another key parameter which was used to determine the potential of the source rock to generate hydrocarbons.

2. In situ produced microbial biomarkers

After the eruption of the volcanoes and the emplacement of mud breccia microbial communities begin to form due to the large flow of chemical energy. The study of biomarkers related to these microbial communities provides information concerning their distribution and composition. More specifically, studied lipids include DGDs (glycerol dialkyl diethers) such as archaeol and sn-2-hydroxyarchaeol as well as various fatty acids such as i-$C_{15:0}$, ai-$C_{15:0}$, i-$C_{17:0}$, ai-$C_{17:0}$ which are all characteristic biomarkers of anaerobic methanotrophic Archaea (ANME) and sulfate reducing bacteria (SRB) respectively. Furthermore, biogenic hopanes (29ββ, 31ββ) and hopenes (TNH, NH13, Diploptene) which are ubiquitous in most hopanoid producing bacteria were also analysed. Our aim was to evaluate the potential differences in lipid biomarker distributions at various depths throughout the cores.

Studied cores

As mentioned in chapter 4, both multi- and gravity-cores were retrieved and analysed for the purpose of this study. More specifically, four multi-cores (LEV1MC, LEV3MC, LEV5MC and LEV7MC) and five gravity-cores (LEV1GC, LEV3GV, LEV5GV, LEV7GC and LEV9GC) were used. Multi-core samples were used extensively for the analysis of biomarkers related to microbial processes whereas gravity-core samples were used in order to assess the indigenous characteristics of the mud matrix.

PART I
INDIGENOUS CHARACTERISTICS OF THE MUD BRECCIA

The extruded mud breccia (which represents the solid part of the eruptional material) from the Olimpi MV field and generally the Mediterranean Ridge is mainly composed of a mud matrix along with clasts of various sizes. After its deposition on the seafloor surface this complex material can provide information concerning palaeoenvironments, stratigraphy as well as the hydrocarbon potential of the area. For the purpose of this study the mud matrix was separated from the macroscopically visible clasts and subsequently analysed for various diagnostic biomarkers and non-biomarker parameters.

5.1 ORIGIN OF THE ORGANIC MATTER AND POSSIBLE ERUPTIONAL EVENTS

In order to determine the origin/source of the organic matter in the extruded mud breccia, focus was given to the distribution of aliphatic hydrocarbons and specifically to the n-alkanes as well as some characteristic isoprenoid hydrocarbons. Alicyclic alcohols (n-alkanols) were also analysed as well as some other characteristic compounds concerning the depositional environment, such as gammacerane and perylene. Differences in the distribution of these compounds were also used in order to assess the existence of possible eruptional events within our sediment cores which may otherwise not have been apparent from visual lithological description.

5.1.1 n-alkanes and n-alkanols

Even though n-alkanes are widely distributed amongst organisms, their distribution patterns can give us a general idea of the origin of the organic carbon (OC). Long-chain homologues, mostly in the range of nC21-nC35 with peaks at nC27, nC29 and nC31, which exhibit an odd-over-even predominance (OEP) are characteristic of higher plant waxes [141].The occurrence of these alkanes therefore signifies important terrestrial inputs to the organic content. Shorter-chain homologues of around nC15-nC20 in chain length (nC17 in particular), are mainly of algal origin [225].

The Carbon Preference Index (CPI), which is the ratio of odd to even numbered n-alkanes in the nC24-nC35 range [226], as well as the odd-to-even predominance (OEP) [227] are indexes used for maturity but can also be affected by source and biodegradation processes. Relative high CPI values (4-10) are indicative of terrestrial organic matter and low maturity whereas lower CPI values, close to 1, are typical of petroleum-derived compounds and thermal maturation.

Finally, the alicyclic alcohols, n-alkanols, can also be used along with n-alkanes in order to assess the origin of the organic matter. Even-chain C22-C32 are found in most marine sediments and can be attributed to higher plant waxes, especially when there is further support from the n-alkane distribution (long-chain alkanes with an odd-over-even predominance). Shorter chain n-alkanols from C14-C22 can be attributed to marine sources. Hydrolysis of the wax esters of zooplankton leads to saturated and unsaturated alcohols in the C14-C22 range, with a predominance of 16:0, 20:1, 22:1. It has also been suggested that the 22:0 alcohol has a specific, but unidentified, marine source [228].

Apolar compounds (Figure 5.1), which dominate the total organic extract, contain abundant n-alkanes ranging in general from nC17-nC35 in carbon chain length. In all samples, their compositional profile showed an odd-over-even carbon-number predominance in the long-chain nC23-nC25 range which also presented the highest concentrations. Short-chain n-alkanes ranging from nC17-nC22 were found in lower concentrations with only a few exceptions.

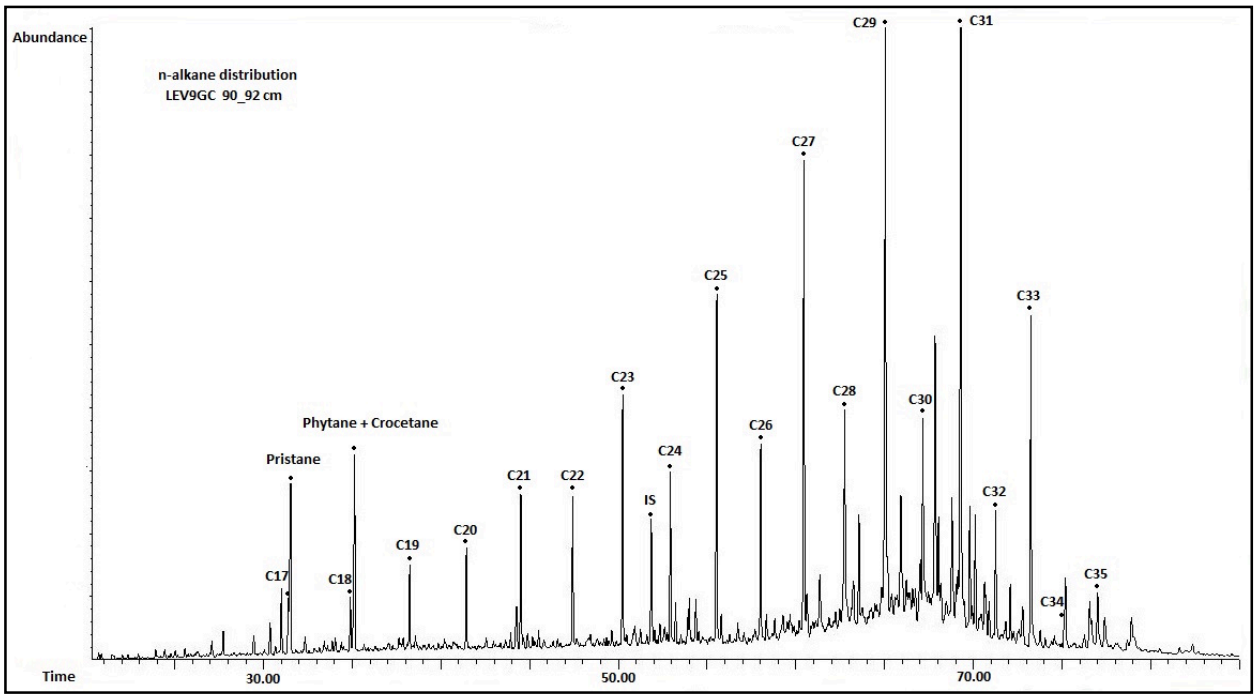

Figure 5.1. Characteristic total ion current (TIC) chromatogram of the aliphatic hydrocarbon fraction from the LEV9G 90_92 cm sample. Isoprenoid hydrocarbons (pristane and phytane) and n-alkanes are depicted.

Gelendzhik

The gravity-core taken from Gelendzhik (LEV1GC) (Figure 5.2) contains abundant long chain n-alkanes (nC23-nC35) with peaks at either nC29 or nC31 and similar distributions throughout the core. $CPI_{(22-35)}$ values are high, between 3.43 and 4.10, but relatively steady, indicating immature contributions from higher terrestrial plants. Based on sedimentological descriptions (Rousakis et al., Leveco Report, 2017) the top 3-cm-thick layer is considered to be pelagic, whereas the deepest mud phase, at around 62-72 cm b.s.f, presents oxidized horizons which are considered to be created by older mud-flows mixed with pelagic sediments. Both layers (0-3cm b.s.f and 62-72 cm b.s.f) are also visible through the slightly higher concentrations of both short (nC17-nC20) and long chain n-alkanes in comparison to the rest of the core (3-62 cm b.s.f).

The multi-core (LEV1MC) (Figure 5.3), taken from approximately the same location, also contains n-alkanes which range between nC17 and nC35 with a strong odd-over-even predominance of their long-chain homologues. Peaks are observed at nC29 or nC31, and $CPI_{(22-35)}$ values between 2.5 and 3.2 suggest relatively immature organic matter with terrestrial higher plant contributions. N-alkanols range between nC14-OH and nC32-OH with an even-over–odd predominance. The surficial sediment (0-1cm b.s.f) has an abundance of the short-chain marine nC16-OH whereas the longer-chain higher plant homologues are in small concentrations. The rest of the core shows an increase in the terrestrial input and a decrease in the marine signal. The top part of the core, from about 0-15 cm b.s.f, displays a slightly different compositional profile. It presents much higher concentrations of the acyclic isoprenoids pristane (C19) and phytane (C20), as well as the short-chain homologues (nC17-nC20) which peak at nC17 suggesting algal inputs. The rest of the core from about 15-40 cm b.s.f seems to differ since it presents lower concentrations of both short and long-chain n-alkanes as well as slightly higher $CPI_{(22-35)}$ values. These differences could either be attributed to two different mud phases/eruptional events within the core or to post-eruptional anaerobic microbial biodegradation processes.

No Name

Gravity-core LEV3GC (Figure 5.4), taken from a previously undocumented location, presents many variations of its n-alkane compositional profile. Once again the range is between nC17 and nC35 with the long-chain nC27, nC29, nC31 being the most abundant and $CPI_{(22-35)}$ values between 2.04 and 3.42. Short-chain homologues (nC17-nC20) and the isoprenoids pristane (C19) and phytane (C20) are present throughout the core with various abundances. Based on the distributions and abundances of these compounds there seem to be indications of various mud phases/eruptional events within the core.

The top layer at around 0-10 cm b.s.f is characterized by high terrestrial inputs (nC27, nC29, nC31) which also reflect on the $CPI_{(22-35)}$ values (over 3). From 10 cm b.s.f until about 25-30 cm b.s.f the concentrations of all n-alkanes (as well as the $CPI_{(22-35)}$ values) decrease significantly except for phytane which shows a slight increase, indicating the possible presence of a different mud phase. At around 30-50 cm b.s.f there appears to be another mud phase characterized by an increase in all compounds which intensifies at around 50 cm b.s.f. At this point terrestrial inputs nC27, nC29, nC31 increase from ~ 200-600 ng/g dw to ~ 1000-1500 ng/g dw and their distribution also shows differences, with a clear peak at nC29 instead of nC31, indicating another difference concerning the mud flow. From about 50 cm b.s.f until the end of the core $CPI_{(22-35)}$ values keep increasing. One of the main characteristics of this core seems to be the high concentrations of phytane and to a lesser extent pristane throughout the core. Sedimentological description (Rousakis et al., Leveco Report, 2017) also reveals the presence of multiple mud phases (visible in Figure 5.4) which correlate approximately to the ones presented from the biomarker distributions.

On the other hand, the multi-core (LEV3MC) (Figure 5.5) taken from the same mud volcano doesn't seem to be as complicated. The first few centimeters, from 0-10 cm b.s.f approximately, contain long-chain n-alkanes (nC27, nC29, nC31) in considerable amounts indicating the terrestrial character of the organic matter. The rest of the core, from 10-32 cm b.s.f, presents higher concentrations of the short-chain alkanes (nC17-nC20) along with pristane and phytane. $CPI_{(22-35)}$ values range between 2.61 and 3.49 throughout the core remaining relatively stable. N-alkanols range between nC14-OH and nC32-OH in the first ~ 10 cm b.s.f whereas the rest of the core shows a strong decrease in the long-chain terrestrial homologues. A marine signal (nC16-OH) is present throughout all the core with varying abundances. The difference between the first ~ 10 cm and the rest of the core could either be attributed to two different mud phases or could be due to microbial biodegradation of the short-chain alkanes in the uppermost layer.

Moscow

Moving on to the gravity-core taken from Moscow (LEV5GC) (Figure 5.6), n-alkanes range between nC17 and nC40 showing an odd-over-even predominance of the long-chain homologues nC27, nC29, nC31, nC33 and peaks at nC31. $CPI_{(22-35)}$ values remain relatively steady throughout the core between 2.18 and 3.16 once again indicating mixed sources of organic matter. Sedimentological analysis (Rousakis et al., Leveco Report, 2017) reveals an upper 1-cm-thick pelagic layer followed by four mud phases. Based on the compositional profiles of n-alkanes the core could be divided into three layers. Approximately, the top 0-15 cm b.s.f layer appears to be separate containing abundant

long-chain homologues from nC23-nC40. It is then followed by a second unit which shows a decrease in all compounds including an absence of the long-chain nC36-nC40, which extends from about 15-102 cm b.s.f. Finally, the last part of the core could also be considered a separate phase since it shows a slight increase in the short (nC17-nC20) and long-chain (nC36-nC40) homologues.

The multi-core (LEV5MC) (Figure 5.7) taken from the same mud volcano presents a compositional profile which is relatively steady throughout the whole core, with high $CPI_{(22\text{-}35)}$ values between 3.01 and 3.84. The concentrations of long-chain n-alkanes are much higher in comparison to all other cores with the terrestrial nC27, nC29 and nC31 reaching up to 5000-30000 ng/g dw, whereas the short-chain (nC17-nC20) homologues are absent. The first (0-1) cm b.s.f presents the highest $CPI_{(22\text{-}35)}$ value at 3.84 and a predominance of the odd-over-even long-chain homologues, indicating the possibility of pelagic sedimentation. N-alkanols range between nC16-OH and nC32-OH without major differences in their compositional profile and abundances. From 1-35 cm b.s.f there seems to be a separate mud phase with lower $CPI_{(22\text{-}35)}$ values and similar characteristics throughout its length. Finally, at around 35 cm b.s.f until the end of the core, a third unit appears which is characterized by a severe increase in terrestrial inputs (up to 30000 ng/g dw) and a slight increase in $CPI_{(22\text{-}35)}$ values.

Milano

The gravity-core from Milano (LEV7GC) (Figure 5.8) does not show many compositional variations. Once again n-alkanes range from nC17-nC35 with a predominance of the long-chain terrestrially derived homologues and $CPI_{(22\text{-}35)}$ values are between 2.87 and 3.62. Short-chain (nC17-nC20) algal inputs and the isoprenoids pristane and phytane exist but in much lower concentrations. Sedimentological description (Rousakis et al., Leveco Report, 2017) separates this core into five phases but these don't seem to reflect on the molecular composition which only shows minor differences in concentrations. $CPI_{(22\text{-}35)}$ values on the other hand show increasing values from around 50 cm b.s.f until the end of the core.

The multi-core (LEV7MC) (Figure 5.9) taken from Milano is the core that shows the strongest characteristics of immature terrigenous inputs. Short-chain algal influences are negligible whereas long-chain homologues show a strong odd-over-even predominance which reflects in high $CPI_{(22\text{-}35)}$ values of 4.01-4.58. N-alkanols range between nC14-OH and nC34-OH with minor inputs of the marine homologues. Longer-chain terrestrial inputs have a relatively steady profile throughout the core. There are no prominent separate mud phases within this core which could be due to its short length (26 cm).

Leipzig

Finally, the gravity-core from Leipzig (LEV9GC) (Figure 5.10) contains abundant long-chain (nC27, nC29, nC31, nC33) n-alkanes as well as pristane and phytane. $CPI_{(22\text{-}35)}$ values are lower than in other cores ranging between 2.28 and 2.75 indicating a more mixed source of organic matter. Sedimentological descriptions (Rousakis et al., Leveco Report, 2017) recognize four mud phases and a lack of modern pelagic sedimentation. Differences in compositional profiles of n-alkanes and isoprenoids could perhaps suggest three different mud phases. The first unit from ~ 0-22 cm b.s.f, characterized by abundant pristane, phytane and long-chain n-alkanes, is followed by a second phase which shows a decrease in all compounds and especially the isoprenoids. Finally, the rest of the core which represents a third mud phase appears to be relatively homogenous.

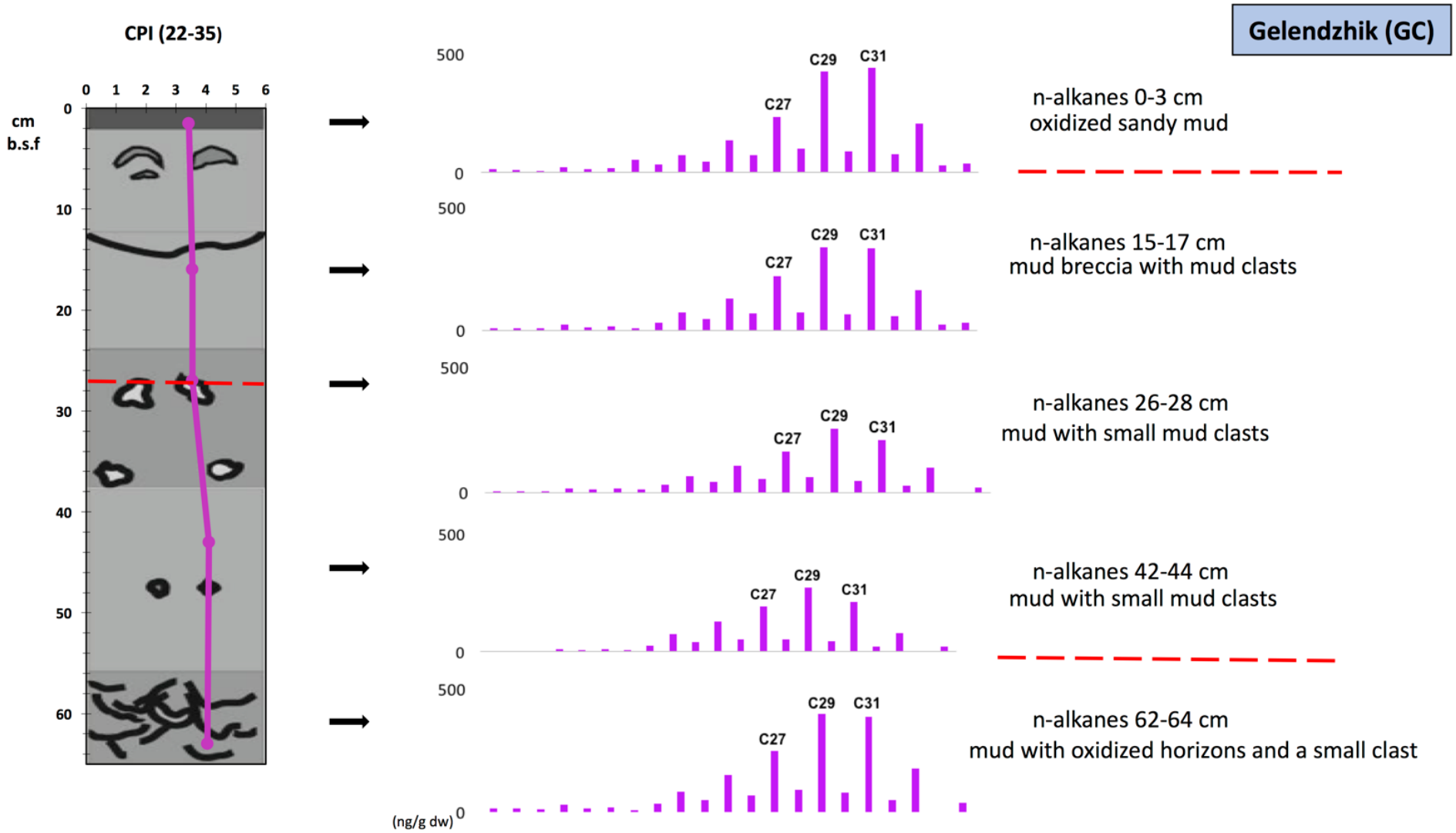

Figure 5.2. CPI, n-alkane distribution and brief description of each sample from Gelendzhik GC (LEV1CGC). Red lines represent possibly different mudflow events (sedimentological description of core was taken from Rousakis et al., Leveco Report, 2017).

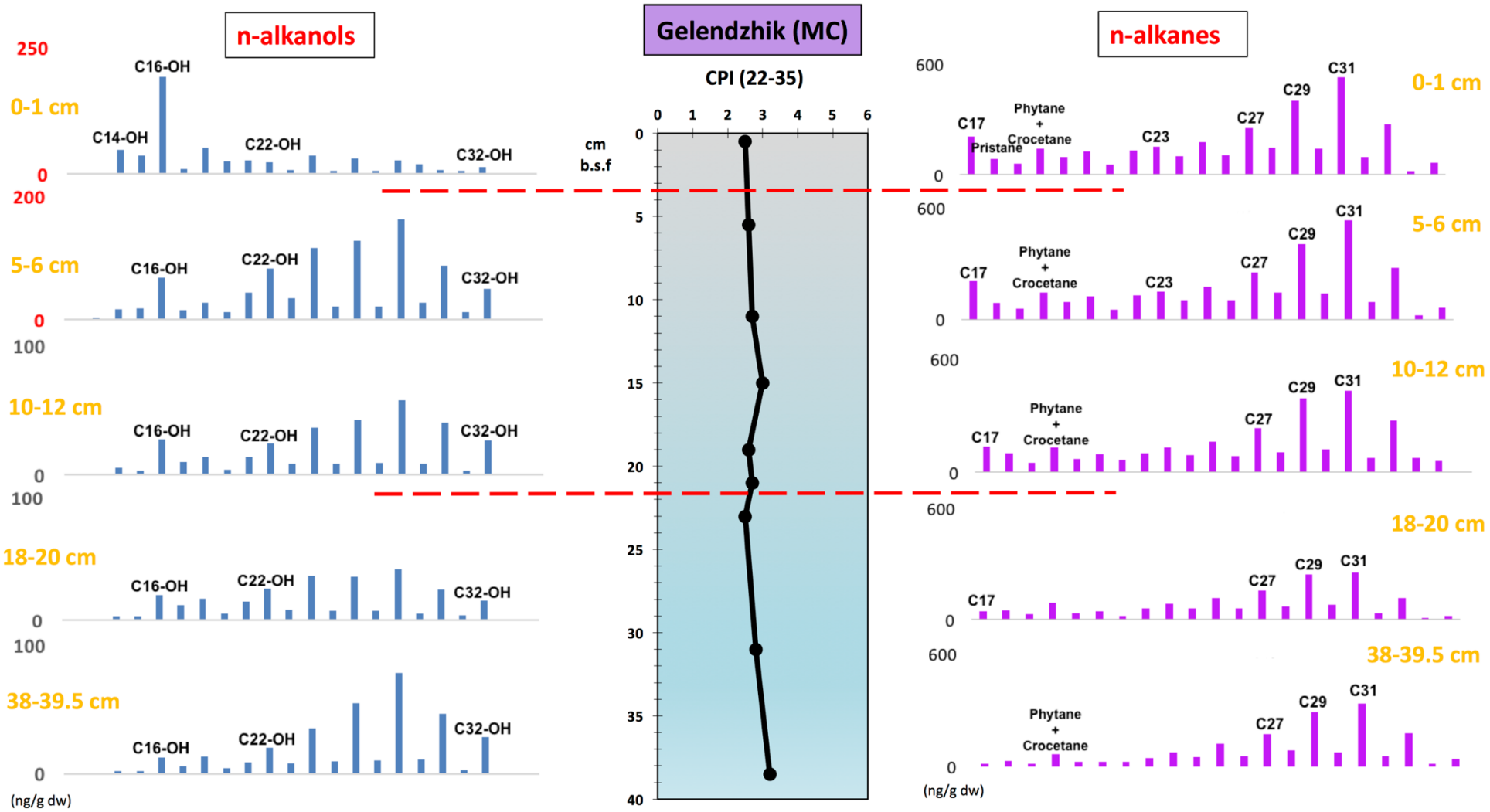

Figure 5.3. CPI, n-alkane and n-alkanol distribution of Gelendzhik MC (LEV1CMC). Red lines represent possibly different mudflow events.

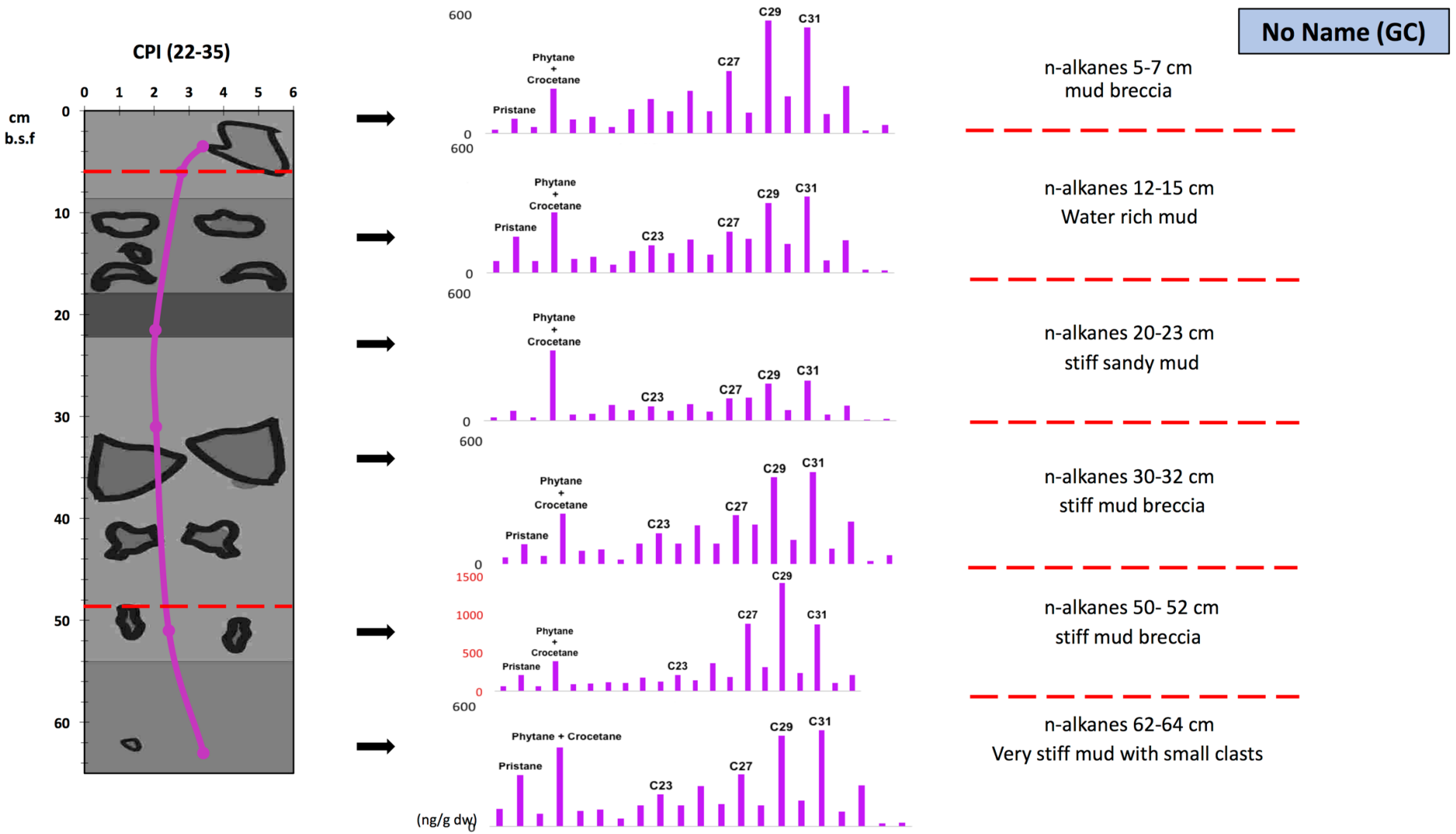

Figure 5.4. CPI, n-alkane distribution and brief description of each sample from No Name GC (LEV3GC). Red lines represent possibly different mudflow events (sedimentological description of core was taken from Rousakis et al., Leveco Report, 2017).

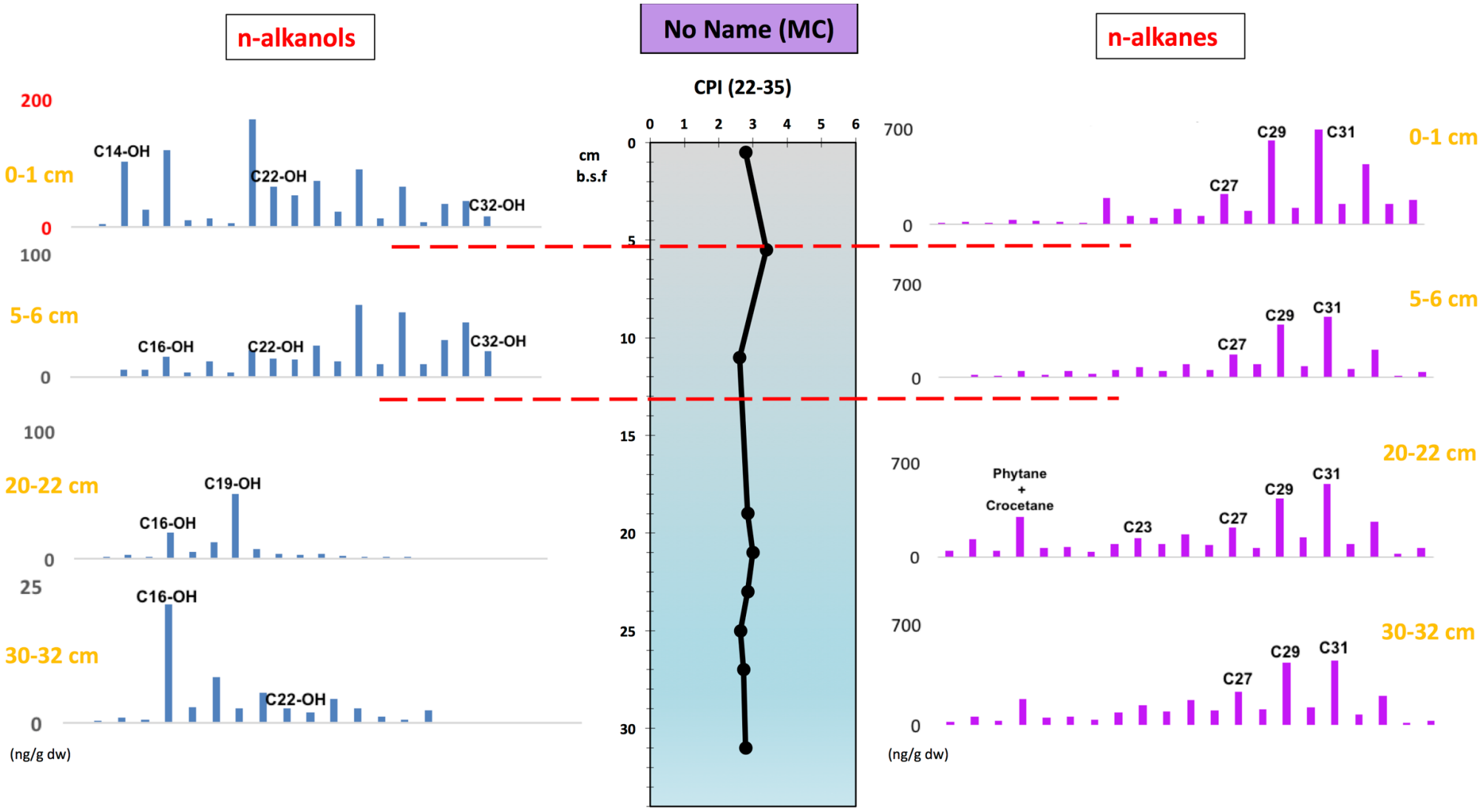

Figure 5.5. CPI, n-alkane and n-alkanol distribution of No Name MC (LEV3MC). Red lines represent possibly different mudflow events.

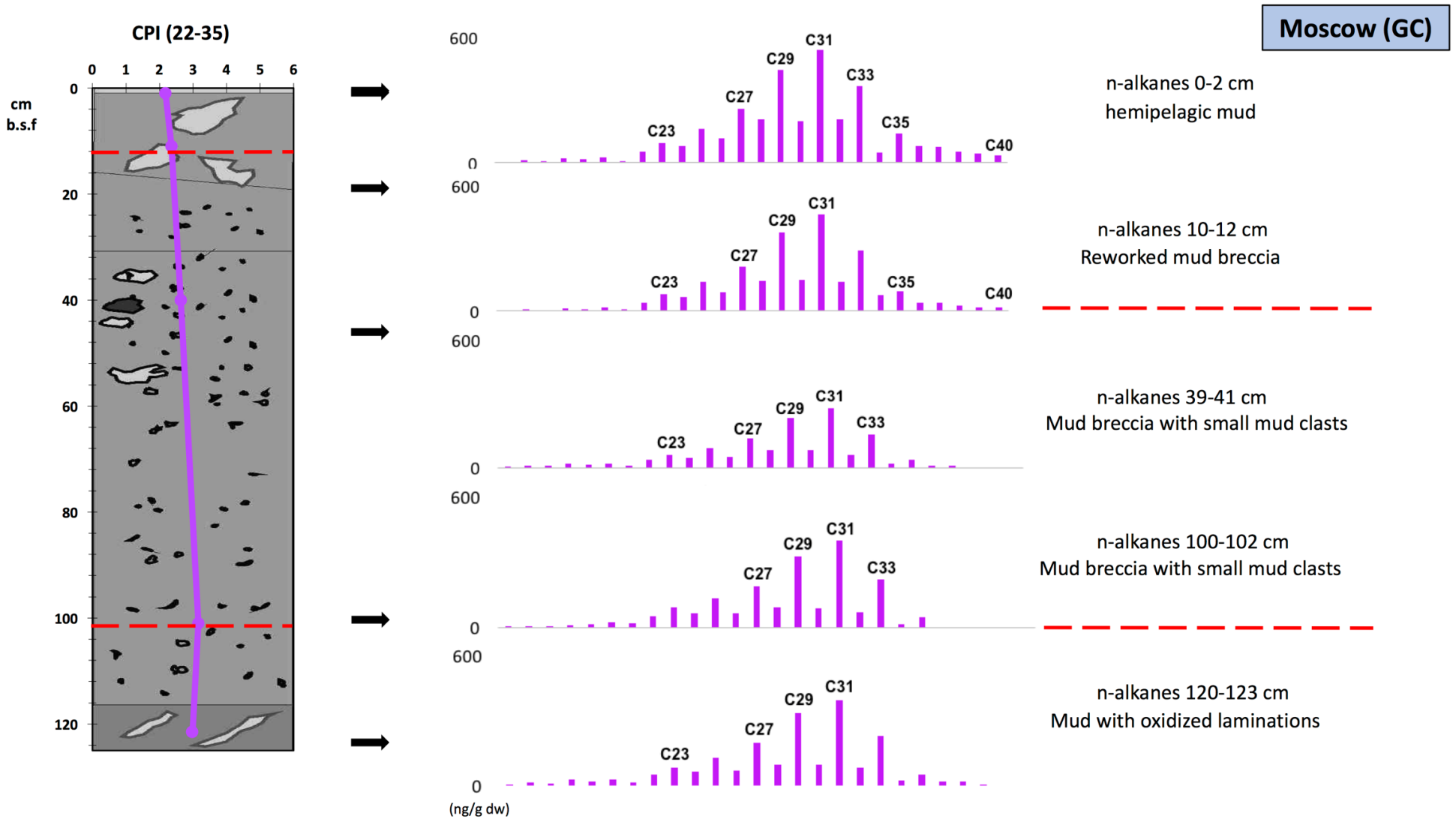

Figure 5.6. CPI, n-alkane distribution and brief description of each sample from Moscow GC (LEV5GC). Red lines represent possibly different mudflow events (sedimentological description of core was taken from Rousakis et al., Leveco Report, 2017).

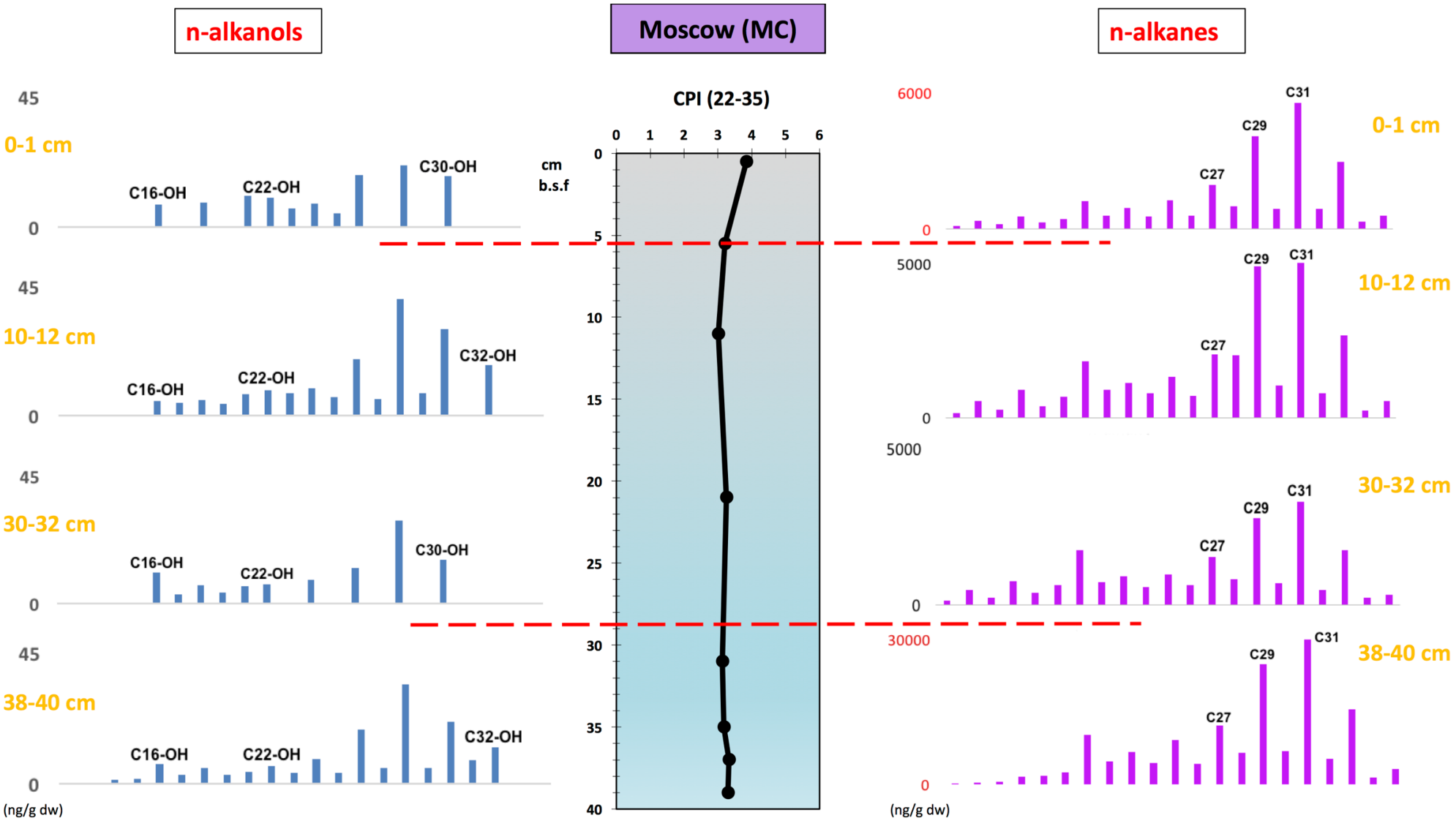

Figure 5.7. CPI, n-alkane and n-alkanol distribution of Moscow MC (LEV5MC). Red lines represent possibly different mudflow events.

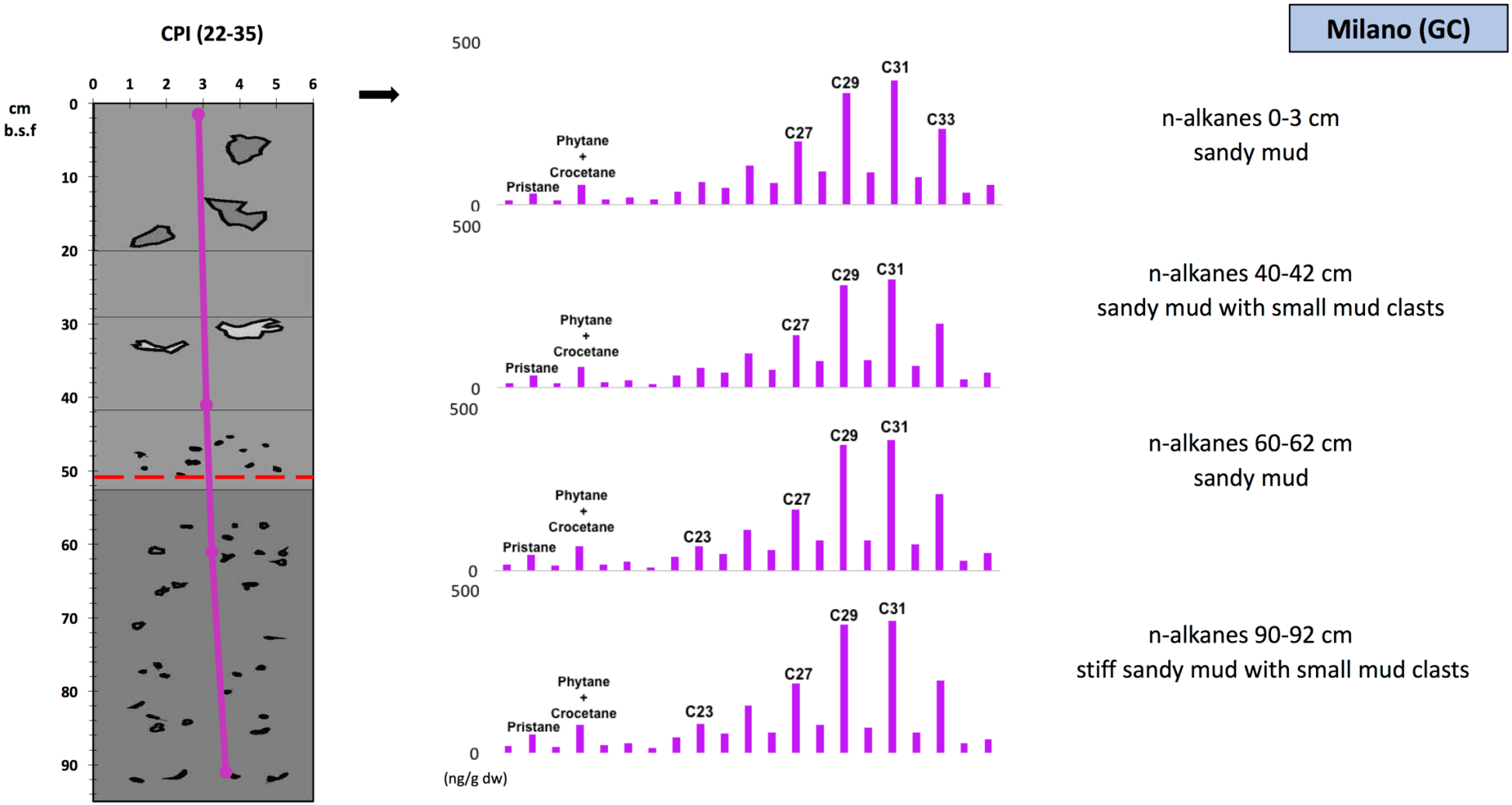

Figure 5.8. CPI, n-alkane distribution and brief description of each sample from Milano GC (LEV7GC). Red lines represent possibly different mudflow events (sedimentological description of core was taken from Rousakis et al., Leveco Report, 2017).

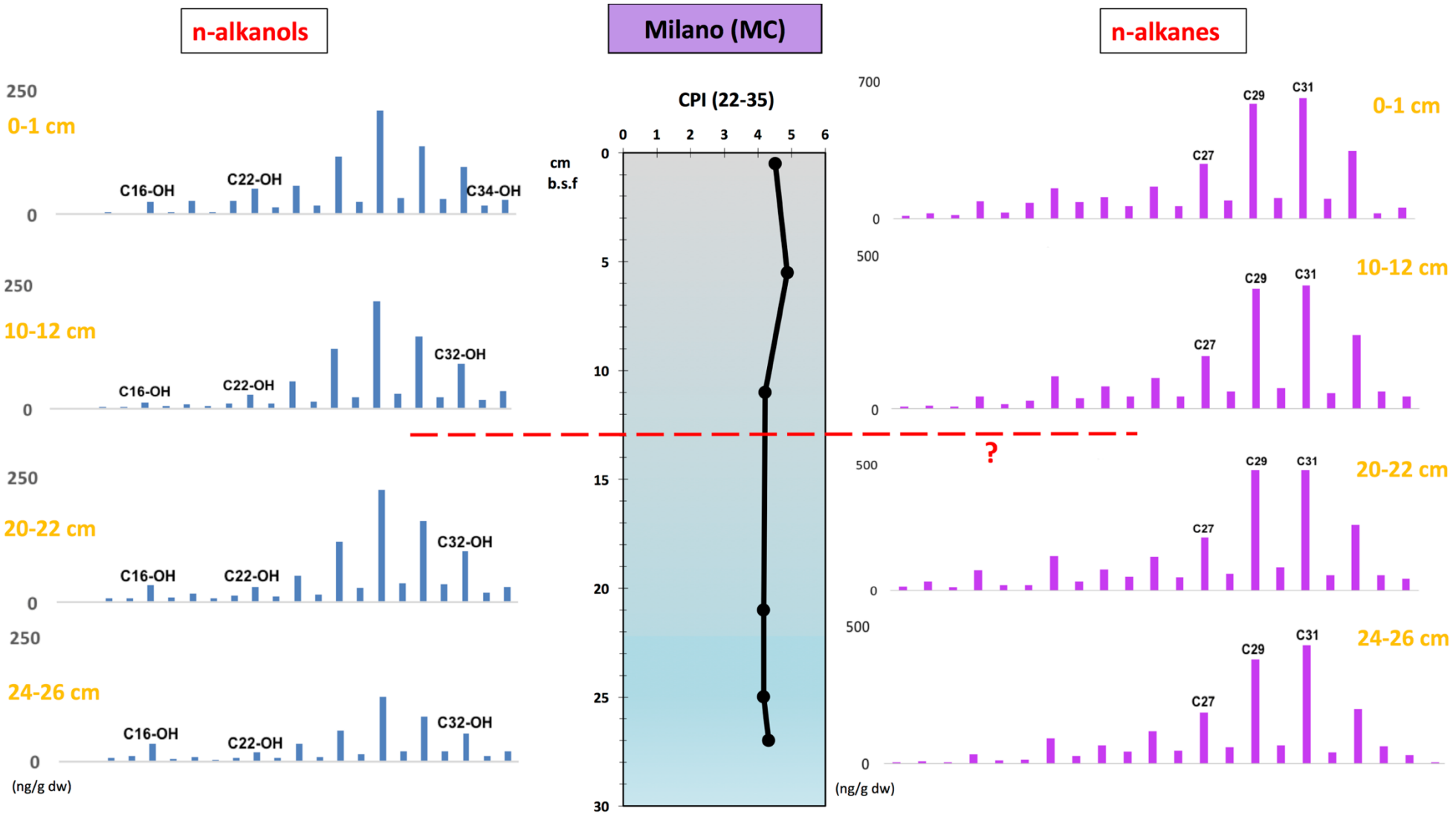

Figure 5.9. CPI, n-alkane and n-alkanol distribution of Milano MC (LEV7MC). Red lines represent possibly different mudflow events.

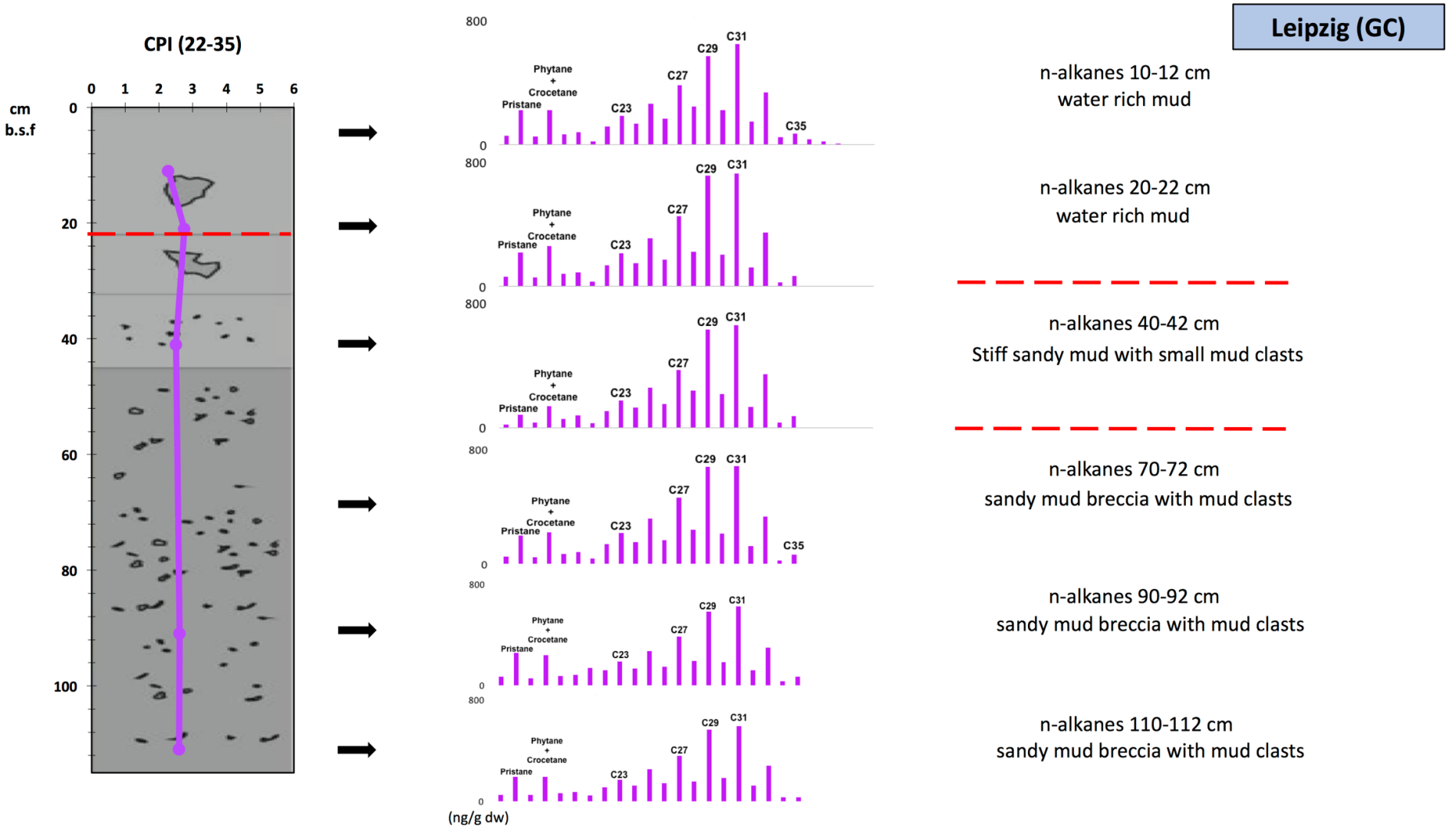

Figure 5.10. CPI, n-alkane distribution and brief description of each sample from Leipzig GC (LEV9GC). Red lines represent possibly different mudflow events (sedimentological description of core was taken from Rousakis et al., Leveco Report, 2017).

5.1.2 Isoprenoid hydrocarbons and gammacerane - Possible palaeosalinity indexes

Other compounds used to determine the origin of the organic carbon include the acyclic isoprenoids pristane (C19) and phytane (C20). These compounds are ubiquitous in the geosphere and have been assumed to be diagenetic products of the phytyl side chain of chlorophyll [159,229,230]. As mentioned in Chapter 2, anoxic conditions during diagenesis lead to the production of phytane whereas oxic conditions to pristane and therefore the ratio Pr/Ph has been previously used as an indicator of the oxicity of the depositional environment [231]. The origins of these compounds though are way more complex than the reduction or oxidation of the phytyl side chain in chlorophylls. For example, [232] suggested that pristane could also derive from tocopherols (which are minor constituents in plants and algal lipid membranes, primarily serving as antioxidants), whereas [233] that dihydrophytol is a component in archaeal cell membranes.

Coming back to the Pr/Ph ratio, Ten Haven et al., 1987 suggested that conclusions about the oxicity of the depositional environment should not be driven by this ratio alone. On the other hand, the ratio appears to be a good indication of hypersaline depositional environments. Sediments from hypersaline environments are characterized by low Pr/Ph (<1) ratios which can be attributed to the high amounts of complex lipids containing phytanyl moieties found in the halophilic bacteria that exist there [234]. Maturity also plays an important role since an increase of the Pr/Ph ratio has been observed in uniform sedimentary sequences [235] as well as in non-uniform strata [61].

Considering the salinity of a depositional environment the Pr/Ph ratio has been found to have a relationship with the gammacerane index. The origin of gammacerane is relatively uncertain, but it could form by reduction of tetrahymanol [236] which is a lipid that replaces steroids in the cell membranes of various organisms. The main source of tetrahymanol appears to be bacterivorious ciliates which occur in stratified water columns between the oxic and anoxic zone [237]. Abundant gammacerane has therefore been found to indicate a stratified water column in marine and non-marine depositional environments most likely due to hypersalinity at depth. A few studies of source rocks in Angola as well as petroleum from Tertiary rocks in offshore China [238] and Tertiary dolomites from the Biyang Basin in China [239] indicate that increased water salinity during sediment deposition results in higher gammacerane indices and lower Pr/Ph.

Another limitation involving these isoprenoids is the fact that there seems to be analytical uncertainty since both of them co-elute with other isoprenoids. On most capillary columns pristane co-elutes with the highly branched irregular isoprenoid 2,6,10-trimethyl-7(3-methylbutyl)-dodecane [240]. Phytane on the other hand also co-elutes with crocetane (2,6,11,15-tetramethylhexadecane) [241] which is an irregular isoprenoid hydrocarbon

diagnostic for methanogenic and methanotrophic Archaea. It is therefore apparent that in this study both absolute values (Table 5.1), as well as the ratio or pristane and phytane should not be used on their own to draw any conclusions.

Table 5.1. Gammacerane and the pristane/phytane ratio for all multi- and gravity- cores.

Core	Pristane/Phytane	Gammacerane (ng/g)
Gelendzhik (LEV1MC)		
0-1 cm	0.6	3.8
5-6 cm	0.8	2.9
10-12 cm	0.6	3.3
14-16 cm	0.7	2.9
18-20 cm	0.6	2.5
20-22 cm	0.4	3.6
22 -24 cm	0.4	4.7
30-32 cm	0.4	2.8
38-39.5 cm	0.5	2.4
No Name MC (LEV3MC)		
0-1 cm	0.6	11.2
5-6 cm	0.5	3.2
10-12 cm	0.6	5.4
18-20 cm	0.5	7.5
20-22 cm	0.4	6.7
22-24 cm	0.6	4.7
24-26 cm	0.6	4.7
26-28 cm	0.4	4.7
30-32 cm	0.3	5.1
Moscow MC (LEV5MC)		
0-1 cm	0.7	3.9
5-6 cm	0.8	4.4
10-12 cm	0.6	6.0
20-22 cm	0.7	2.6
30-32 cm	0.6	4.4
34-36 cm	0.7	3.3
36-38 cm	0.4	2.7
38-40 cm	0.2	11.1
Milano MC (LEV7MC)		
0-1 cm	0.3	2.0
4-6 cm	0.4	1.9
10-12 cm	0.3	1.0
20-22 cm	0.4	1.9
24-26 cm	0.2	1.2
26-28 cm	0.4	2.0

Core	Pristane/Phytane	Gammacerane (ng/g)
Gelendzhik (LEV1GC)		
0-3 cm	0.4	0.8
15-17 cm	0.5	1.3
26-28 cm	0.3	1.1
42-44 cm	0.2	1.0
62-64 cm	0.4	0.9
No Name (LEV3GC)		
2-5 cm	1.1	1.8
5-7 cm	0.3	4.6
12-15 cm	0.6	3.2
20-23 cm	0.1	1.5
30-32 cm	0.4	3.7
50-52 cm	0.5	
62-64 cm	0.6	4.0
Moscow (LEV5GC)		
0-2 cm	0.6	3.3
10-12 cm	0.6	2.2
39-41 cm	0.6	2.4
100-102 cm	0.1	3.9
120-123 cm	0.5	2.9
Milano (LEV7GC)		
0-3 cm	0.6	2.6
40-42 cm	0.5	2.0
60-62 cm	0.6	2.5
90-92 cm	0.7	3.5
Leipzig (LEV9GC)		
10-12 cm	1.0	4.2
20-22 cm	0.8	5.0
40-42 cm	0.6	4.6
70-72 cm	1.1	5.4
90-92 cm	0.9	5.5
110-112 cm	1.0	4.5

Gammacerane and pristane/phytane values (Table 5.1) were calculated in all multi- and gravity-cores during this study. As mentioned previously the pristane/phytane ratio should be used with caution due to possible co-elutions. However, most cores seem to present similarly low values between 0.2 and 1.1. Gammacerane is also present in all cores ranging between 0.8-11.1 ng/g dw. No core seems have any substantial differences with a slight exception in the No Name MC which shows slightly higher concentrations throughout its length. Although it is hard to draw reliable conclusions about the oxicity or salinity of the depositional environments it is pretty clear all cores present relatively similar values of gammacerane and a low pristane/phytane ratio with only minor exceptions. These values could perhaps be an indication of a hypersaline depositional environment but other parameters must be evaluated in order to make this conclusion.

5.1.3 Perylene

The polyaromatic hydrocarbon (PAH), perylene, is considered to be a diagenetic product which is derived from its natural precursors post-depositionally, during the stages of early diagenesis. Combustion or abnormal thermal exposure of organic matter only produces trace amounts of perylene which is probably due to its thermodynamic instability [242].

Natural precursors of perylene could be structurally related to perylenequinones and their derivatives, which are types of black pigments present in modern plants, insects, fungi and crinoids. However, whether perylene precursors are of terrestrial or aquatic sources has not yet been clarified. [243] for example, concluded that perylene originates from more than one precursor including both aquatic and continental organic matter as well as different microbial processes. On the other hand, perylene has long been considered to be an indicator of terrestrial inputs including plants, fungi and insects [244]. One of the most important facts about perylene is that its present in more than trace amounts (>0.010 ppm) is a palaeo-environmental indicator of syn- and post- depositional anoxia [244]. This can be explained by the fact that quinone compounds are sensitive to oxidation and their presence in sediments requires reducing conditions. Its presence also indicates that transportation and sedimentation of perylene precursors has had to be rapid in order to prevent degradation prior to deposition [244].

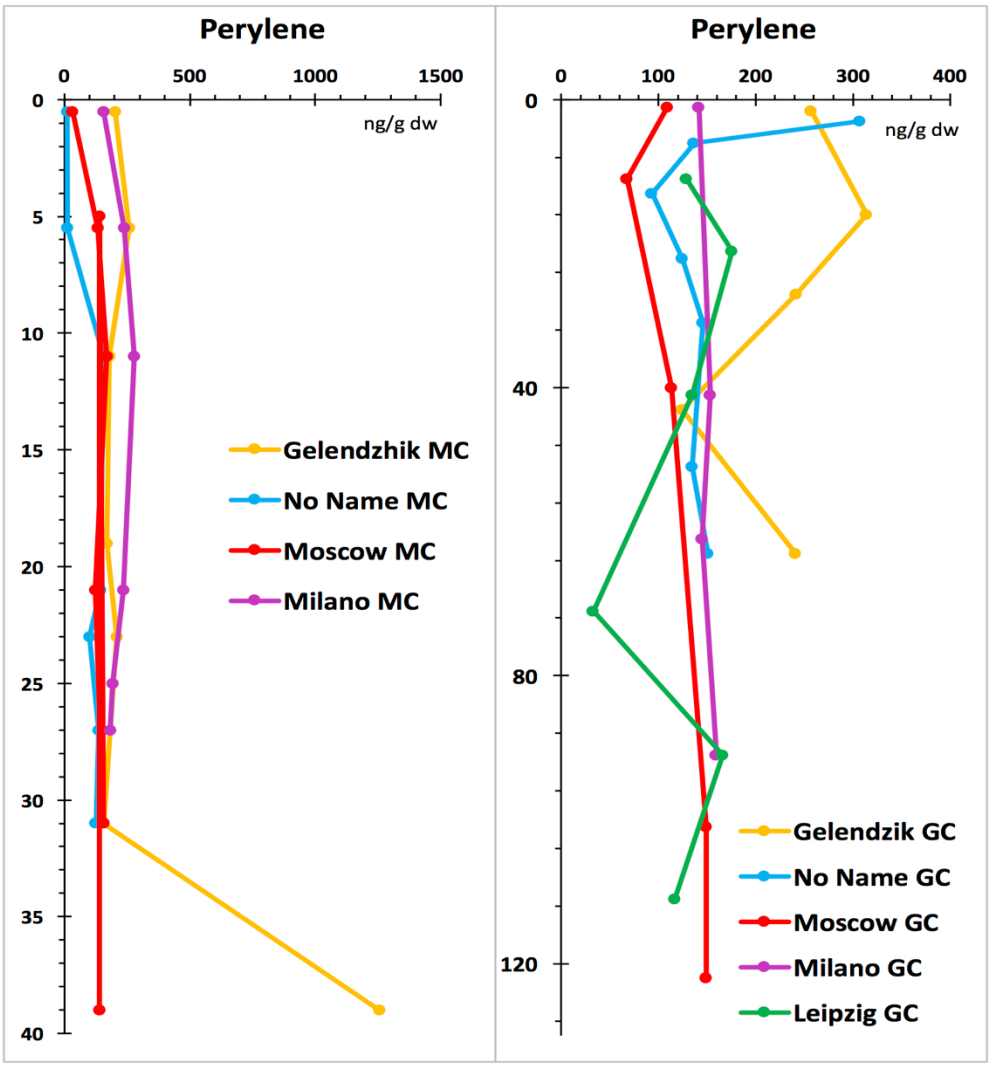

Figure 5.11. Perylene concentrations in all multi- and gravity-cores.

All studied multi- and gravity-cores contain considerable amounts of perylene (Figure 5.11), with concentrations ranging between 33 and 314 ng/g for all gravity cores and between 11 and 1255 ng/g for all muti-cores. A prominent difference is observed in the deepest part of the Gelendzhik MC core at 38-40 cm b.s.f where concentrations rise to 1255 ng/g, whereas throughout the rest of the core concentrations are steady at ~ 200 ng/g. This difference doesn't seem to correspond with other terrigenous markers such as the n-alkanes in the same depth and as a result it is hard to attribute it to a different mud phase/origin of mud. The distributions of perylene in the gravity-cores seem to be not as steady as those in the multi-cores. These variations are likely due to the presence of different mud phases within each core. Despite all of these variations, the abundance of perylene could be used as an indication of reducing/anoxic depositional environments.

5.2 THERMAL MATURITY OF ORGANIC MATTER AND MUD MOBILIZATION DEPTH

Introduction

Diagenesis and thermal maturity

In an organic geochemistry context, the process of diagenesis affects the products of primary production prior to deposition as well as during the early stages of burial. Diagenetic conditions are characterized by relatively low temperatures and pressures and the transformations are usually a result of biological and to a lesser extent chemical reasons (for example catalysis by mineral surfaces).

Diagenesis leads to the thermal alteration of sedimentary organic matter. Specifically, thermal maturity describes all heat-driven reactions that convert organic matter trapped in sediments into petroleum and other gas hydrocarbons. These potential source rocks only become effective at appropriate levels of thermal maturity. In general, organic matter can be described as immature, mature or postmature, depending on its relation to the oil-generative window [245]. Immature organic matter has been biologically, physically and chemically altered but only through diagenesis. Increase in temperature slowly leads to the stage of catagenesis during which biological activity is restricted, and thermally mediated alteration of organic matter prevails. In this stage, which is equivalent to the oil-generative window, organic matter is described as mature. Finally, organic matter that has been heated to extremely high temperatures and has been reduced to a hydrogen-poor residue is described as postmature. This matter is only capable of generating small amounts of hydrogen gases.

It is therefore evident, that the thermal maturity of organic matter within a source rock is an extremely important factor to take into account when searching for potential hydrocarbon sources. This maturity level can also be used in order to infer the approximate burial depth of our sediment or in our case, extruded mud. As mentioned previously thermal maturity correlates to the oil-generative window which is also characterized by a specific temperature range. The temperature gradient of the area in combination with thermal maturity rates could estimate a maximum burial depth of the extruded sediment.

In order to describe the thermal maturity of organic matter various parameters have been developed over the years. Conventional geochemical methods include Vitrinite Reflectance (Ro), Thermal Alteration Index (TAI) and the Carbon Preference Index (CPI) which has been described in the previous part of this chapter. Since the 1970s, molecular

parameters based on distributions and rates of specific biomarkers have been used extensively.

Molecular maturity parameters

Molecular maturity parameters have been used since the recognition of systematic changes in biomarker composition with increasing depth and thus thermal maturity in burial sequences [246,247]. These maturity parameters are based on the relative abundances of two stereoisomers and involve an increase in the more thermally stable (non-biological) isomer compared to the isomer with the original biologically-inherited stereochemistry. The processes which control the fate of individual maturity parameters are complex, and each parameter may be influenced to different extents by the underlying mechanisms of intervonversion (isomeration), generation and thermal degradation [248].

Some of the most applied thermal maturity indicators are the ratios of saturated and aromatic biomarkers. Cracking reactions as well as configurational isomerization at certain asymmetric carbon atoms are the two types of reactions that control these indicators, with isomerizations being more widely applied. Figure 5.12 depicts various maturity parameters in correlation with the vitrinite reflectance (Ro%) and various stages of oil and gas generation.

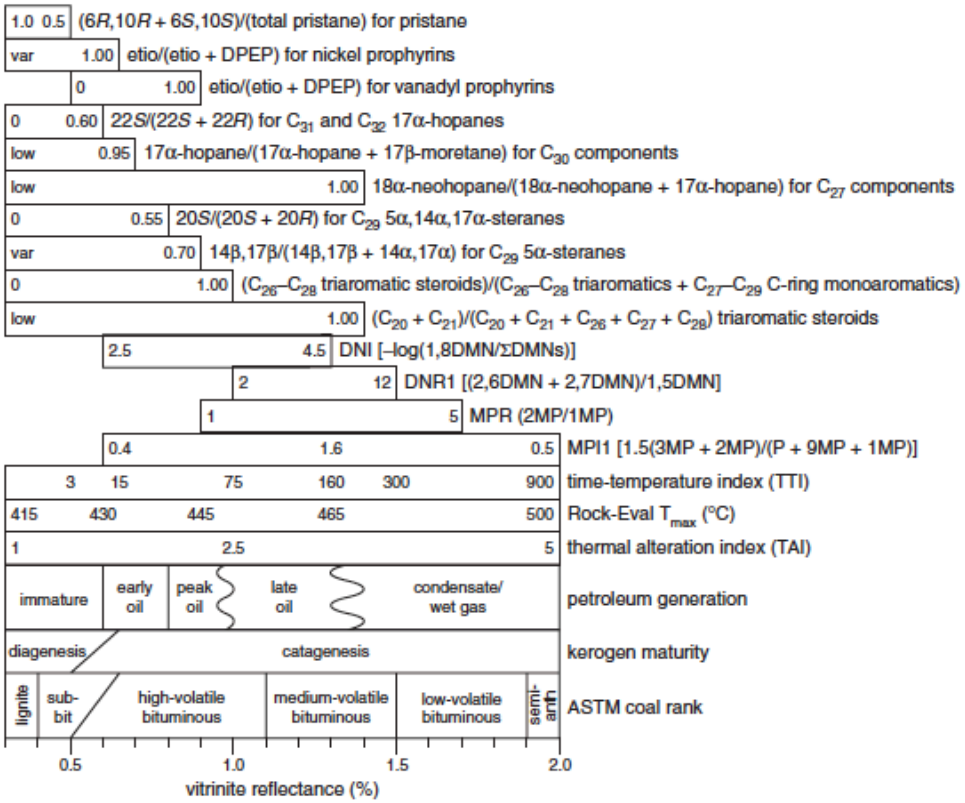

Figure 5.12. Approximate correlations of various maturity parameters and stages of coalification and petroleum generation (taken from Killops and Killops, 2005).

5.2.1 Hopanes

Hopanes are ubiquitous in marine sediments, reflecting the importance of bacterial activity during diagenesis. During the early stages of diagenesis reduction of the hopanoidal acids and polyols leads to the formation of hopanes with a 17(β),21(β) configuration, a configuration which also occurs in living organisms (Figure 5.13) [249]. This 17(β),21(β) isomer is much less thermally stable than the 17(β),21(α) and 17(α),21(β) isomers (these do not occur in living organisms) and therefore it is quickly converted to a mixture of these two [249]. With increasing temperature 17(β),21(α) is almost completely converted into the more stable 17(α),21(β). Similarly, the biologically conferred 22R configuration which appears in the C31-C35 hopanes is only preserved during the initial stages of diagenesis. Throughout time isomerisation results in equal amounts of 22R and 22S isomers [249].

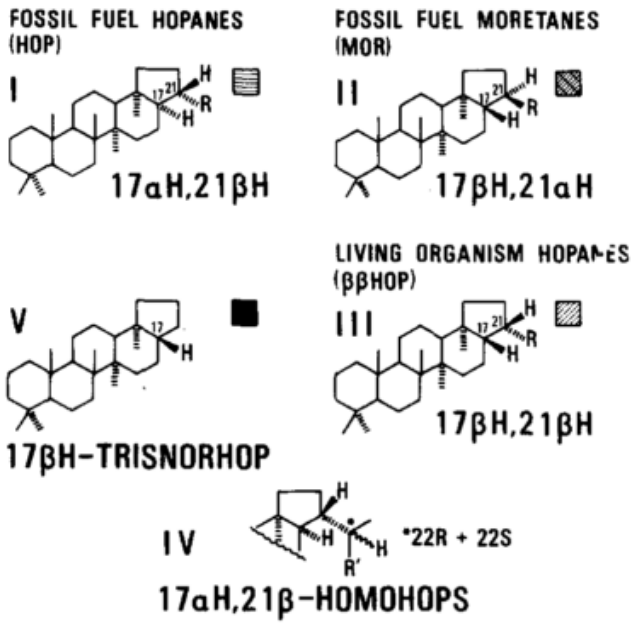

Figure 5.13. Hopane stereochemistry in immature ancient shales (taken from [246]).

For the purpose of this study the distribution of hopanes (m/z 191) (Figure 5.14 and Table 5.2) was analysed in all nine multi- and gravity-cores. The most important ratios concerning the thermal maturation of organic matter are discussed below.

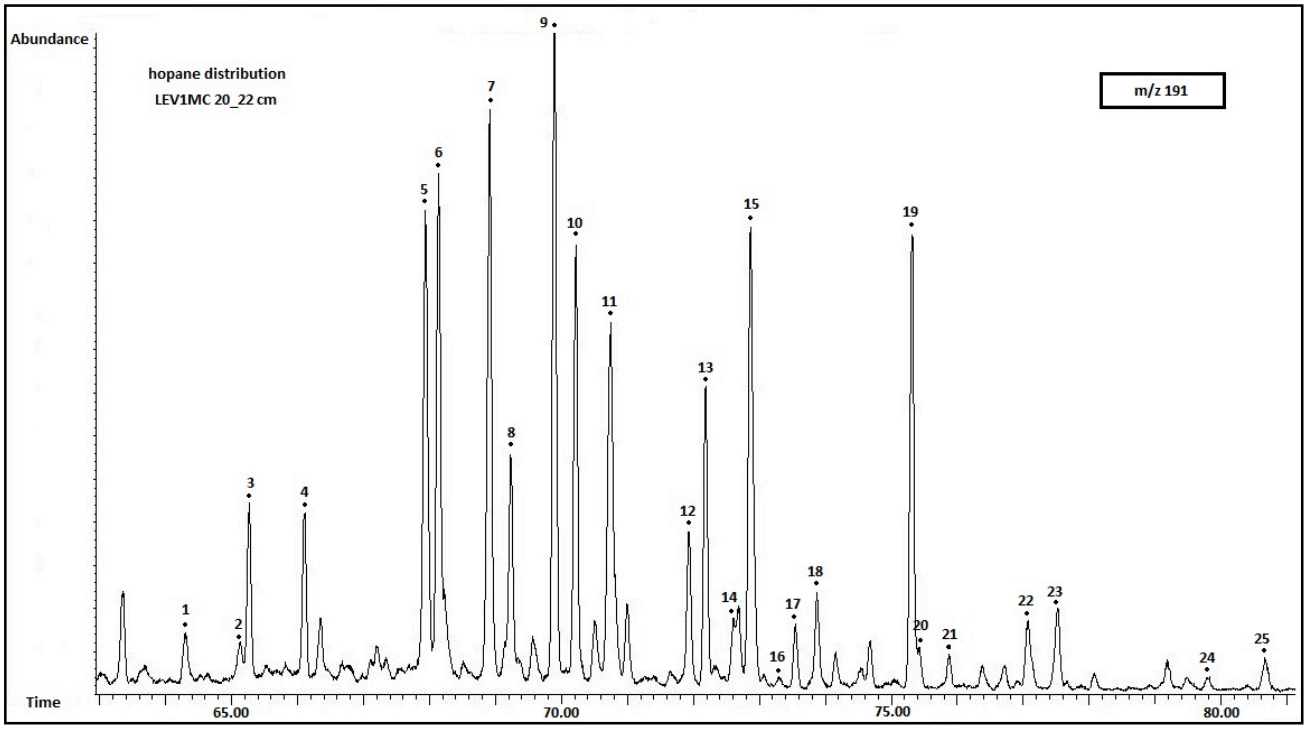

Figure 5.14. Typical m/z 191 chromatogram showing the distribution of hopanes present in the LEV1MC 20_22 cm sample. Numbers refer to compounds listed in Table 5.1.

Table 5.2. List of hopanes found in sediment samples from Olimpi MV field.

Peak number	Compound name	Abbreviation	Carbon number
1	18α(H)-22,29,30-trisnorneohopane	Ts	C27
2	22,29,30-Trisnorhop-17(21)-ene	TNH	C27
3	17α(H)-22,29,30-trisnorhopane	Tm (27a)	C27
4	17β(H)-22,29,30-trisnorhopane	27β	C27
5	17α-bisnormoretane		C28
6	17α,21β(H)-30-norhopane	29αβ	C29
7	hop-17(21)-ene		C30
8	17β,21α(H)-30-norhopane (or normoretane)	29βα	C29
9	17α(H),21β(H)-hopane	30αβ	C30
10	Neohop-13(18)-ene	NH13	C30
11	17β(H),21α(H)-hopane (moretane)	30βα	C30
12	17α(H),21β(H)-homohopane 22S	C31 αβ S	C31
13	17α(H),21β(H)-homohopane 22R	C31 αβ R	C31
14	gammacerane		
15	17β(H),21α(H)-homomoretane	C31 βα	C31
16	hop-22(29)-ene (diploptene)	D	C30
17	17α(H),21β(H)-bishomohopane 22S	C32 αβ S	C32
18	17α(H),21β(H)-bishomohopane 22R	C32 αβ R	C32
19	17β(H),21β(H)-homohopane	C31 ββ	C31
20	17α(H),21β(H)-trishomohopane 22S	C33 αβ S	C33
21	17α(H),21β(H)-trishomohopane 22R	C33 αβ R	C33
22	17α(H),21β(H)-tetrakishomohopane 22S	C34 αβ S	C34
23	17α(H),21β(H)-tetrakishomohopane 22R	C34 αβ R	C34
24	17α(H),21β(H)-pentakishomohopane 22S	C35 αβ S	C35
25	17α(H),21β(H)-pentakishomohopane 22R	C35 αβ R	C35

A. 22S/(22S+22R) homohopane isomerization, (%22S)

The %22S parameter is one of the most widely applied hopane maturity parameters with high specificity for immature to early oil generation organic matter. It records the relative enrichment of the more thermally stable 22S isomer in comparison to the biologically derived 22R one. Isomerization at the C-22 of the C31-C35 homohopanes occurs earlier than many other biomarker reactions therefore making it a reliable parameter for immature matter. The 22S/(22S+22R) ratio differs slightly between the C31-C35 17α-homohopanes. Thermodynamic equilibrium of these ratios is around 0.6 but this number can vary slightly. [250] calculated the average equilibrium of the ratio for C31, C32, C33, C34, C35 to be at 0.55, 0.58, 0.60, 0.62 and 0.59, respectively.

The C31 and C32 homohopanes are typically used to calculate this ratio, which rises from 0 to approximately 0.6 during maturation. The thermodynamic equilibrium is between 0.57 and 0.60 according to [251] for both C31 and C32. 22S/(22S+22R) ratios between 0.50 and 0.54 imply that the sediment has barely entered oil generation, whereas ratios between 0.57 and 0.62 mean that the main phase of oil generation has happened or has even been surpassed. After reaching equilibrium the ratio remains constant since there are no other changes in the 22S and 22R isomers.

For the purpose of this study the 22S/(22S+22R) ratio for both C31 and C32 homohopanes was calculated and results are presented below in Figure 5.15. The values of the 22S/(22S+22R) ratio for the C31 homohopane range between 0.25 and 0.52 for the multi-cores, and between 0.22 and 0.35 for the gravity cores. Values of the ratio for the C32 homohopane are slightly elevated between 0.28 and 0.55 for the gravity-cores. The gravity core taken from Gelendzhik seems to differ from the rest as it presents much higher values, nearing equilibrium in some parts. All multi-cores present higher ratios for the C32 homohopane in the top layer from around 0-10 cm b.s.f. These higher values could possibly be due to co-elution of a biogenic hopane (such as diploptene) with the C32 αβ S peak. It is therefore evident that all our samples fall into the category of immature organic matter, presenting relatively similar values. The cores taken from Gelendzhik are the only ones that systematically exhibit slightly higher values than the rest of the cores but without reaching equilibrium.

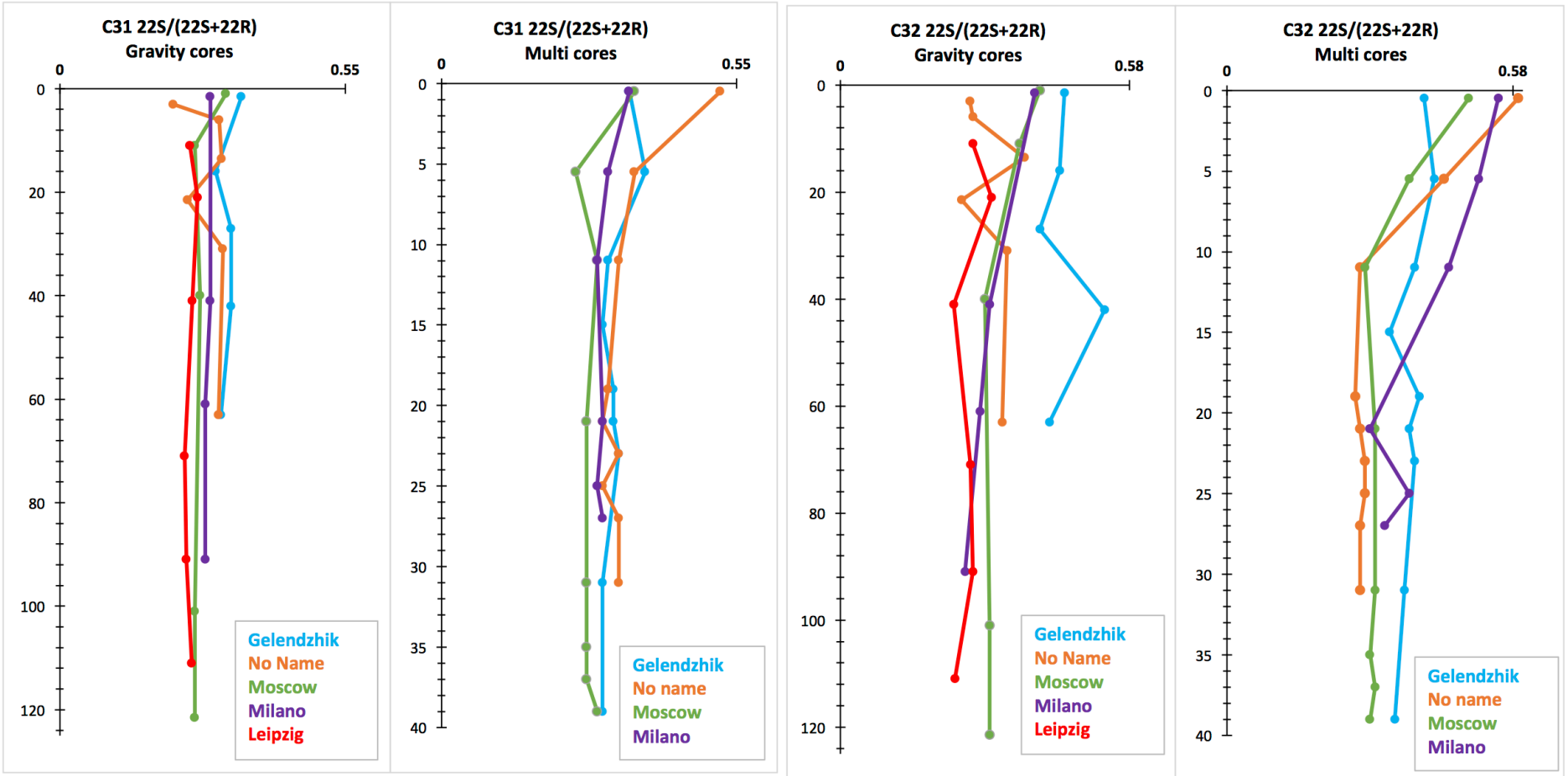

Figure 5.15. C31 and C32 22S/(22S+22R) distributions for all gravity and multi-cores.

B. Ts/Ts +Tm

The Ts/Ts +Tm, also expressed as Ts/Tm, is a frequently used parameter which depends on both the source of the organic matter and its maturity [252]. This thermal parameter is based on the stability of the C27 hopanes, and it is applicable for immature to mature and postmature organic matter. During diagenesis, Tm appears to be less stable than Ts [246]. Caution must be taken when using this ratio since lithology and oxicity of the depositional environment seem to play some role. Caution should also be taken since Tm and Ts commonly co-elute with tricyclic or tetracyclic terpanes on m/z 191 mass chromatograms.

The Ts/Ts+Tm ratio in all multi-cores (Figure 5.16) ranged between 0.18 and 0.40. Most cores showed relatively similar values but a slight exception was observed in the Milano core from around 0-10 cm b.s.f. Gravity-cores (Figure 5.16) show values between 0.11 and 0.36, which are slightly lower than the ones presented in the multi-cores. Values are similar throughout the cores with an exception in the 10-40 cm b.s.f layer of Gelendzhik. This decrease could either be due to a difference in maturity or even in the source of the organic matter present in that mud phase even though this different phase doesn't seem to reflect on any other maturity parameters. As we can see all results point out to relatively immature organic matter.

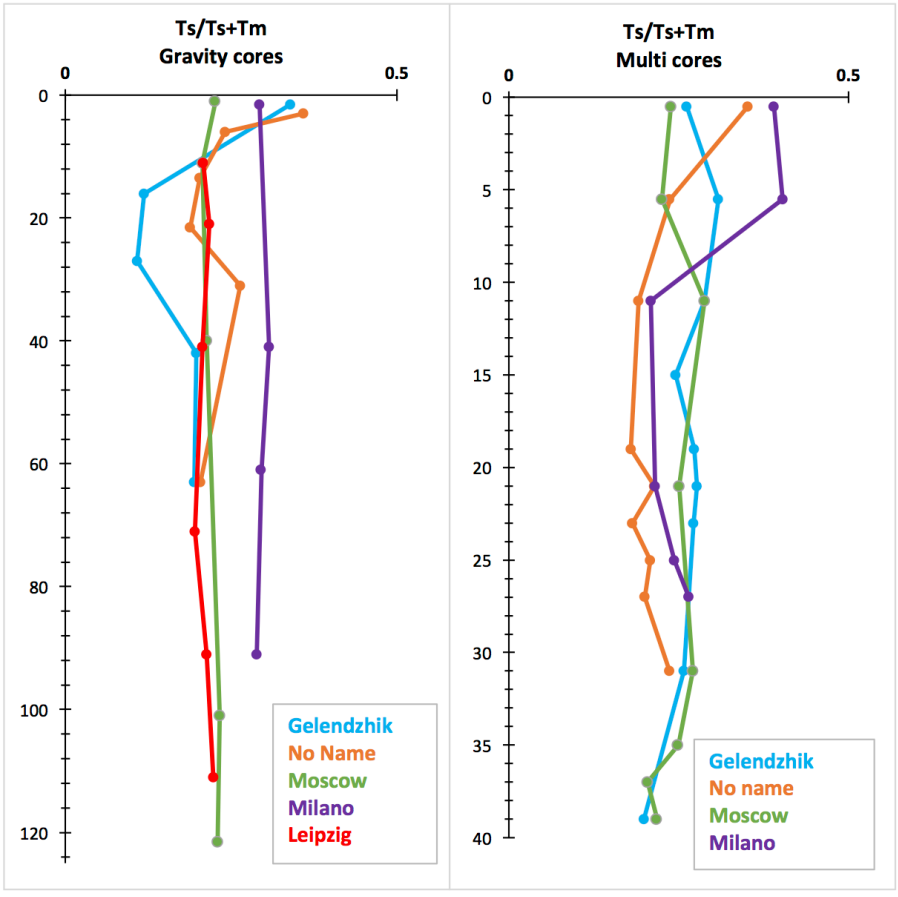

Figure 5.16. Ts/Ts+Tm ratios for all gravity- and multi-cores.

5.2.2 Steranes

Just like hopanes, steranes are the diagenetic product of sterols and their presence in sediments implies thermal alteration of the organic matter. Stenols are the predominant biogenic sterols which along with stanols are the major steroidal input in the sediment. During the early stages of diagenesis hydrogenation, via a microbially mediated process under anaerobic conditions [253], of the free unsaturated stenols leads to their saturated counterparts stanols. The next diagenetic transformation is the dehydration of stanols and stenols to sterenes. Finally, fully saturated steranes with a predominant 5α configuration occur after hydrogenation (reduction) of sterenes.

At the end of diagenesis steranes have a 5α(H), 8β(H), 9α(H), 10β(CH3), 13β(CH3), 14α(H),1 7α(H), 20R configuration. As diagenesis continues isomerization reactions around the C-20 carbon center take place. The carbon number of the biogenic precursors (sterols) is preserved in steranes but some source specifity is lost and therefore the attempt to evaluate the organic matter source from steranes can be difficult.

In terms of thermal maturity two ratios have been used during this study. The distribution of steranes (m/z 217+218) (Figure 5.17and Table 5.3) was analysed in all 9 gravity- and multi-cores.

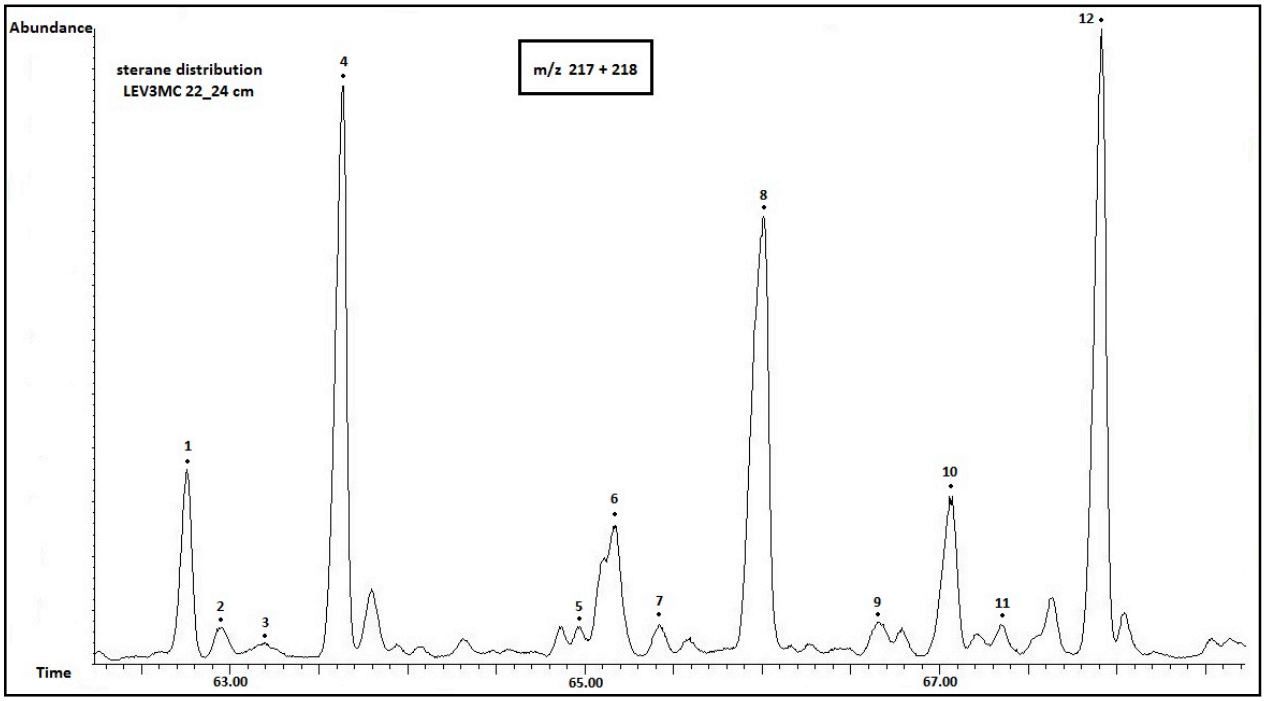

Figure 5.17. Typical m/z 217 + 218 chromatogram showing the distribution of steranes in the LEV3MC 22_24 cm sample. Numbers refer to compounds listed in Table 5.3.

Table 5.3. List of steranes found in sediment samples from Olimpi MV field.

Peak number	Compound name	Abbreviation	Carbon number
1	20S-5α(H),14α(H),17α(H)-cholestane	27αααS	C27
2	5α(H),14β(H),17β(H),20(R)-cholestane	27αββR	C27
3	5α(H),14β(H),17β(H),20(S)-cholestane	27αββS	C27
4	20R-5α(H),14α(H),17α(H)-cholestane	27αααR	C27
5	24-Methyl-20S-5α(H),14α(H),17α(H)-cholestane	28αααS	C28
6	24-Methyl-5α(H),14β(H),17β(H),20(R)-cholestane	28αββR	C28
7	24-Methyl-5α(H),14β(H),17β(H),20(S)-cholestane	28αββS	C28
8	24-Methyl-20R-5α(H),14α(H),17α(H)-cholestane	28αααR	C28
9	24-Ethyl-20S-5α(H),14α(H),17α(H)-cholestane	29αααS	C29
10	24-Ethyl-5α(H),14β(H),17β(H),20(R)-cholestane	29αββR	C29
11	24-Ethyl-5α(H),14β(H),17β(H),20(S)-cholestane	29αββS	C29
12	24-Ethyl-20R-5α(H),14α(H),17α(H)-cholestane	29αααR	C29

A. 20S/20S+20R isomerization or %20S

Steroidal precursors in living organisms only contain the R configuration at C-20 which is gradually converted during maturation to a mixture of R and S sterane configurations. This isomerization at C-20 of the C29 5α, 14α, 17α (H) sterane causes the 20S/20S+20R ratio to rise from 0 to about 0.5 with increasing thermal maturity, while the equilibrium is at 0.52-0.55 [254]. This ratio shows high specificity for organic matter in the immature to mature range, and it is the C29 compounds which are most often used. Isomerization ratios of the C27 and C28 commonly show interference by other co-eluting peaks since C27βαα20R usually co-eultes with C27ααα20R and C28βαα20R with C28αββ20R. In order to determine the onset of petroleum generation this ratio should be used with caution since different source rocks exhibit different equilibrium values. Sterane isomerization can also be affected by other factors such as differences in organofacies, weathering [255], and biodegradation. Biodegradation specifically can lead to an increase in the ααα 20S/20S+20R ratio (of all C27, C28, C29) above 0.55 most likely due to selective removal of the ααα 20R epimer by bacteria [256].

The 20S/20S+20R ratio of the C29 ααα sterane (Figure 5.18) was exceptionally low in all gravity- and multi- cores. Values were under 0.1 for all samples with an exception in the surficial (0-1 cm b.s.f) sample from the No Name multi-core (LEV3MC) which was at 0.29. The same ratio was also calculated for the C27 ααα sterane (Figure 5.18) which showed higher values which were relatively steady around 0.3. Once again, the cores from the No Name (LEV3) location presented a few exceptions. The multi-core (LEV3MC) specifically showed a much higher value around 0.5 in the surficial 0-1 cm b.s.f sample,

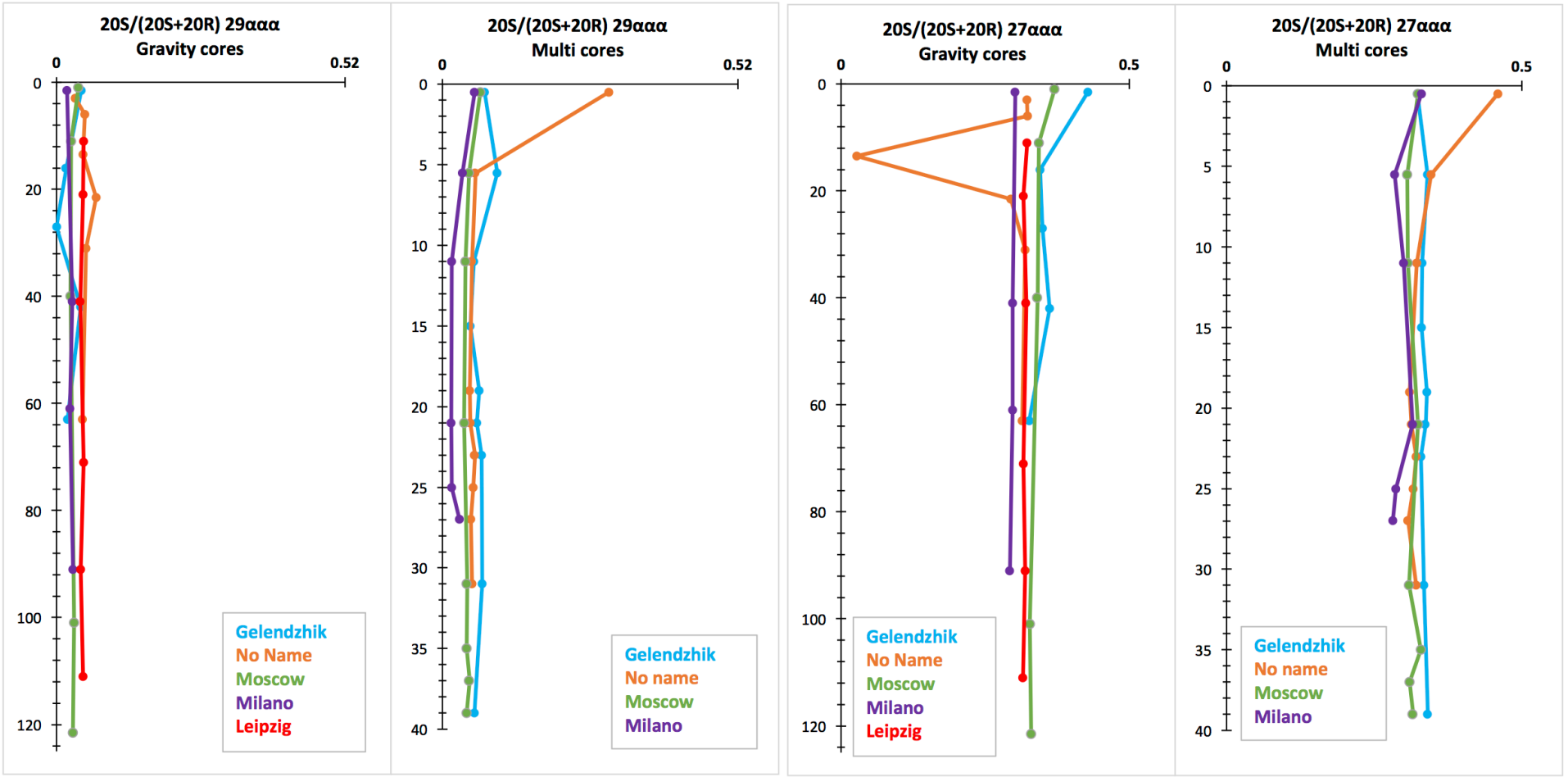

Figure 5.18. C29ααα and C27ααα 22S/(22S+22R) distributions for all gravity and multi-cores.

a trend which appears in all separate maturity parameters. This difference in the surficial sample could be attributed to the intense biological activity which appears to take place on the surface of this core which could lead to a co-elution of a biogenic compound with our studied parameters.

B. αββ/(αββ+ααα) isomerization

This maturity parameter is based on the higher thermal stability of the αββ isomer in comparison to the biologically derived ααα form. It is a widely applied due to its high specificity in the immature to mature range of the organic matter, even though various anomalous values have been linked to different organic facies (Rullkoter and Marzi,1988), or specific precursors (ten Haven et al.,1986). Isomerization of the C-14 and C-17 in the C29 20S and 20R steranes leads to an increase in the αββ/αββ+ααα ratio from 0 to approximately 0.7 (the equilibrium is at 0.67-0.71) with increasing maturity [254].

All our samples (Figure 5.19) presented values below the thermodynamic equilibrium indicating immature organic matter just like all previously mentioned parameters. More specifically, all gravity- and multi- cores displayed similar values at around 0.3 for the C29 sterane with once again an exception in the surficial sample (0-1 cm b.s.f) of LEV3MC. The ratio for the C27 sterane presented much lower values at around 0.1, in both gravity- and multi- cores.

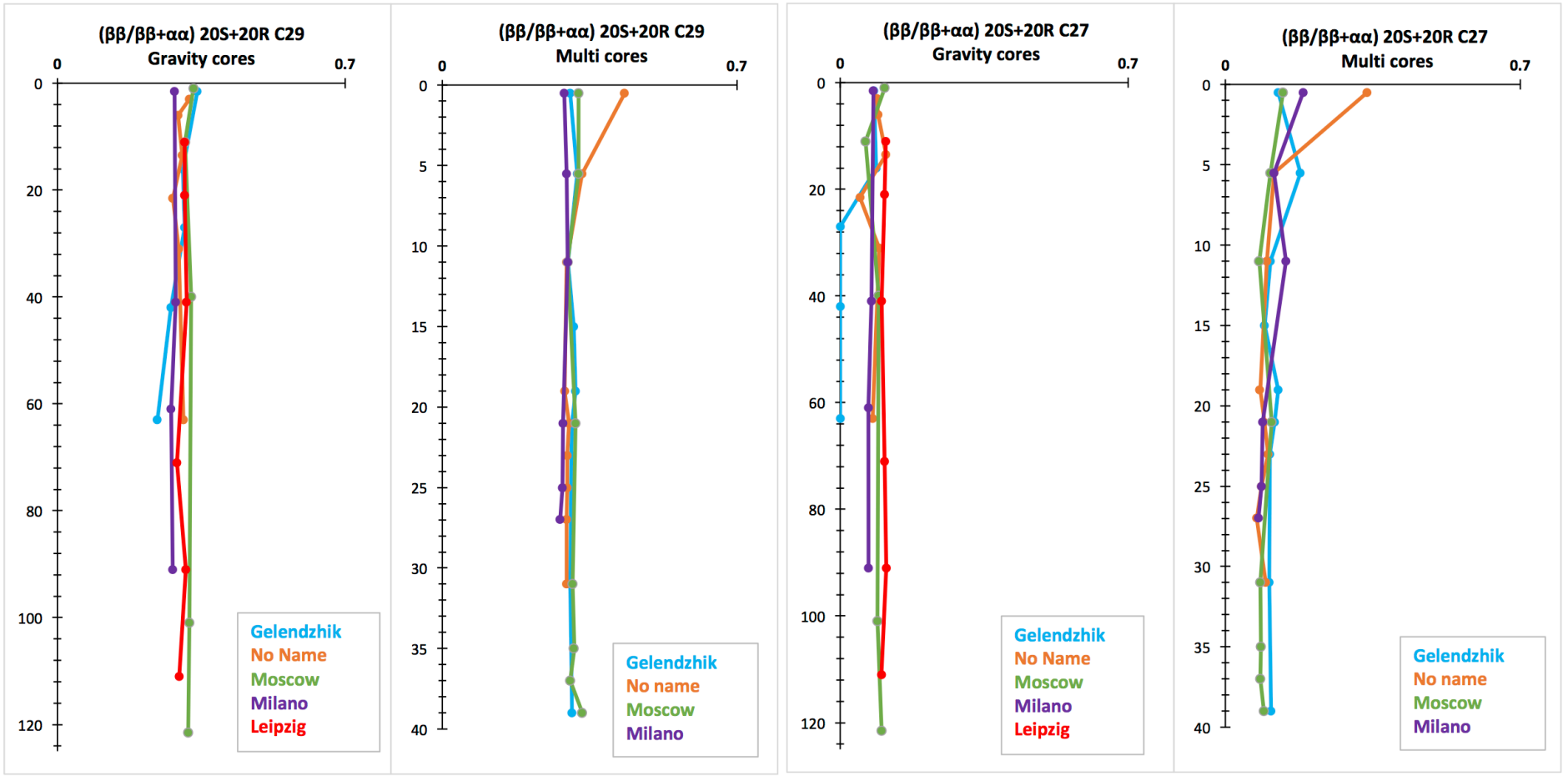

Figure 5.19. C29 and C27 (ββ/ββ+αα) 20S+20R distributions for all gravity and multi-cores.

PART II
POST-ERUPTIONAL MICROBIAL PROCESSES

Cold seep environments are considered to be 'hotspots' of increased biological activity and over the years they have been documented in a number of seafloor sites [6]. These environments are characterized by the presence of chemosynthetic communities and large emissions of methane and sulfide. Following the eruption of mud volcanoes and the emplacement of the hydrocarbon-rich extruded material, in situ microbial processes start taking place. The main microbial processes that can be distinguished in such settings are 1) the anaerobic oxidation of methane (AOM), which is coupled to 2) sulfate reduction (SR) and finally 3) microbial methanogenesis (mentioned in detail in Chapter 1). Each of these processes is performed by a specific group of prokaryotic microorganisms and can be distinguished by the distribution of their specific biomarkers.

For the purpose of this study, characteristic biomarkers related to the chemosynthetic communities were analysed in order to quantify microbial activity and distribution and to evaluate the dynamics between these communities and the biogeochemical processes that take place. Even though these processes are related to each other (AOM is coupled to SR) and should be described together, results are presented in two separate sections involving archaeal and bacterial biomarkers.

5.3 ANAEROBIC OXIDATION OF METHANE / ANAEROBIC METHANOTROPHS

The anaerobic oxidation of methane (described in Chapter 1) is a microbial process mediated by a syntrophic consortium of Archaea and sulfate reducing bacteria which form dense aggregates [90–92,97,105]. So far, the archaeal partners, also called ANaerobic MEthanotrophs (ANME), have been found to belong to three groups (ANME-1, ANME-2 and ANME-3) related to the methanogenic *Methanosarcinales* and *Methanomicrobiales*. One of the main characteristics of archaeal biomarkers derives from the fact that these ANaerobic MEthanotrophs consume/oxidize the isotopically light CH4 therefore leading to extremely light C-isotope signals (measured by compound specific isotopic analysis).

During this study, characteristic archaeal biomarkers such as isoprenoidal glycerol ethers (archaeol and sn-2-hydroxyarchaeol) (Figure 5.20) and the isoprenoidal hydrocarbon PMI were analysed in all four multi-cores. Results are presented alongside the bulk organic carbon (OC%) and δ13Corg parameters as well as with the CH4 fluxes for each core.

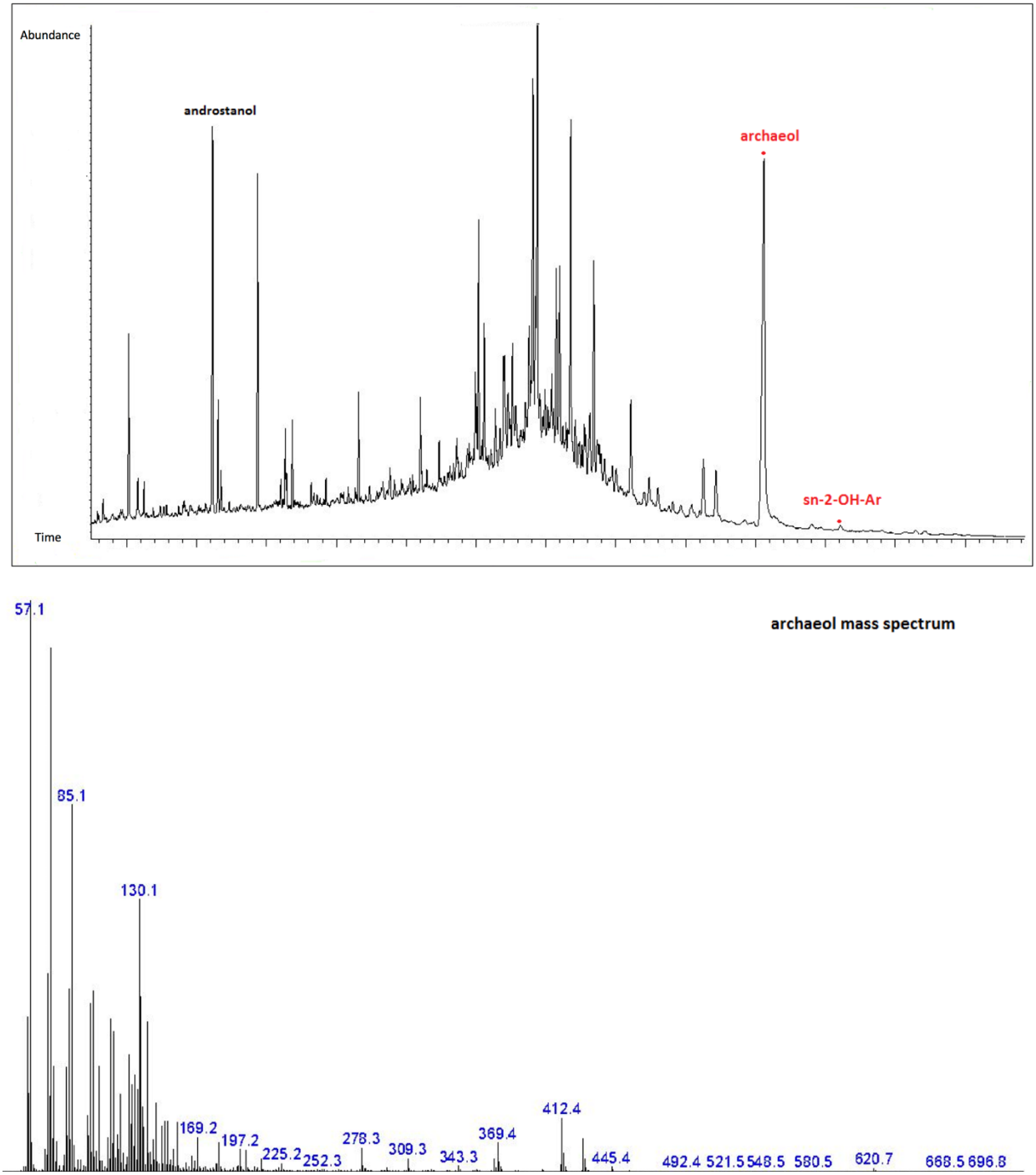

Figure 5.20. Top: Characteristic chromatogram of the polar fraction depicting the archaeal biomarkers archaeol and sn-2-hydroxyarchaeol, Bottom: Mass spectrum of archaeol.

The bulk geochemical parameter of δ13Corg has been used to differentiate the origin of organic matter [257]. According to δ13Corg, organic carbon in marine sediments can be classified into three groups which include 1) predominant marine organic matter with δ13Corg values between −20‰ and −22‰, 2) a mixture of marine and terrestrial organic matter with δ13Corg values between −22‰ and −25‰ and 3) predominant supply of terrestrial organic matter with δ13Corg values lower than −25‰. Characterization of

organic matter should not be performed based on δ13Corg values alone, since both terrestrial and marine sources have been found to produce slightly different values therefore leading to inaccurate results.

Methane concentrations were measured on board right after the recovery of each core but since δ13Corg analysis has not been performed yet it is unclear if this methane is biogenic or thermogenic. Furthermore, since compound specific δ13Corg analysis has also not been performed yet on the archaeal biomarkers it is also unclear if these belong to methanogens which produce biogenic methane or if they belong to anaerobic methanotrophs (ANME) which perform anaerobic methane oxidation (AOM). Therefore, whenever the process of AOM is mentioned during the description of each core caution should be taken since microbial methanogenesis could actually be the prevailing process taking place.

Gelendzhik MC (LEV1MC)

Bulk characteristics of the core taken from Gelendzhik (Figure 5.21) show relatively steady OC% values at ~ 0.5% which increases to ~ 1% in the surficial layer due to increased biological activity. Similarly, δ13Corg values remain steady throughout the core at ~ −25‰ and slight decreases to ~ −28‰ are observed in the top 0-5 cm b.s.f and towards the end of the core. These values point to predominately terrestrial organic matter inputs which is in agreement with other measured parameters mentioned previously. Elevated methane concentrations at around 25 mmol/L are observed in the 20-25 cm b.s.f layer, and they are actually the highest concentrations found in comparison to the rest of the cores. Archaeal biomarkers such as the dialkyl glycerol diethers (DGDs) archaeol and sn-2-hydroxyarchaeol are found throughout the core. Archaeol values are considerably higher, between 30-420 ng/g dw, whereas sn-2-hydroxyarchaeol is a minor constituent at 0-38 ng/g dw. The distribution of DGDs and especially that of archaeol show a clear bimodal or even trimodal pattern. The lower peak, at 20-25 cm b.s.f, correlates with the peak of methane concentrations which could imply that the process taking place at that depth is either microbial methanogenesis or anaerobic oxidation of methane. Conclusions regarding the actual process taking place cannot be made until further analysis of compound specific isotopic composition is performed. The shallower peaks at 0 cm b.s.f and 10 cm b.s.f could be indications of aerobic microbial activity or palaeo-AOM/aerobic activity respectively .The irregular isoprenoid PMI which is another archaeal biomarker, shows a similar bimodal distribution but with much lower concentrations. A strong peak is observed at around 5 cm b.s.f indicating palaeo-AOM or palaeo-aerobic activity due to the absence of methane. Generally speaking, the top layer of the core, at 0-5 cm b.s.f, shows increased microbial activity which could be a sign of an active system.

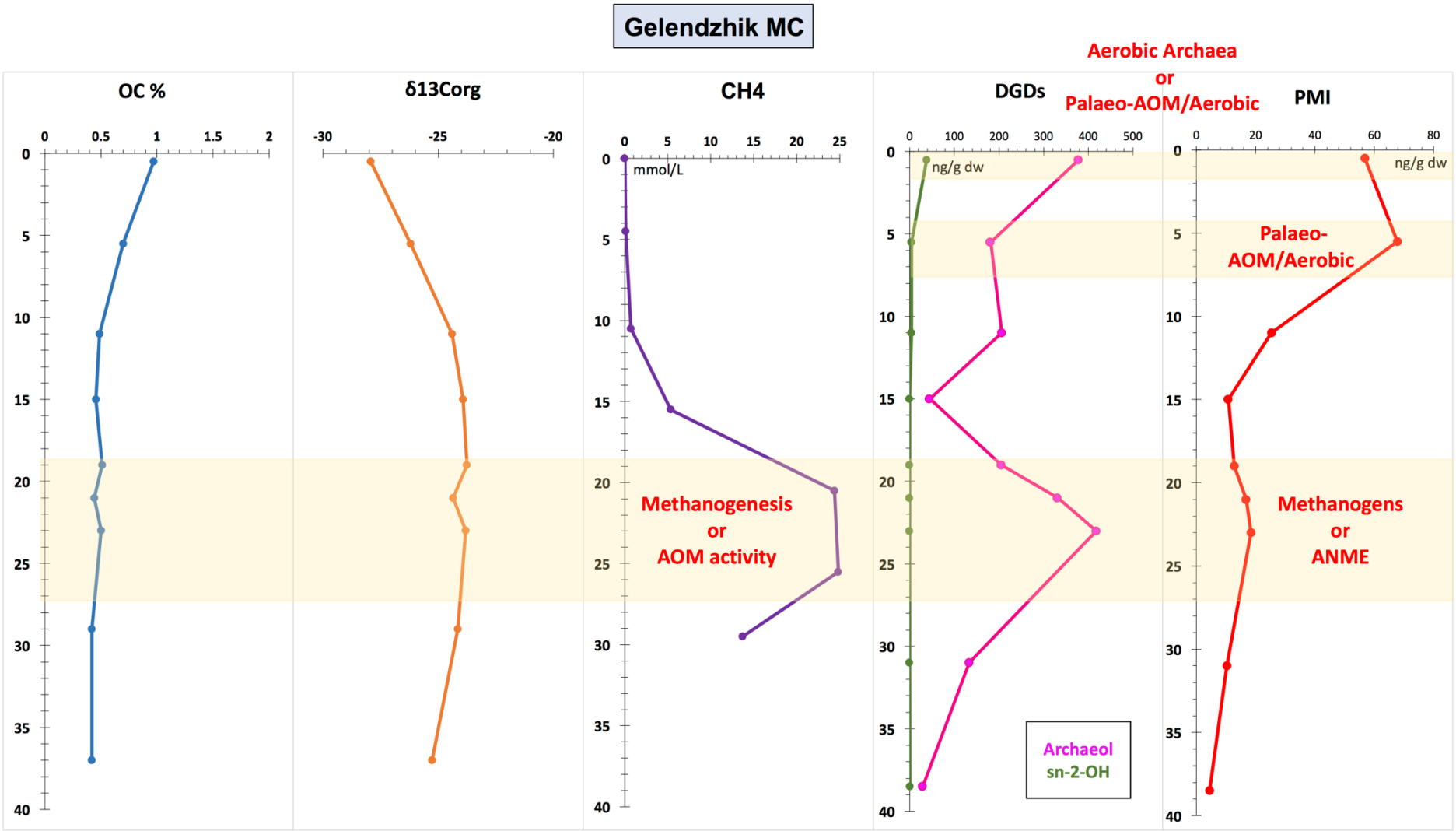

Figure 5.21. Bulk parameters (OC%, δ13Corg), CH4 flux and archaeal biomarkers (DGDs and PMI) for Gelendzhik MC.

No Name MC (LEB3MC)

The bulk characteristics of this core (Figure 5.22) present some slight variation in their distributions, especially in the zone of higher methane concentrations. OC% values are ~ 0.43-0.8% and increase up to ~2% in the surficial sediment indicating increased biological activity. δ13Corg values also show some differences in the same zone, at around 20-27 cm b.s.f, but other than that values throughout the core remain similar ~ −25‰ indicating a strong input of terrestrial organic matter. Unlike LEV1MC this core only presents a slight decrease in δ13Corg values in the top 0-5 cm b.s.f layer. Methane concentrations are low, showing a slight increase of up to about 3mmol/L in the 20-27 cm b.s.f layer. Archaeal biomarkers, archaeol and sn-2-hydroxyarchaeol, are present throughout the core, with archaeol concentrations being much higher than those of sn-2-hydroxyarchaeol. Archaeol shows a peak at 31 cm b.s.f, deeper than the methane peak observed at 28 cm b.s.f, which could be an indication of microbial methanogenesis instead of AOM. Compound specific isotopic analysis is necessary in order to draw any specific conclusion since the archaeol peak could instead be indicative of palaeo-AOM/methanogenesis. PMI is also observed throughout the core with the highest concentrations in the top 0-5 cm b.s.f layer indicating recent or palaeo- activity. At around 22 cm b.s.f there seems to an almost negligible second increase in methane concentration. Despite its small intensity, this increase seems to reflect on both bulk (OC% and δ13C) parameters and in PMI concentrations and could possibly represent palaeo-activity. High microbial activity in the surficial layer could be due to current aerobic activity or a previous signal.

Moscow MC (LEV5MC)

Bulk characteristics from Moscow MC (Figure 5.23) present steady values throughout the core, with an exception at the bottom layer which also seems to be the layer with the highest methane concentration. OC% is around 0.5% and shows no increase in the surficial layer whereas δ13Corg values are consistent at around −26‰. At 36-37 cm b.s.f the OC% shows a small increase whereas the δ13Corg a decrease to about −30‰. At the same time methane concentration presents its peak at the same depth. Archaeol, which is present throughout the core, begins to increase just above where the peak of methane is observed (at 36-27 cm b.s.f). PMI shows a similar strong peak, around 35 ng/g dw, within the zone of methane depletion. This strong decrease in δ13Corg in combination with an increase in archaeal biomarkers in the zone where methane decreases can be assumed to be evidence of the anaerobic oxidation of methane (AOM), taking place in the 28-37 cm b.s.f layer.

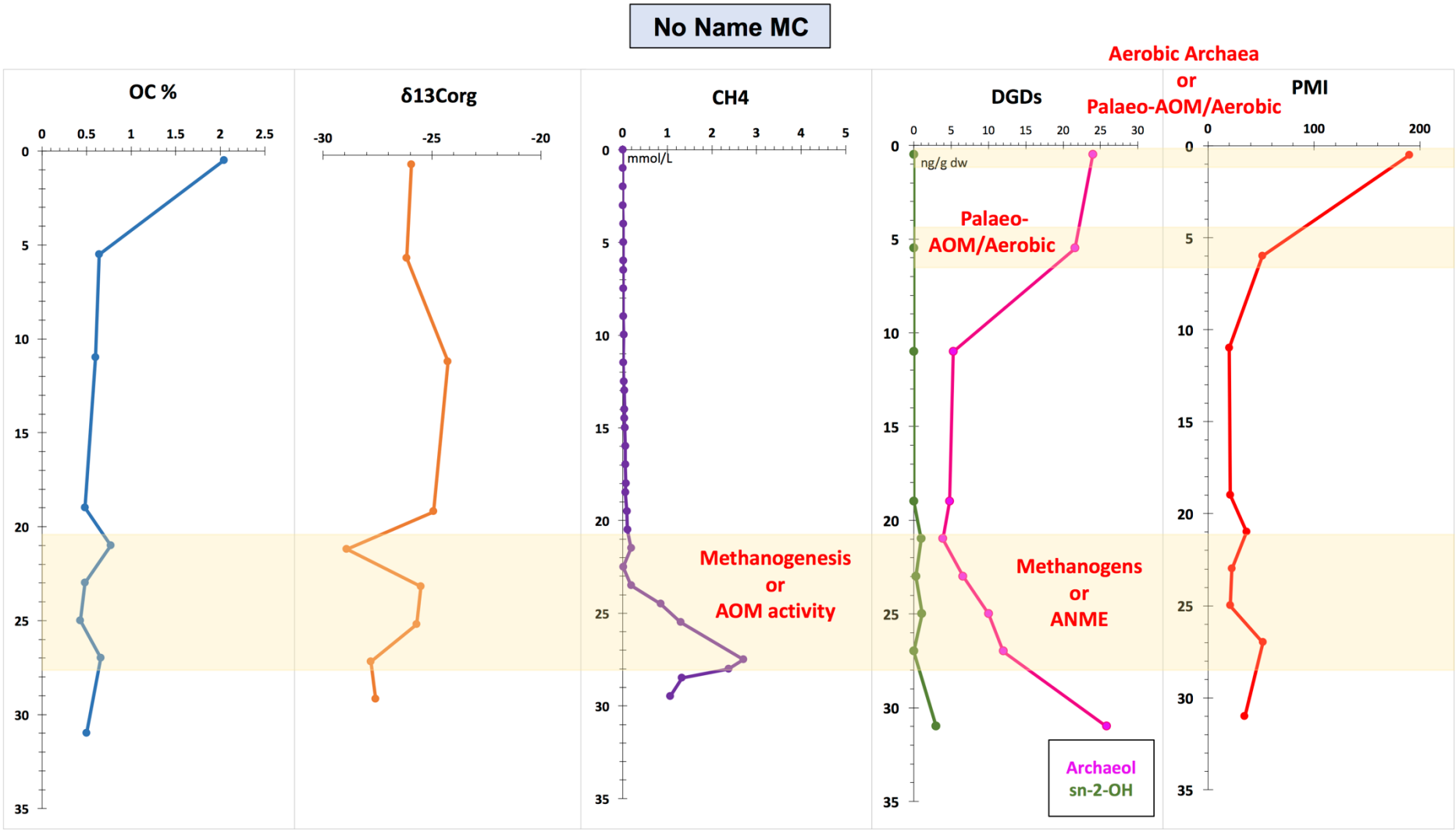

Figure 5.22. Bulk parameters (OC%, δ13Corg), CH4 flux and archaeal biomarkers (DGDs and PMI) for No Name MC.

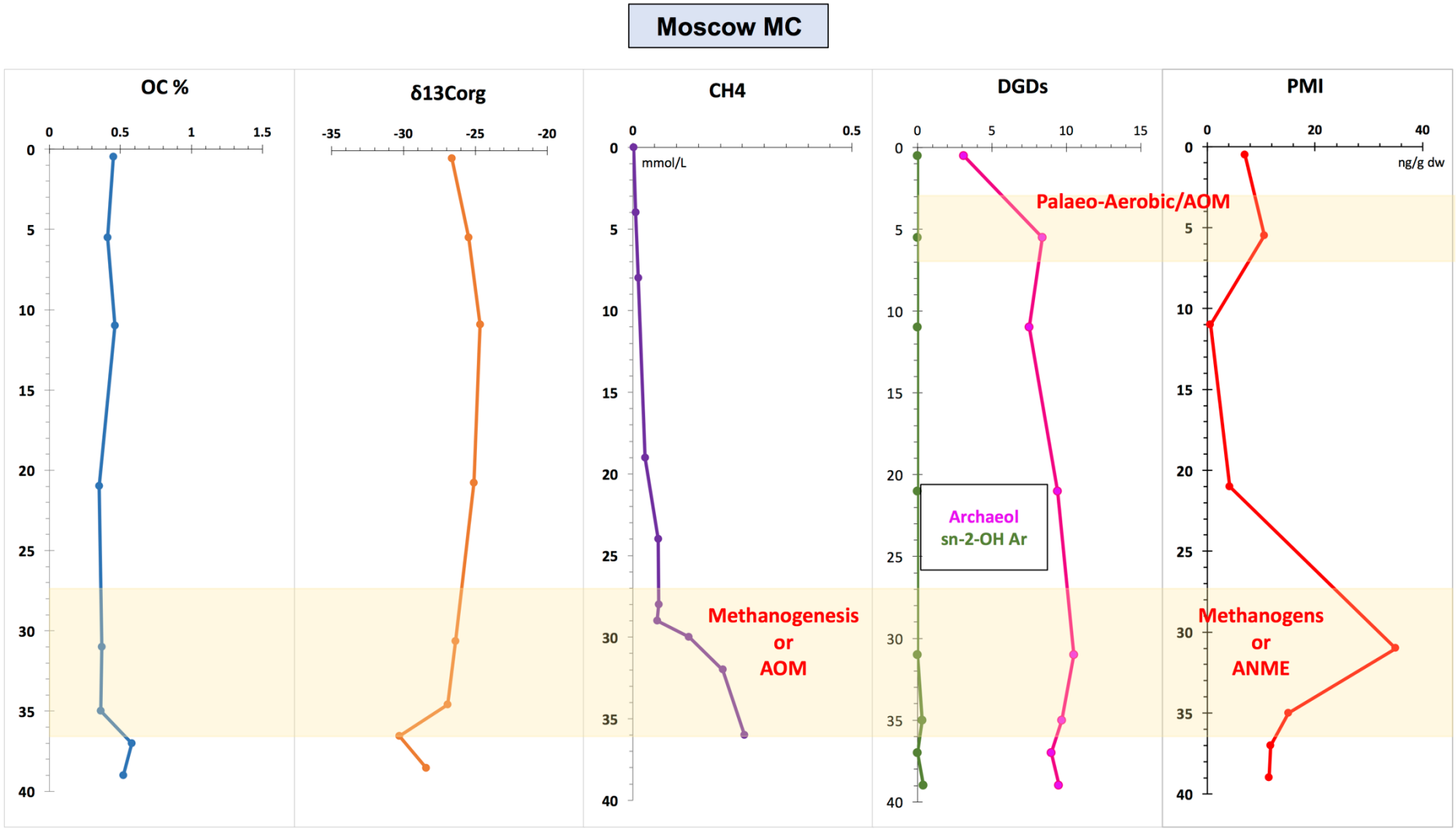

Figure 5.23. Bulk parameters (OC%, δ13Corg), CH4 flux and archaeal biomarkers (DGDs and PMI) for Moscow MC.

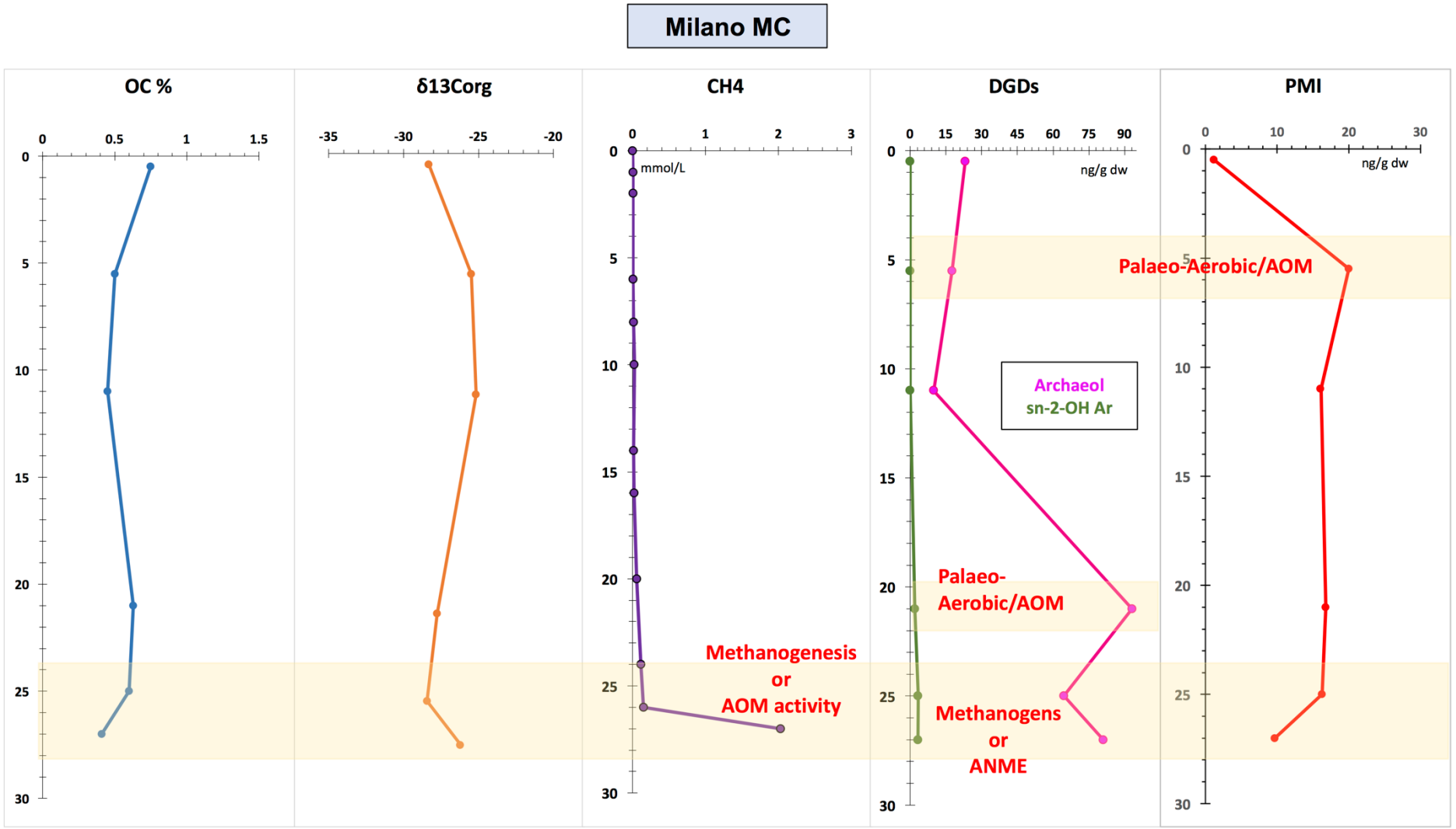

Figure 5.24. Bulk parameters (OC%, δ13Corg), CH4 flux and archaeal biomarkers (DGDs and PMI) for Milano MC.

Milano MC (LEV7MC)

The bulk geochemical characteristics from Milano MC (Figure 5.24) present a few variations throughout the core, with OC% values between 0.4-0.8% and δ13Corg between −29‰ and −25‰. The top layer at 0-5 cm b.s.f shows a slight increase in the OC% content which can be attributed to an increase in biological content, whereas δ13Corg throughout the whole core point to a terrigenous input of organic matter. Methane concentrations are low throughout the core but show a slight increase between 20-27 cm b.s.f of up to about 2mmol/L. Once again archaeol is in much higher concentrations than sn-2-hydroxyarchaeol and seems to present 2 peaks at around 21 cm b.s.f and 27 cm b.s.f. The deepest peak could represent active methanogenesis or AOM activity whereas the shallower peak could be a sign of palaeo-AOM/methanogenesis. PMI begins to increase at 5 cm b.s.f and remains steady until ~25 cm b.s.f where its concentration begins to decrease. Its peak at around 5 cm b.s.f could be an indication of palaeo-aerobic activity.

5.4 SULFATE REDUCTION AND BACTERIAL ACTIVITY

The process of sulfate reduction (described in Chapter 1) has been found to be coupled to the anaerobic oxidation of methane (AOM) in anoxic sediments. This linkage between sulfate-reducing bacteria (SRB) and methane oxidizing archaea (ANME) was confirmed in a study that microscopically identified a consortium of these microbes from the Cascadia margin [90].

Despite the fact that sulfate reducers are clearly implicated in the process of AOM there are very few biomarkers that can be exclusively attributed to the SRB partners [258]. Unlike archaeal membranes, bacterial membranes are thought to contain alkyl chains ester-linked to glycerol. Fatty acids have been used widely as SRB biomarkers, especially the iso and anteiso C15 and C17 [90,217], but these compounds are also produced by other bacteria and cannot be used as tracers of particular prokaryotic processes. However, fatty acids with site-specific methyl groups, cyclic moieties and double bonds which are less common have been found to be more abundant in anaerobic bacteria [259].

Hopanoid compounds (pentacyclic triterpenoids) are also well-documented biomarkers for bacteria [148], but up until recently these structures had not been found in cultures of anaerobic bacteria and were considered to be diagnostic for aerobic organisms. However, during the study of modern methane seeps [217] suggested that the observed 13C depleted C30 hopanoids belonged to anaerobic organisms. [260] also suggested that

the common hopanoid diplopterol can be derived from anaerobic chemoorganotrophic bacteria (even though aerobic methanotrophic bacteria were not exluded as source organisms). This anaerobic bacterial source of diplopterol and diploptene has also been confirmed recently by various studies [261–263].
It is therefore evident that when studying the source of hopanoids extreme caution must be taken before assigning them to a source organism [258].

During this study, the distribution of fatty acids was analysed while focus was given to the diagnostic iC15:0/aiC15:0, iC17:0/aiC17:0 and C16:1ω5. Biogenic hopanes (27β and C31ββ) and biogenic hopenes (TNH, NH13 and Diplotene) (Table 5.4) were also detected in all cores. All fatty acids and diploptene are presented seperately for each core. The surficial 0-1 cm b.s.f layer of Gelendzhik MC and No Name MC presented such high concentrations of bacterial fatty acids that it overshadowed all other values and was therefore not used in the graphs.

Gelendzhik MC

The core retrieved from Gelendzhik (
Figure 5.25) showed really high fatty acid and diploptene concentrations in the 0-1 cm b.s.f, therefore implying increased recent or palaeo- bacterial activity on the cores surface. A second peak in both fatty acids and diploptene was observed at 5 cm b.s.f and it is most likely a signal of palaeo- bacterial activity. At around 10 cm b.s.f all concentrations are minimized. Between 20 and 25 cm b.s.f there is a second but much smaller peak in all fatty acids which is in good agreement with the archaeal distributions mentioned previously and could imply the activity of sulfate reducing bacteria. However, none of the characteristic fatty acids seem to have any prominent differences in distributions at that depth as one would expect. Diploptene on the other hand does not show any significant fluctuations below 10 cm b.s.f mark.

No Name

The core taken from the No Name MC (Figure 5.26) location shows similar patterns of the fatty acid and diploptene distributions. Once again, the surficial sediment 0-1 cm b.s.f contained very high concentrations of fatty acids and is therefore not depicted in the graph. This high FA presence presents itself once again at ~ 10 cm b.s.f and is associated with palaeo- bacterial activity. The values of diploptene are also elevated in the same layers. At 27 cm b.s.f there is a slight increase in the fatty acid concentrations which is also were an increase in the archaeal signal is observed. This FA increase is minimal and as a result the possibility of sulfate reduction taking place in the area cannot be said with certainty.

Moscow MC

The core taken from Moscow MC (Figure 5.27) also shows increased concentrations (although not as high as in the previous two cores) of fatty acids and diploptene in the surficial layer thus proving current or perhaps previous bacterial activity. At around 5 cm b.s.f a peak of SRB fatty acids is observed which can most likely be attributed to palaeo-SRB activity. In contrast to the previous two cores, there is a prominent increase of the aiC15:0 FA in the 25-35 cm b.s.f layer. This fatty acid in particular is a diagnostic biomarker of sulfate reducing bacteria and especially the ones associated with the ANME-1 cluster. Furthermore, archaeal biomarkers also presented a maximum in this layer during which a methane decrease was also observed. As a result, we could assume that anaerobic oxidation of methane coupled to sulfate reduction is being performed at this depth.

Milano MC

Bacterial biomarkers from Milano MC (Figure 5.28) exhibit similar distributions with the previously mentioned ones from Moscow MC. The surficial layer is characterized by an abundance of fatty acids and diploptene indicating the presence of aerobic bacterial organisms. Similarly to Moscow MC at around 5 cm b.s.f the aiC15:0 FA presents a significant peak which is an indication of palaeo- SRB activity. From about 10 cm b.s.f downwards all concentrations present minimum values until around 22 cm b.s.f where a second peak of fatty acids is observed. Once again, the aiC15:0 acid presents the highest concentrations in the same zone in which archaeal biomarkers peak, and methane decreases. All this information further supports the possibility of AOM activity coupled to sulfate reduction taking place in the zone beneath 20 cm b.s.f.

A general conclusion concerning the bacterial activity found in all four multi-cores would have to be that the surficial layer of each core as well as the layer at around 5 cm b.s.f presents high bacterial activity which is apparent from the concentrations of the hopanoid diploptene and from specific bacterial fatty acids. This activity can either be recent or can represent a palaeo-signal. Presumed sulfate reduction also takes place at the same depth in all cores, which is between 20 and 35 cm b.s.f.

Core	Biogenic hopanes (ng/g)		Biogenic hopenes (ng/g)		
Gelendzhik (LEV1MC)	**27β (Tβ)**	**31ββ**	**TNH**	**NH13**	**D**
0-1 cm	15,29	23,20	4,52	31,71	20,68
5-6 cm	16,11	24,13	11,24	60,23	91,83
10-12 cm	14,71	35,22	6,32	30,32	6,81
14-16 cm	13,34	33,56	5,04	22,41	4,39
18-20 cm	9,64	18,75	3,15	20,93	4,45
20-22 cm	11,87	32,38	4,33	31,42	3,78
22 -24 cm	15,39	36,80	5,21	32,10	6,19
30-32 cm	11,39	23,26	4,46	23,01	3,16
38-39.5 cm	10,80	36,68	7,29	17,70	3,76
No Name MC (LEV3MC)					
0-1 cm	6,87	19,86	7,12	13,21	145,58
5-6 cm	10,49	16,14	10,49	11,23	20,98
10-12 cm	13,20	23,39	5,27	23,81	9,72
18-20 cm	13,84	28,76	4,42	26,42	4,22
20-22 cm	15,33	24,14	5,07	28,06	6,76
22-24 cm	11,57	17,57	16,96	19,15	4,26
24-26 cm	10,85	18,57	2,91	20,03	6,52
26-28 cm	9,92	22,80	3,67	23,51	6,02
30-32 cm	11,71	21,66	18,23	25,20	8,58
Moscow MC (LEV5MC)					
0-1 cm	8,10	18,53	2,51	8,92	14,69
5-6 cm	10,42	27,44	6,17	21,78	18,79
10-12 cm	9,56	27,87	6,05	21,26	8,15
20-22 cm	6,13	17,74	3,70	15,44	3,22
30-32 cm	8,39	23,92	5,04	19,44	7,37
34-36 cm	6,46	18,45	3,99	15,45	5,59
36-38 cm	5,05	16,24	3,05	12,73	4,05
38-40 cm	8,36	23,72	4,94	18,28	5,82
Milano MC (LEV7MC)					
0-1 cm	14,17	45,85	12,52	11,18	39,68
4-6 cm	11,96	42,88	14,55	12,90	19,94
10-12 cm	12,73	47,01	14,29	9,37	4,53
20-22 cm	12,95	49,93	15,39	12,77	5,97
24-26 cm	10,55	42,41	12,61	12,34	6,04
26-28 cm	9,79	38,89	11,53	12,86	4,66

Core	Biogenic hopanes (ng/g)		Biogenic hopenes (ng/g)		
Gelendzhik (LEV1GC)	**27β (Tβ)**	**31ββ**	**TNH**	**NH13**	**D**
0-3 cm	9,14	31,00	9,00	5,58	2,54
15-17 cm	10,27	30,31	8,49	6,86	2,24
26-28 cm	9,91	33,59	7,54	6,84	2,64
42-44 cm	9,83	34,65	14,02	7,07	1,80
62-64 cm	11,23	39,09	13,02	8,56	2,50
No Name (LEV3GC)					
2-5 cm	6,47	15,10	7,33	28,81	2,02
5-7 cm	8,27	13,94	3,91	18,18	6,18
12-15 cm	10,29	6,42	4,02	19,64	88,59
20-23 cm	3,99	3,96	1,29	6,49	1,86
30-32 cm	8,72	13,86	3,66	18,52	5,77
62-64 cm	9,09	15,96	3,50	18,67	3,34
Moscow (LEV5GC)					
0-2 cm	7,35	15,15	4,44	13,56	8,19
10-12 cm	6,83	11,66	2,68	7,21	6,75
39-41 cm	5,32	11,35	3,55	11,38	3,44
100-102 cm	9,38	19,14	5,79	19,29	9,39
120-123 cm	7,33	14,61	4,29	15,02	4,99
Milano (LEV7GC)					
0-3 cm	10,60	33,69	7,20	19,55	13,69
40-42 cm	9,05	31,34	8,19	18,61	3,45
60-62 cm	9,30	32,36	7,37	20,65	3,42
90-92 cm	11,68	37,07	8,78	20,81	4,35
Leipzig (LEV9GC)					
10-12 cm	13,81	16,29	4,01	25,86	3,66
20-22 cm	17,07	24,36	7,76	33,40	15,01
40-42 cm	15,34	20,39	6,63	27,82	7,91
70-72 cm	14,05	22,81	5,97	29,73	5,23
90-92 cm	15,00	21,65	6,15	34,45	5,22
110-112 cm	13,22	18,63	5,14	24,98	4,52

Table 5.4. Concentrations (ng/g) of biogenic hopanes and hopenes in multi- and gravity-cores. Full compound names are mentioned previously, in Table 5.2.

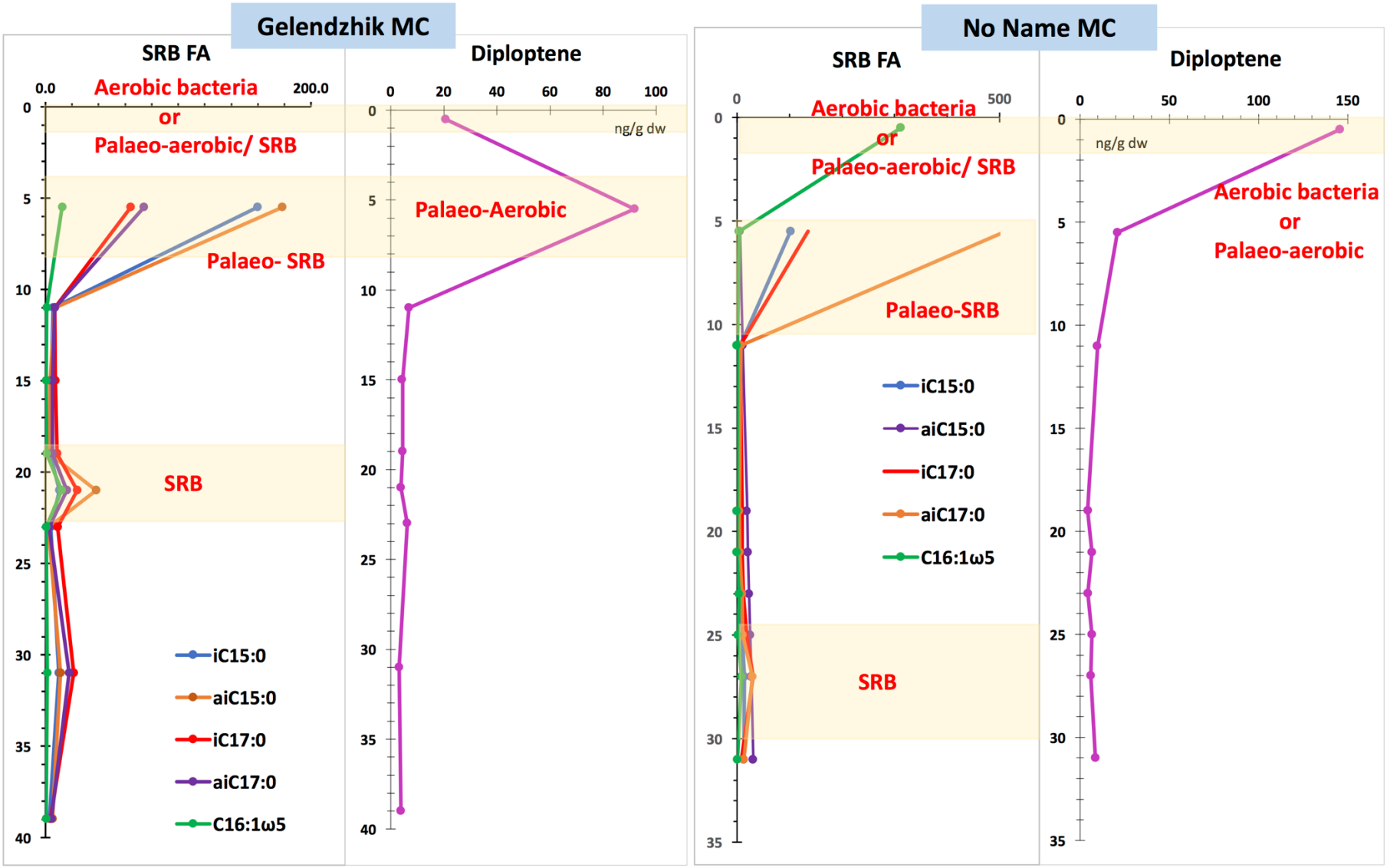

Figure 5.25 and Figure 5.26. SRB fatty acids and diploptene distributions at Gelendzhik MC and No Name MC.

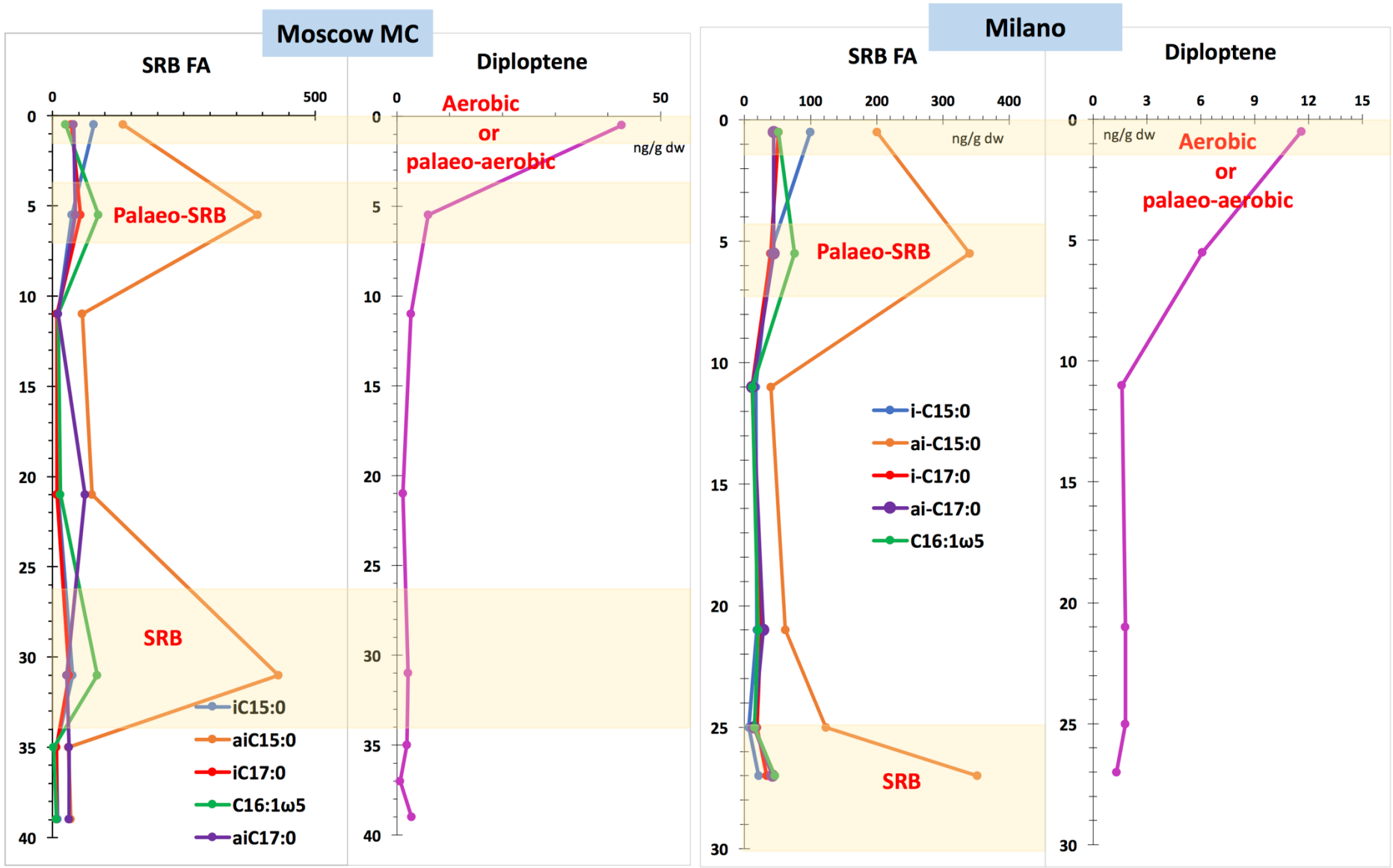

Figure 5.27 and Figure 5.28. SRB fatty acids and diploptene distributions at Moscow MC and Milano MC.

5.5 CHARACTERIZATION OF AOM COMMUNITIES

Phylogenetic analysis (ribosomal RNA (rRna) gene sequences) of the communities mediating the anaerobic oxidation of methane have revealed that there are three distinct lineages amongst the Euryarchaeota, which are responsible for this process. These ANaerobic MEthanotrophs (ANME) include the 1) lineage ANME-1, which so far does not have any cultured relatives [92,105,124], 2) lineage ANME-2, which is affiliated to the cultuterd members of the genus *Methanosarcinales* [90,92,97], and 3) lineage ANME-3, which is also affiliated with *Methanosarcinales* but more closely to *Methanococcoides spp.* than are the ANME-1 and ANME-2 [92,93].

In terms of the lipid membrane composition of these ANME, this is likely to be different as well, but since no cultures exist so far there are no conclusive data. However, a clear distinction between the lipids of ANME-1 and ANME-2 was made by [172] during the study of archaeal communities in microbial mats from the northwestern Black Sea. According to the study the distinction is made based on the relative abundances of archaeol and sn-2-hydroxyarchaeol. When methanotrophs affiliated with the ANME-2 cluster were the prevailing community, sn-2-hydroxyarchaeol was found in higher concentrations in comparison to archaeol. The abundance of archaeol on the other side, in combination with high concentrations of GDGTs, is linked to the ANME-1 cluster.

As has been mentioned before ANME-1 and ANME-2 Archaea have been found in consortia with sulfate reducing bacteria of the Seep-SRB1 cluster, which belongs to the *Desulfosarcina/Desulfococcus* group (DSS) [91,97]. Apart from the differences in the lipid content of archaeal communities, compositional variations in these SRB could also be used to differentiate between ANME clusters. Even though the *iso*- and *anteiso*- branched C15:0 fatty acids have been found in all AOM communities [174], their ratio (aiC15:0/iC15:0) has been found to be higher in ANME-1/Seep-SRB1 in comparison to ANME-2/Seep-SRB1 communities [174]. A value over 2 is usually indicative of the ANME-1 associated SRB, but there seems to be a large overlap between the two SRB ecotypes so this ratio should be used with caution [174]. Furthermore, the characteristic fatty acid C16:1ω5 has been found in high concentrations in ANME-2/Seep-SRB1 dominated systems [172,177]. The C16:1ω5/iC15:0 ratio is used to distinguish between these communities since the C16:1ω5 concentrations are significantly higher in the SRB eco-types associated with ANME-2, and a value below 1.8 for the ratio is considered to be a strong indicator for the Seep-SRB1 associated with ANME-1 [174]. However, this ratio doesn't seem to apply for the distinction between ANME-2 and ANME-3 since it appears to be similar. [177] found that the presence of the cyC17:1ω5 is restricted to the Seep-SRB1 communities associated with ANME-2 and therefore it is used to distinguish between those two. Finally, [93] found

that the DBB group associated with ANME-3 show high amounts of the characteristic C17:1ω6 fatty acid.

In all studied cores (Figure 5.29) the archaeal lipid ratio, sn-2-hydroxyarchaeol/archaeol, exhibits values way below the 0.8 mark used to distinguish between ANME-1 and ANME-2, therefore classifying the communities as ANME-1. Bacterial lipids on the other hand were a bit more inconclusive. The C16:1ω5/iC15:0 ratio also supports the presence of ANME-1 communities since it was mostly below the 1.8 mark. Some small exceptions are present in the Moscow and Milano core which are due to higher concentrations of the C16:1ω5 fatty acid. Finally, the aiC15:0/iC15:0 ratio is much higher in the Moscow MC and Milano MC cores than it is in Gelendzhik MC and No Name MC. Specifically, the first two cores (Moscow and Milano) show values (>2) which clearly indicate that the communities formed belong to the ANME-1 cluster, whereas the other two cores (Gelendzhik and No Name) show much lower values for most parts of the cores.

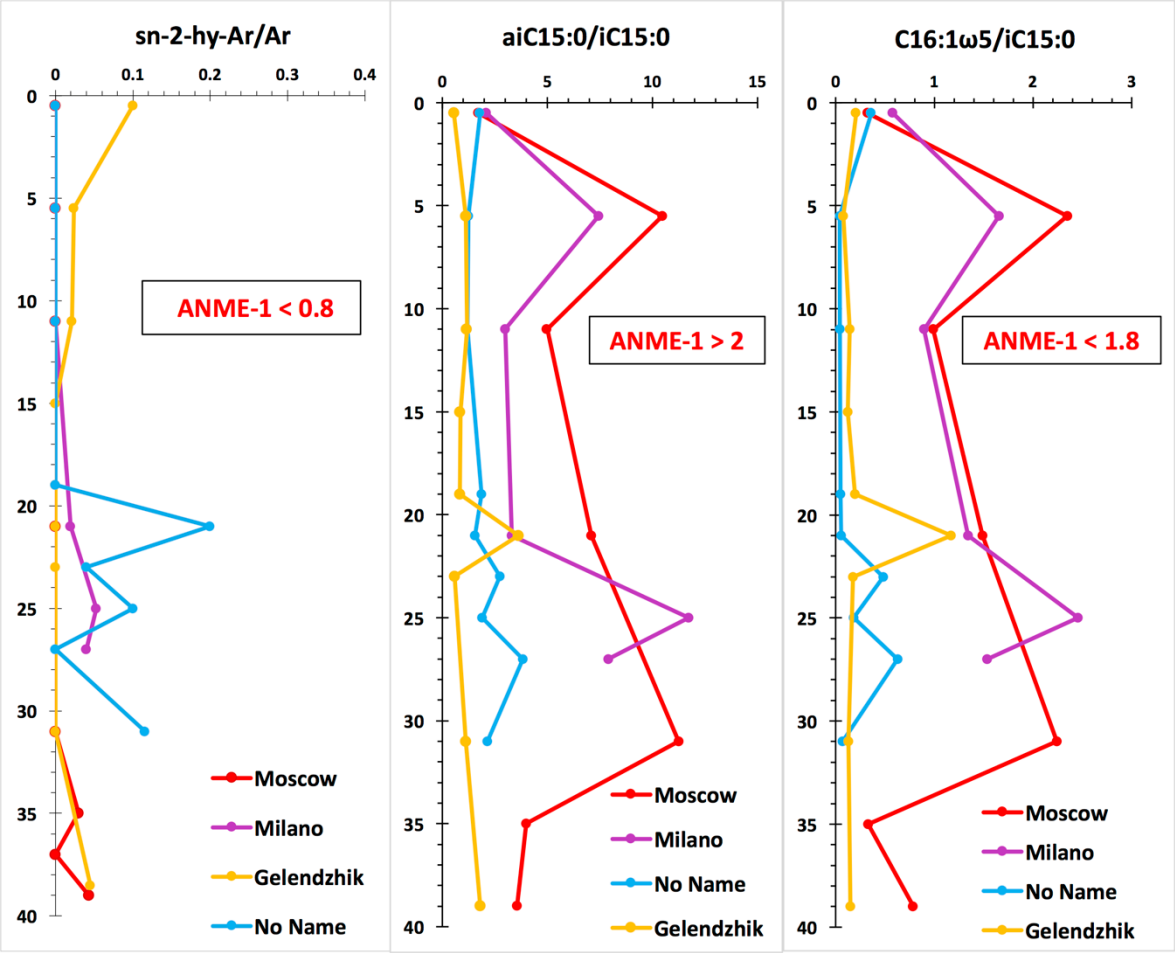

Figure 5.29. Diagnostic ratios of archaeal and bacterial membrane lipids for the identification of AOM communities.

CHAPTER 6 - CONCLUSIONS

The analysis of lipid biomarkers in both multi and gravity cores reveals that the organic matter is a complex mixture of components indigenous to the ascending mud matrix, a variety of in situ formed archaeal and bacterial lipids and finally, recent pelagic contributions which take place after the mud breccia deposition.

The main conclusions of this study are presented in two separate parts concerning the eruptional events, the source and thermal maturity of the indigenous organic matter and the microbial processes that take place after the eruption and mud breccia emplacement.

Possible eruptional events, source and thermal maturity of the organic matter

The organic matter which is associated with the ascending mud matrix provides information on the mud volcano dynamic processes. More specifically, separate events of mud flow expulsion as well as the thermal maturity and source origin of the organic matter can be inferred through the study of specific lipid biomarkers.

The lipid biomarker composition revealed relatively similar characteristics for all studied mud volcanoes with the apolar compounds strongly dominating the total organic extract. The mud matrix is composed of a mixture of recent as well as thermally altered organic matter. Most cores do not present any visible pelagic/hemipelagic mud neither on their surface nor within them, indicating that that the latest mud flow activity is relatively recent. Exceptions could be the gravity cores from Moscow (LEV5GC) and Gelendzhik (LEV1CGC) where a thin layer (~ 1cm-thick) of hemipelagic mud was present on their surface, indicating that at least these parts of the volcanoes are not currently active.

Through the compositional distributions of n-alkanes and n-alkanols as well as the CPI index possible eruptional events can be assumed to exist within each core. However, most distributions do not reveal major differences, especially in the shorter multi-cores. One definite compositional difference can be seen in the bottom sediment layer of the Moscow MC (LEV5MC) revealing a separate mud flow. Despite the relative distributional similarities in all cores there are some slight differences, which in combination with sedimentological descriptions can point out to separate mud flows.

The abundance of long-chain n-alkanes and n-alkanols with an odd-over-even and even-over-odd predominance respectively, in combination with the relatively high CPI values, indicate high inputs of terrestrial organic matter. Shorter-chain marine inputs are also present but in much lower concentrations. As a general result, we could say that this type

of organic material suggests an origin from sediments deposited under considerable terrigenous influence. This finding is in agreement with previous studies which concluded that the extruded sediment was deposited under riverine, lacustrine or even brackish conditions [202].

Information concerning the depositional environment of the sediment can also be obtained through characteristic biomarkers. High perylene concentrations in all cores indicate that the sediment was deposited under reducing/anoxic conditions. The existence of perylene in such concentrations is also an indication of relatively immature and most likely terrigenous organic matter. Low ratios of pristane/phytane and the existence of gammacerane could possibly indicate hypersaline depositional environments, although these results should be treated with caution due to analytical difficulties. Furthermore, the high abundance of C29 ααα steranes, which are thought to be absent in immature hypersaline sediments, is another indicator that contradicts this possibility of a hypersaline environment.

In terms of the maturity of the organic matter, all ratios of hopanes and steranes as well as the Methylphenanthrere Index (MPI1) suggested the presence of a thermally immature mud matrix with a shallow mobilization depth. This depth, between 1.5-2 km, can be inferred by the geothermal gradient of the area, which is at 30-35^{O}C/km [180]. Our results are in accordance to previous studies performed in the area [188] and are also supported by a high presence of immature biogenic hopenes and hopanes.

It is therefore apparent that the primary source of the erupted material in the Olimpi mud volcano field is located within similar stratigraphic units, from a shallow depth no deeper than 2 km. Previous studies have found a Middle-Upper Miocene (Messinian) age of the mud matrix, during which sedimentation in the area was lacustrine and fluvial in the non-evaporative basins [264]. The high terrigenous contributions and low marine ones found in all our cores seems to fit this description.

Microbial processes

The study of the organic matter which is formed after the emplacement of the sediment on the seafloor provides information on the distribution, composition and finally dynamics of the archaeal and bacterial communities.

In all studied cores, characteristic biomarkers of ANME and SRB communities were identified in the SMTZ in which the AOM activity presents its highest rates. The core taken from Gelendzhik MC presented the highest values of archaeal biomarkers indicating

higher AOM activity. Bacterial biomarkers such as characteristic fatty acids of sulfate reducing bacteria are also found in all cores, and present higher values in the sulfate-methane transition zone. Diploptene and other aerobic bacterial biomarkers presented their maximum concentrations in the surficial zones of Gelendzhik MC and No name MC, indicating higher surficial bacterial activity.

The ANaerobic MEthanotrophs (ANME) found in the area can be classified as ANME-1/Seep-SRB1 communities, based on the low ratios of sn-2-hydroxyarchaeol/archaeol and C16:1ω5/iC15:0 and the high ai-$C_{15:0}$/i-$C_{15:0.}$ ANME-1 communities usually present in subsurface sediments characterized by low-medium methane fluxes.

LIST OF ABBREVIATIONS

MV	Mud Volcano
OMV	Olimpi Mud Volcano
ANME	ANaerobic MEthanotrophs
AOM	Anaerobic Oxidation of Methane
SR	Sulfate Reduction
SRB	Sulfate Reducing Bacteria
SMI	Sulfate Methane Interaction
DIC	Dissolved Inorganic Carbon
GHSZ	Gas Hydrate Stability Zone
BSR	Bottom Simulating Reflector
SMTZ	Sulfate Methane Transition Zone
OC	Organic Carbon
FAME	Fatty Acid Methyl Esters
PAH	Polycyclic Aromatic Hydrocarbons
VPDB	Vienna Pee Dee Belemnite
MC	Multi Core
GC	Gravity Core
GC-MS	Gas Chromatography-Mass Spectrometry
SIM	Selected Ion Monitoring
R/V	Research Vessel
CPI	Carbon Preference Index
KIF	Kinetic Isotope Effects
FA	Fatty Acids
Bsf	Bellow sea floor
MPI1	Methylphenanthrene Index

APPENDIX I. Glossary

Accretionary prism/accretionary wedge: Body of fluid-rich sediment being accumulated at the leading edge of the overriding plate in a subduction zone; its base is a highly permeable fault called the decollement.

Argillokinetic: Caused by the mobility of clay-rich sediment.

Avalanche: Landslide on continental forearcs and slopes, often triggered by rapid fluid flow and/or gas- charged sediments.

Backstop: Mechanical abutment of the overriding continental plate to allow an accretionary wedge to build up; often the leading edge of the continental crust or older accreted rock of high strength.

BSR: Bottom-simulating reflector; a characteristic reflection in seismic data with reversed polarity relative to the seafloor reflection. It usually follows the seafloor topography at a certain depth, which is defined by the thermal gradient of the area. The cause of the reflection is free gas beneath the zone of gas hydrate stability.

Cauldron: Subsided crater area, often used as a synonym for crater.

Chemoherm: Seafloor feature of variable geometry, which is mostly composed of authigenic carbonate from inorganic precipitation.

Chimney: Precipitates of more or less cylindrical shape around the wall of a conduit.

Conduit: Cylindrical or odd-shaped feeder channel through which mud ascends.

Conglomerate: Here, like mud breccia, but with rounded rather than angular clasts and rock fragments.

Crater: Depression in the crestal area of cone-shaped MVs.

Decollement: Plate boundary fault in subduction zones that represents the main detachment in which many thrust faults root.

Diapir: Clay- and fluid-rich intrusion.

Diapirism: Intrusion of a sedimentary body into its overburden without reaching the surface.

Diatreme: Type of mud extrusive feature that evolved from a violent eruption of overpressured mud, cross-cutting.

Eruption: Extrusive outflow of mud and fluids that may be quiescent (mostly degassing) or vigorous (see diatreme).

Ejecta: Material extruded during violent eruptions.

Extrusiva: All extruded material. Fumarole: Product of volcanic devolatilization, sometimes in conjunction with precipitation of, for ex- ample, sulfur.

Gryphon: Small cones or mud craters off the crest, or at the flank of the mud volcano.

Hydrofracturation: Brittle failure of rock due to enhanced pore fluid pressures; a common phenomenon in overpressured strata of, for example, accretionary wedges.

Liquefaction: Process of rehydrating a partly compacted claystone or shale, in which the internal friction is zero as all stress is taken up by the fluid.

Melange: Deformed mixture of usually clay-bearing lithologies, often found in tectonic fault zones and accretionary prisms.

Mud breccia: Type of sediment that is characterized by a clay mineral-rich matrix in which various amounts of (firmer) rock fragments and clasts (usually of the overburden rock through which the mud ascended) are embedded.

Mud diapir: Intrusive body of shale or clay that does not reach the surface.

Mud lump: Small mud volcano (a few meters in size and height).

Mud mound: Accumulation of mud debris, biogenetic detritus, etc., that is usually cemented by carbonate precipitated by organisms. In contrast to mud diapirs or volcanoes, mud mounds do not necessarily involve the movement of a mud body and hence are excluded from this summary. Owing to the carbonate cementation, they are often preserved over long periods of time (i.e., since the Precambrian).

Mud pie: Flat (slope angle $<5^{o}$) mud extrusive feature.

Mud pool: Soupy mud accumulation in the crater (or, more generally speaking, central) area of a mud volcano or diatreme; a synonym is tassik.

Mud pot: Small mud mound.

Mud ridge: Elongated mud extrusive feature, supposedly related to faulting or folding.

Mud volcano: Surface expression of mud that originated from depth. Depending on the geometry of the conduit and the physical properties of the extrusiva, the feature may be a dome (cone; see Figure 2a) or a pie with low topographic relief.

Olistolith: Rock carried by an olistostrome.

Olistostrome: Deposit of a fluid-rich mudflow, often containing debris that was accumulated during emplacement.

Overpressured: Here, sediment with porosities higher than predicted from compaction law under a certain lithostatic pressure, i.e., undercompacted sediment.

Parent bed: Stratigraphic horizon that provides the bulk of material that ascends and extrudes; often under- compacted and rich in clay or fluids.

Plasticity: Difference between the water content of a material at its liquid and plastic limit, given in wt% H2O.

Pockmark: Seafloor expression of high fluid discharge (venting) through a conduit, often resulting in a depression relative to the surrounding seafloor. Scaly fabrics: Texture of clays and claystones having been dewatered and sheared, often with striations.

Seepage: See vent.

Tassik: See mud pool.

Toe: Frontal tip of an accretionary wedge.

Vent: Location (on the seafloor) at which fluids escape

APPENDIX II. Chronostratigraphic Chart

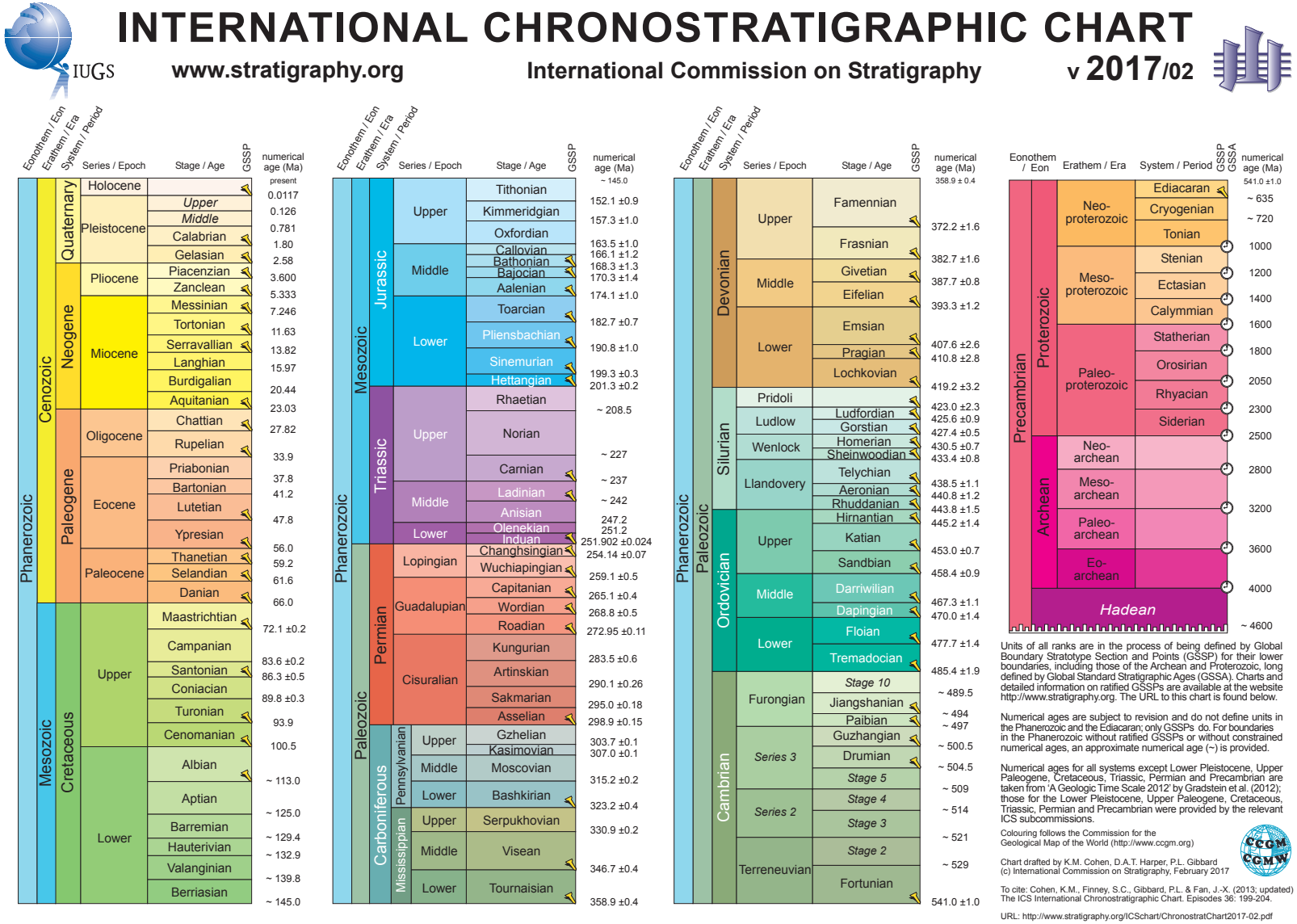

BIBLIOGRAPHY

1. Dimitrov L. Mud volcanoes – the most important pathways for degassing deeply buried sediments. *Earth Science Review*. 2002; 59:49-76.
2. Milkov A V. Worldwide distribution of submarine mud volcanoes and associated gas hydrates. 2000.
3. Dimitrov LI. Mud volcanoes—a significant source of atmospheric methane.
4. Kopf AJ. Significance of mud volcanism. *Reviews of Geophysics*. 2002; 40(2):1005.
5. Brown KM. The nature and hydrogeologic significance of mud diapirs and diatremes for accretionary systems. *Journal of Geophysical Research*. 1990; 95(B6):8969.
6. Judd AG., Hovland M. Seabed fluid flow: the impact of geology, biology and the marine environment. *ResearchGate*. 2007; (February):1-442.
7. Higgins., Saunders. *Mud Volcanoes: Their Nature and Origin*.; 1974.
8. Ivanov MK., Limonov AF., Van Weering TCE. Comparative characteristics of the Black Sea and Mediterranean Ridge mud volcanoes. *Marine Geology*. 1996; 132(1-4):253-271.
9. Woodside J. Shallow gas and gas hydrates in the Anaximander Mountains regions, eastern Mediterranean Sea. 1998.
10. Ginsburg and Soloviev. Submarine Gas Hydrates, VNIIOkeangeologia, St. Petersburg. 1994:199pp.
11. Limonov AF., Woodside JM., Cita MB., Ivanov MK. The mediterranean ridge and related mud diapirism: A background. *Marine Geology*. 1996.
12. Prior D., Doyle E., Kaluza M. Evidence for sediment eruption on deep sea floor, Gulf of Mexico. *Science*. 1989.
13. Akhmanov GG., Woodside JM. Mud volcanic samples in the context of the Mediterranean Ridge mud diapiric belt. *Proceeding of the Ocean Drilling Program, Scientific Results, Vol 160*. 1998; 160:597-605.
14. Hovland M., Hill A., Stokes D. The structure and geomorphology of the Dashgil mud volcano, Azerbaijan. *Geomorphology*. 1997; 21(1):1-15.
15. Deville E., Battani A., Griboulard R., Guerlais S., Herbin JP., Houzay JP., Muller C., Prinzhofer A. The origin and processes of mud volcanism: new insights from Trinidad. *Geological Society, London, Special Publications*. 2003; 216(1).
16. Judd A. Gas Emissions from Mud Volcanoes. Significance to Global Climate Change. *Mud Volcanoes, Geodynamics and Seismicity*. 2005; (51):295.
17. Kopf AJ. Significance of mud volcanism. *Reviews of Geophysics*. 2002; 40(2):1-52.
18. Martinelli G., Panahi B., eds. *Mud Volcanoes, Geodynamics and Seismicity*. Vol 51. Berlin/Heidelberg: Springer-Verlag; 2005.
19. Dimitrov L., Woodside J. Deep sea pockmark environments in the eastern Mediterranean. *Marine Geology*. 2003; 195(1-4):263-276.
20. Milkov A V., Sassen R., Apanasovich T V., Dadashev FG. Global gas flux from mud volcanoes: A significant source of fossil methane in the atmosphere and the ocean. 2003.
21. Tinivella U., Giustiniani M. An Overview of Mud Volcanoes Associated to Gas Hydrate System. In: *Updates in Volcanology - New Advances in Understanding Volcanic Systems*. InTech; 2012.
22. Söderberg P., Flodén T. Gas seepages, gas eruptions and degassing structures in the seafloor along the Str??mma tectonic lineament in the crystalline Stockholm Archipelago, east Sweden. *Continental Shelf Research*. 1992;

12(10):1157-1171.
23. Kopf A., Klaeschen D., Mascle J. Extreme efficiency of mud volcanism in dewatering accretionary prisms. *Earth and Planetary Science Letters*. 2001; 189(3-4):295-313.
24. Delisle G., von Rad U., Andruleit H., von Daniels C., Tabrez A., Inam A. Active mud volcanoes on- and offshore eastern Makran, Pakistan. *International Journal of Earth Sciences*. 2002; 91(1):93-110.
25. Etiope G., Klusman RW. Geologic emissions of methane to the atmosphere. *Chemosphere*. 2002; 49(8):777-789.
26. Yassir N. The role of shear stress in mobilizing deep-seated mud volcanoes: geological and geomechanical evidence from Trinidad and Taiwan. *Geological Society, London, Special Publications*. 2003; 216(1).
27. Shakirov R., Obzhirov A., Suess E., Salyuk A., Biebow N. Mud volcanoes and gas vents in the Okhotsk Sea area. *Geo-Marine Letters*. 2004; 24(3):140-149.
28. Stewart SA., Davies RJ. Structure and emplacement of mud volcano systems in the South Caspian Basin. *AAPG Bulletin*. 2006; 90(5):771-786.
29. Martinelli G. Mud volcanoes of Italy: a review. *Giornale di geologia*. 1999.
30. Motyka ' RJ., Poreda RJ., Jeffrey~ AWA. Geochemistry, isotopic composition, and origin of fluids em~ating from mud volcanoes in the Copper River basin, Alaska. 53:29-41.
31. Robertson P., Burke K. Evolution of southern Caribbean Plate boundary, vicinity of Trinidad and Tobago. *AAPG Bulletin*. 1989; 73(4).
32. Brown K., Westbrook GK. Mud diapirism and subcretion in the Barbados Ridge Accretionary Complex: The role of fluids in accretionary processes. *Tectonics*. 1988; 7(3):613-640.
33. Muller C., Theilen F., Milkereit B. Natural Gas: Igniting New Markets. *World Oil*. 2001; 222(1):60-65.
34. Kenyon NH., Lvanov MK., Akhmetzhanov AM. Geological processes on the Northeast Atlantic margin: preliminary results of geological and geophysical investigations during the TTR-8 cruise of R/V Professor Logachev, June-August 1998; IOC. Technical series; Vol.:54; 1999. *IOC Technical Series UNESCO*. 1999; 54.
35. Pérez-Belzuz F., Alonso B., Ercilla G. History of mud diapirism and trigger mechanisms in the Western Alboran Sea. *Tectonophysics*. 1997; 282(1-4):399-422.
36. Neurauter -H H Roberts TW. Three generations of mud volcanoes on the Louisiana continental slope. 1994; 14:120-125.
37. Orudjieva DS, Vorobiev VT RA (1982). Space-born investigations of oil prospective areas of Northeastern Caspian Basin (in Russian). 1982.
38. Ginsburg GD., Milkov A V., Soloviev VA., Egorov A V., Cherkashev GA., Vogt PR., Crane K., Lorenson TD., Khutorskoy MD. Gas hydrate accumulation at the Håkon Mosby Mud Volcano. *Geo-Marine Letters*. 1999; 19(1-2):57-67.
39. Mascle J., Mary F., Praeg D., Brosolo L., Camera L., Ceramicola S., Dupré S. Distribution and geological control of mud volcanoes and other fluid/free gas seepage features in the Mediterranean Sea and nearby Gulf of Cadiz. *Geo-Marine Letters*. 2014; 34(2-3):89-110.
40. Cita MB., Broglia C., Malinverno A., Spezzibottiani G., Tomadin L., Violanti D. Pelagic sedimentation in the southern Calabrian ridge and western Mediterranean ridge. *Rapports et Proces-Verbaux des Reunions - Commission Internationale pour l'Exploration Scientifique de la Mer Mediterranee*. 1981; 27(8).
41. Praeg D., Ceramicola S., Barbieri R., Unnithan V., Wardell N. Tectonically-driven mud volcanism since the late Pliocene on the Calabrian accretionary prism,

central Mediterranean Sea. *Marine and Petroleum Geology*. 2009; 26(9):1849-1865.
42. Blinova VN., Comas MC., Ivanov MK., Poludetkina EN., Matveeva T V. Active mud volcanism in the West Alboran Basin: Geochemical evidence of hydrocarbon seepage. *Marine and Petroleum Geology*. 2011; 28(8):1483-1504.
43. Somoza L., Medialdea T., León R., Ercilla G., Vázquez JT., Farran M., Hernández-Molina J., González J., Juan C., Fernández-Puga MC. Structure of mud volcano systems and pockmarks in the region of the Ceuta Contourite Depositional System (Western Alborán Sea). *Marine Geology*. 2012; 332-334:4-26.
44. Gamberi F., Rovere M. Mud diapirs, mud volcanoes and fluid flow in the rear of the Calabrian Arc Orogenic Wedge (southeastern Tyrrhenian sea). *Basin Research*. 2010; 22(4):452-464.
45. Martinelli G., Judd A. Mud volcanoes of Italy. *Geological Journal*. 2004; 39(1):49-61.
46. Guliev IS., Feizullayev AA. Geochemistry of Hydrocarbon Seepages in Azerbaijan. 1996:63-70.
47. Hovland M. Are there commercial deposits of marine hydrates in ocean sediments? *Energy Explor Exploit*. 2000; 18(4):339–347.
48. Milkov A., Sassen R., Apanasovich T., Dadashev F. Estimate of global gas flux from mud volcanoes. *Proc of the 7th Conference Gas in*. 2002.
49. Hunt JM., Whelan JK. Volatile organic compounds in Quaternary sediments. *Organic Geochemistry*. 1979; 1(4):219-224.
50. Rice., Claypool. *Generation, Accumulation, and Resource Potential of Biogenic Gas*. Vol 51. American Association of Petroleum Geologists; 1981.
51. Floodgate GD., Judd AG. The origins of shallow gas. *Continental Shelf Research*. 1992; 12(10):1145-1156.
52. Hunt JM. Generation of gas and oil from coal and other terrestrial organic matter. *Organic Geochemistry*. 1991; 17(6):673-680.
53. Whiticar MJ. Carbon and hydrogen isotope systematics of bacterial formation and oxidation of methane. *Chemical Geology*. 1999; 161:291-314.
54. Claypool GE., Kvenvolden KA. Methane and other hydrocarbon gases in marine sediments. *Annual Review of Earth and Planetary Sciences*. 1983.
55. Lelieveld J., Crutzen PJ., Dentener FJ. Changing concentration, lifetime and climate forcing of atmospheric methane. *T ellus*. 1998; 50:128-150.
56. Petit J., Jouzel J., Raynaud D., Barkov N., Barnola J-M., Basile I., Bender M., Chappellaz J., Davis M., Delaygue G., Delmotte M., Kotlyakov V., Legrand M., Lorius C., PÉpin L., Ritz C., Saltzman E., Stievenard M. Climate and atmospheric history of the past 420,000 years from the Vostok ice core, Antarctica. *Oceanography*. 1999; 28:63-86.
57. Wuebbles DJ., Hayhoe K. Atmospheric methane and global change.
58. Prinzhofer AA., Huc AY. Genetic and post-genetic molecular and isotopic fractionations in natural gases. *Chemical Geology*. 1995; 126(3-4):281-290.
59. Kvenvolden K. Methane hydrates and global climate. 1988; 2(3):221-229.
60. Kvenvolden KA. Gas hydrates-Geological perspectives and global change. 1993.
61. Brooks JM., Cox HB., Bryant WR., Kennicutt Ii MC., Mann RG., Mcdonald TJ. Association of gas hydrates and oil seepage in the Gulf of Mexico. *Org Geochem*. 1985; 10:221-234.
62. Dallimore SR., Collett TS. Intrapermafrost gas hydrates from a deep core hole in the Mackenzie Delta, Northwest Territories, Canada. *Geology*. 1995; 23(6):527.
63. Sassen R., Joye S., Sweet ST., Defreitas DA., Milkov A V., Macdonald IR. Thermogenic gas hydrates and hydrocarbon gases in complex chemosynthetic

communities, Gulf of Mexico continental slope.
64. Ginsburg GD., Soloviev VA. Methane migration within the submarine gas-hydrate stability zone under deep-water conditions. *Marine Geology*. 1997; 137:49-57.
65. Milkov A. Gas hydrates of the Haakon Mosby mud volcano. 1998.
66. Bohrmann G., Torres ME. Gas Hydrates in Marine Sediments. In: *Marine Geochemistry*. Berlin/Heidelberg: Springer-Verlag; :481-512.
67. E. Dendy Sloan J. Gas Hydrates: Review of Physical/Chemical Properties. 1998.
68. Kvenvolden KA. Reassessment of the rates at which oil from natural souces enters the marine environment. *Mar Environ Res*. 1983; 10:223-243.
69. Makogon YF., Makogon TY., Holditch SA. Gas hydrate formation and dissociation with thermodynamic and kinetic inhibitors. In: Vol 1. Soc Pet Eng (SPE); 1999.
70. Borowski WS., Hoehler TM., Alperin MJ., Rodriguez NM., Paull CK. Significance of anaerobic methane oxidation in methane-rich sediments overlying the blake ridge gas hydratesI. 2000; 164.
71. Kvenvolden K a., Lorenson TD. The Global Occurrence of Natural Gas Hydrate. In: *Natural Gas Hydrates: Occurrence, Distribution, and Detection*. American Geophysical Union; 2001:3-18.
72. Zatsepina OY., Buffett BA. Phase equilibrium of gas hydrate: Implications for the formation of hydrate in the deep sea floor. *Geophysical Research Letters*. 1997; 24(13):1567-1570.
73. Tomkeieff SI., Walton EK., Randall BAO., Battey MH. *Dictionary of Petrology*. Wiley; 1983.
74. Mackay ME., Jarrard RD., Westbrook GK. Origin of bottom-simulating reflectors: Geophysical evidence from the Cascadia accretionary prism Shipboard Scientific Party of Ocean Drilling Program Leg 146.
75. Shipley TH., Ladd JW., Buffler RT., Watkins JS. Tectonic processes along the Middle America Trench inner slope. *Geological Society, London, Special Publications*. 1982; 10(1).
76. Paull CK., Hecker B., Commeau R., Freeman-Lynde RP., Neumann C., Corse WP., Golubic S., Hook JE., Sikes E., Curray J. Biological Communities at the Florida Escarpment Resemble Hydrothermal Vent Taxa. *Science*. 1984; 226(4677).
77. Suess E., Carson B., Ritger SD., Moore JC., Jones ML., Kulm, L. D. and Cochrane GR. Biological communities at vent sites along the subduction zone off Oregon. In: *Biological Communities at Vent Sites along the Subduction Zone off Oregon*. Biological Society of Washington; 1985.
78. Juniper SK., Sibuet M. Cold seep benthic communities in Japan subduction zones: spatial organization, trophic strategies and evidence for temporal evolution. *Marine Ecology Progress Series*. 40:115-126.
79. Sloan ED., Koh CA (Carolyn A. *Clathrate Hydrates of Natural Gases.* CRC Press; 2008.
80. Jørgensen BB., Boetius A. Feast and famine — microbial life in the deep-sea bed. *Nature Reviews Microbiology*. 2007; 5(10):770-781.
81. Henry PE., Foucher J-P., Le Pichon X., Sibuet M., Kobayashi K., Tarits P., Chamot-Rooke N., Furuta T., Schultheiss P. Interpretation of temperature measurements from the Kaiko-Nankai cruise: Modeling of fluid flow in clam colonies. *Earth and Planetary Science Letters*. 1992; 109:355-371.
82. Barry JP., Kochevar RE., Baxter CH. The influence of pore-water chemistry and physiology on the distribution of vesicomyid clams at cold seeps in Monterey Bay: Implications for patterns of chemosynthetic community organization. *Limnol Oceanogr*. 1997; 42(3):18-328.
83. Sahling H., Rickert D., Raymond L., Linke P., Suess E. Macrofaunal community

structure and sulfide flux at gas hydrate deposits from the Cascadia convergent margin, NE Pacific. *Marine Ecology Progress Series*. 2002; 231:121-138.
84. Levin LA., Ziebis W., Mendoza G., Growney V., Tryon M., Brown K., Mahn C., Gieskes J., Rathburn A. Spatial heterogeneity of macrofauna at northern California methane seeps: influence of sulfide concentration and fluid flow. *Marine Ecology Progress Series*. 2003; 265:123-139.
85. De Beer D., Sauter E., Niemann H., Kaul N., Foucher J-P., Witte U., Schlüter M., Boetius A. In situ fluxes and zonation of microbial activity in surface sediments of the Hå kon Mosby Mud Volcano. 2006.
86. Tryon MD., Brown KM. Complex flow patterns through Hydrate Ridge and their impact on seep biota. *Geophysical Research Letters*. 2001; 28(14):2863-2866.
87. Tryon M., Brown K., Dorman L., Sauter A. Instruments and methods A new benthic aqueous flux meter for very low to moderate discharge rates. *Deep-Sea Research I*. 2001; 48:2121-2146.
88. Sibuet M., Olu K. Biogeography, biodiversity and fluid dependence of deep-sea cold-seep communities at active and passive margins. *Deep-Sea Research II*. 1998; 45:517-567.
89. Boetius A., Suess E. Hydrate Ridge: a natural laboratory for the study of microbial life fueled by methane from near-surface gas hydrates. 2004.
90. Boetius A., Ravenschlag K., Schubert CJ., Rickert D., Widdel F., Gleseke A., Amann R., Jørgensen BB., Witte U., Pfannkuche O. A marine microbial consortium apparently mediating anaerobic oxidation methane. *Nature*. 2000; 407(6804).
91. Knittel K., Boetius A., Lemke A., Eilers H., Lochte K., Pfannkuche O., Linke P., Amann R. Activity, Distribution, and Diversity of Sulfate Reducers and Other Bacteria in Sediments above Gas Hydrate (Cascadia Margin, Oregon). *Geomicrobiology Journal*. 2003; 20(4):269-294.
92. Knittel K., Lösekann T., Boetius A., Kort R., Amann R. Diversity and distribution of methanotrophic archaea at cold seeps. *Applied and environmental microbiology*. 2005; 71(1):467-479.
93. Niemann H., Lösekann T., de Beer D., Elvert M., Nadalig T., Knittel K., Amann R., Sauter EJ., Schlüter M., Klages M., Foucher JP., Boetius A. Novel microbial communities of the Haakon Mosby mud volcano and their role as a methane sink. *Nature*. 2006; 443(7113):854-858.
94. Preisler A., De Beer D., Lichtschlag A., Lavik G., Boetius A., Barker Jørgensen B. Biological and chemical sulfide oxidation in a Beggiatoa inhabited marine sediment. *The ISME Journal*. 2007; 150(10):341-353.
95. Hinrichs K-U., Hayes JM., Sylva SP., Brewer PG., DeLong EF. Methane-consuming archaebacteria in marine sediments. *Nature*. 1999; 398(6730):802-805.
96. Valentine DL., Reeburgh WS. New perspectives on anaerobic methane oxidation. *Environmental microbiology*. 2000; 2(5):477-484.
97. Orphan VJ., Sylva SP., Hayes JM., Delong EF. Comparative Analysis of Methane-Oxidizing Archaea and Sulfate-Reducing Bacteria in Anoxic Marine Sediments Comparative Analysis of Methane-Oxidizing Archaea and Sulfate-Reducing Bacteria in Anoxic Marine Sediments. *Applied and environmental microbiology*. 2001; 67(4):1922-1934.
98. Michaelis W., Seifert R., Nauhaus K., Treude T., Thiel V., Blumenberg M., Knittel K., Gieseke A., Peterknecht K., Pape T., Boetius A., Amann R., Jørgensen BB., Widdel F., Peckmann J., Pimenov N V., Gulin MB. Microbial Reefs in the Black Sea Fueled by Anaerobic Oxidation of Methane. *Science*. 2002; 297(5583).
99. Martens CS., Berner RA. Methane Production in the Interstitial Waters of Sulfate-

Depleted Marine Sediments. *Science*. 1974; 185(4157).
100. Barnes RO., Goldberg ED. Methane production and consumption in anoxic marine sediments. *Geology*. 1976; 4(5):297.
101. Reeburgh WS. Methane consumption in Cariaco trench waters and sediments. *Earth and Planetary Scwnce Letters*. 1976; 28:337-344.
102. Sommer S., Pfannkuche O., Linke P., Luff R., Greinert J., Drews M., Gubsch S., Pieper M., Poser M., Viergutz T. Efficiency of the benthic filter: Biological control of the emission of dissolved methane from sediments containing shallow gas hydrates at Hydrate Ridge. *Global Biogeochemical Cycles*. 2006; 20(2):n/a-n/a.
103. Hoehler TM., Alperin MJ., Albert DB., Martens CS. Field and laboratory studies of methane oxidation in an anoxic marine sediment: Evidence for a methanogen-sulfate reducer consortium. *Global Biogeochemical Cycles*. 1994; 8(4):451-463.
104. Niewohner C., Hensen C., Kasten S., Zabel M., Schulz HD. Deep sulfate reduction completely mediated by anaerobic methane oxidation in sediments of the upwelling area off Namibia. 1997.
105. Hinrichs K., Hayes J., Sylva S., Brewer P. Methane-consuming archaebacteria in marine sediments. *Nature*. 1999.
106. Devol A. Methane oxidation rates in the anaerobic sediments of Saanich Inlet1. *NOTES Lin~nol Oceanogr*. 1983; 28(4):738-742.
107. Iversen2 N., Barker Jorgensen B. Anaerobic methane oxidation rates at the sulfate-methane transition in marine sediments from Kattegat and Skagerrak (Denmark)'. *Limnol Oceanogr*. 1985; 30(5):944-955.
108. Borowski WS., Paull CK., Ussler Iii W. Global and local variations of interstitial sulfate gradients in deep-water, continental margin sediments: Sensitivity to underlying methane and gas hydrates. *Marine Geology*. 1999; 159:131-154.
109. Paull CK., Lorenson TD., Dickens G., Borowski WS., Ussler W., Kvenvolden K. Comparisons of In Situ and Core Gas Measurements in ODP Leg 164 Bore Holes. *Annals of the New York Academy of Sciences*. 2006; 912(1):23-31.
110. Borowski WS., Paull CK., Ussler W. Marine pore-water sulfate profiles indicate in situ methane flux from underlying gas hydrate. *Geology*. 1996; 24(7):655.
111. Bohrmann G., Greinert J., Suess E., Torres M. Geology: Authigenic carbonates from the Cascadia subduction zone and their relation to gas hydrate stability. 1998.
112. Naehr TH., Eichhubl P., Orphan VJ., Hovland M., Paull CK., Ussler Iii W., Lorenson TD., Greene HG. Authigenic carbonate formation at hydrocarbon seeps in continental margin sediments: A comparative study. *Deep-Sea Research II*. 2007; 54:1268-1291.
113. Snyder GT., Hiruta A., Matsumoto R., Dickens GR., Tomaru H., Takeuchi R., Komatsubara J., Ishida Y., Yu H. Pore water profiles and authigenic mineralization in shallow marine sediments above the methane-charged system on Umitaka Spur, Japan Sea. *Deep-Sea Research II*. 2007; 54:1216-1239.
114. Aloisi G., Asjes S., Bakker K., Bakker M., Charlou JL., De Lange G., Donval JP., Fiala-Medioni A., Foucher JP., Haanstra R., Haese R., Heijs S., Henry P., Huguen C., Jelsma B., De Lint S., Van Der Maarel M., Mascle J., Muzet S., Nobbe G., Pancost R., Pelle H., Pierre C., Polman W., De Senerpont Domis L., Sibuet M., Van Wijk T., Woodside J., Zitter T. Linking mediterranean brine pools and mud volcanism. *Eos*. 2000; 81(51):625-632.
115. Birgel D., Peckmann J. Aerobic methanotrophy at ancient marine methane seeps: A synthesis. *Organic Geochemistry*. 2008; 39:1659-1667.
116. Borowski WS., Paul1 ' CK., Ussler Iii W. Carbon cycling within the upper methanogenic zone of continental rise sediments: An example from the methane-rich sediments overlying the Blake Ridge gas hydrate deposits. *Marine Chemistry*.

1997; 57:299-311.
117. Hong W., Torres ME., Choi J., Bahk J. *Carbon Cycling within the Sulfate-Methane- Transition-Zone in Marine Sediments from the Ulleung Basin*.
118. Hong W-L., Torres ME., Kim J-H., Choi J., Bahk J-J. Towards quantifying the reaction network around the sulfate–methane-transition-zone in the Ulleung Basin, East Sea, with a kinetic modeling approach. *Geochimica et Cosmochimica Acta*. 2014; 140:127-141.
119. Yoshinaga MY., Holler T., Goldhammer T., Wegener G., Pohlman JW., Brunner B., Kuypers MMM., Hinrichs K-U., Elvert M. Carbon isotope equilibration during sulphate-limited anaerobic oxidation of methane. *Nature Geosci*. 2014; 7(3):190-194.
120. Casciotti KL. Inverse kinetic isotope fractionation during bacterial nitrite oxidation. *Geochimica et Cosmochimica Acta*. 2009; 73(7):2061-2076.
121. Holler T., Wegener G., Niemann H., Deusner C., Ferdelman TG., Boetius A., Brunner B., Widdel F. Carbon and sulfur back flux during anaerobic microbial oxidation of methane and coupled sulfate reduction. *Proceedings of the National Academy of Sciences of the United States of America*. 2011; 108(52):E1484-90.
122. Pohlman JW., Riedel M., Bauer JE., Canuel EA., Paull CK., Lapham L., Grabowski KS., Coffin RB., Spence GD. Anaerobic methane oxidation in low-organic content methane seep sediments. 2013.
123. Nauhaus K., Treude T., Boetius A., Krüger M. Environmental regulation of the anaerobic oxidation of methane: A comparison of ANME-I and ANME-II communities. *Environmental Microbiology*. 2005; 7(1):98-106.
124. Orphan VJ., House CH., Hinrichs K-U., Mckeegan KD., Delong EF. Multiple archaeal groups mediate methane oxidation in anoxic cold seep sediments. 2002.
125. Lösekann T., Knittel K., Nadalig T., Fuchs B., Niemann H., Boetius A., Amann R. Diversity and abundance of aerobic and anaerobic methane oxidizers at the Haakon Mosby Mud Volcano, Barents Sea. *Applied and Environmental Microbiology*. 2007; 73(10):3348-3362.
126. Schonheit P., Keweloh H., Thauer RK. Factor F420 degradation in Methanobacterium thermoautotrophicum during exposure to oxygen. *FEMS Microbiology Letters*. 1981; 12:347-349.
127. Hedderich R., Whitman WB. Physiology and biochemistry of the methane-producing archaea. In: *The Prokaryotes: Prokaryotic Physiology and Biochemistry*. Berlin, Heidelberg: Springer Berlin Heidelberg; 2006:635-662.
128. Ferguson TJ., Mah RA. Effect of H2-CO2 on Methanogenesis from Acetate or Methanol in Methanosarcina spp. *Applied and environmental microbiology*. 1983; 46(2):348-355.
129. Jones WJ., Nagle DP., Whitman WB. Methanogens and the diversity of archaebacteria. *Microbiological reviews*. 1987; 51(1):135-177.
130. Kasting JF. When Methane made climate. *Scientific American*. 2004.
131. Treude T., Boetius A., Knittel K., Wallmann K., Barker Jørgensen B. Anaerobic oxidation of methane above gas hydrates at Hydrate Ridge, NE Pacific Ocean. *Marine Ecology Progress Series*. 2003; 264:1-14.
132. Jørgensen BB. Mineralization of organic matter in the sea bed—the role of sulphate reduction. *Nature*. 1982; 296(5858):643-645.
133. Claypool GE., Kaplan IR. The Origin and Distribution of Methane in Marine Sediments. In: *Natural Gases in Marine Sediments*. Boston, MA: Springer US; 1974:99-139.
134. Froelich PN., Klinkhammer GP., Bender ML., Luedtke NA., Heath GR., Cullen D., Dauphin P., Hammond D., Hartman B., Maynard V. Early oxidation of organic matter in pelagic sediments of the eastern equatorial Atlantic: suhoxic diagenesis.

135. Sansone FJ., Martens CS. Methane Production from Acetate and Associated Methane Fluxes from Anoxic Coastal Sediments. *Science*. 1981; 211(4483).
136. Kasten S., Jørgensen BB. Sulfate Reduction in Marine Sediments. In: *Marine Geochemistry*. Berlin, Heidelberg: Springer Berlin Heidelberg; 2000:263-281.
137. Carbonero F., Benefiel AC., Alizadeh-Ghamsari AH., Gaskins HR. Microbial pathways in colonic sulfur metabolism and links with health and disease. *Frontiers in Physiology*. 2012; 3.
138. Rabus R., Brüchert V., Amann J., Könneke M. Physiological response to temperature changes of the marine, sulfate-reducing bacterium Desulfobacterium autotrophicum. *FEMS Microbiology Ecology*. 2002; 42(3):409-417.
139. Hines M. Acetate concentrations and oxidation in salt-marsh sediments. *Limnol Oceanogr*. 1994; 39(1l):140-148.
140. Eglinton G., Calvin M. Chemical fossils. *Scientific American*. 1967; 216:32-43.
141. Eglinton G., Hamilton RJ. Leaf epicuticular waxes. *Science (New York, NY)*. 1967; 156(3780):1322-1335.
142. Woese CR., Magrum LJ., Fox GE. Archaebacteria. *Journal of Molecular Evolution*. 1978; 11(3):245-252.
143. White D. *The Physiology and Biochemistry of Prokaryotes*. Vol 27. 2nd editio. Oxford University Press; 1999.
144. Cranwell I PA., Eglinton G., Robinson N. Lipids of aquatic organisms as potential contributors to lacustrine sediments--II*. *Org Geochem*. 1987; 11(6):513-527.
145. Itoh YH., Sugai A., Uda I., Itoh T. The evolution of lipids. *Advances in Space Research*. 2001; 28(4):719-724.
146. Finean JB., Coleman R., Michell RH. Membranes and their cellular functions. *Membranes and their cellular functions*. 1984; (Ed. 3).
147. Ourisson G., Albrecht P., Rohmer M. The hopanoids. Palaeochemistry and biochemistry of a group of natural products. *Pure Applied Chemistry*. 1979; 51:709-729.
148. Ourisson G., Albrecht P. Hopanoids. 1. Geohopanoids: the most abundant natural products on Earth? *Accounts of Chemical Research*. 1992; 25(9):398-402.
149. Harwood JL., Russell NJ. *Lipids in Plants and Microbes*. Springer Netherlands; 1984.
150. Rohmer EL., Ourisson3 Y. Distribution of Hopanoid Triterpenes in Prokaryotes. *Journal of General Microbiology*. 1984; 1558(1):137-1.
151. Farrimond P., Griffiths T., Evdokiadis E. Hopanoic acids in Mesozoic sedimentary rocks: their origin and relationship with hopanes.
152. Kannenberg EL., Poralla K. Hopanoid Biosynthesis and Function in Bacteria. *Naturwissenschaften*. 1999; 86:168-176.
153. Rohmer M., Bouvier P., Ourisson G. Molecular evolution of biomembranes: structural equivalents and phylogenetic precursors of sterols. *Proceedings of the National Academy of Sciences of the United States of America*. 1979; 76(2):847-851.
154. Berry AM., Harriot T., Moreau RA., Osman SF., Benson DR., Jones AD. Hopanoid lipids compose the Frankia vesicle envelope, presumptive barrier of oxygen diffusion to nitrogenase. *Microbiology*. 1993; 90:6091-6094.
155. Mahato SB., Sen S. Advances in triterpenoid research, 1990-1994. *Phytochemistry*. 1997; 44(7):1185-1236.
156. Killops SD., Frewin NL. Triterpenoid diagenesis and cuticular preservation. *Org Geochem*. 1994; 21(12):146-6380.
157. Mackenzie AS., Lamb NA., Maxwell JR. Steroid hydrocarbons and the thermal history of sediments. *Nature*. 1982; 295(5846):223-226.
158. de Leeuw JW., Cox HC., van Graas G., van de Meer FW., Peakman TM., Baas

JMA., van de Graaf B. Limited double bond isomerisation and selective hydrogenation of sterenes during early diagenesis. *Geochimica et Cosmochimica Acta*. 1989; 53(4):903-909.
159. Bendoraitis J., Brown B., Hepner L. Isolation and identification of isoprenoids in petroleum. In: *6th World Petroleum Congr.Prod.* ; 1962:13-29.
160. Boschker HTS., Middelburg JJ. Stable isotopes and biomarkers in microbial ecology. *FEMS Microbiology Ecology*. 2002; 40(2):85-95.
161. Boschker HTS., Nold SC., Wellsbury P., Bos D., de Graaf W., Pel R., Parkes RJ., Cappenberg TE. Direct linking of microbial populations to specific biogeochemical processes by 13C-labelling of biomarkers. *Nature*. 1998; 392(6678):801-805.
162. Bian L. Isotopic biogeochemistry of individual compounds in a modern coastal marine sediment (Kattegat, Denmark and Sweden) (Book, 1994) [WorldCat.org]. 1994.
163. Bian L., Hinrichs K-U., Xie T., Brassell SC., Iversen N., Fossing H., Jørgensen BB., Hayes JM. Algal and archaeal polyisoprenoids in a recent marine sediment: Molecular isotopic evidence for anaerobic oxidation of methane. *Geochemistry, Geophysics, Geosystems*. 2001; 2(1):n/a-n/a.
164. Kates M. Membrane lipids of archaea. *The Biochemistry of Archaea (Archaebacteria)*. 1993:261-295.
165. Kushwaha SC., Kates M. 2,3-Di-O-phytanyl-sn-glycerol and prenols from extremely halophilic bacteria. *Phytochemistry*. 1978:2028-2029.
166. Koga Y., Kyuragi T., Nishihara M., Sone N. Did Archaeal and Bacterial Cells Arise Independently from Noncellular Precursors? A Hypothesis Stating That the Advent of Membrane Phospholipid with Enantiomeric Glycerophosphate Backbones Caused the Separation of the Two Lines of Descent. *Journal of Molecular Evolution*. 1998; 46(1):54-63.
167. Koga Y., Nishihara M., Morii H., Akagawa-Matsushita M. Ether polar lipids of methanogenic bacteria: Structures, comparative aspects, and biosyntheses. 1993; 57(1):164-182.
168. Koga Y., Morii H. Recent Advances in Structural Research on Ether Lipids from Archaea Including Comparative and Physiological Aspects. *Bioscience, Biotechnology, and Biochemistry*. 2005; 69(11):2019-2034.
169. Stadnitskaia A., Bouloubassi I., Elvert M., Hinrichs KU., Sinninghe Damsté JS. Extended hydroxyarchaeol, a novel lipid biomarker for anaerobic methanotrophy in cold seepage habitats. *Organic Geochemistry*. 2008; 39(8):1007-1014.
170. De Rosa M., Gambacorta A. The lipids of archaebacteria. *Progress in lipid research*. 1988; 27(3):153-175.
171. Schouten S., J.L. Hoefs M., P. Koopmans M., Bosch H-J., Sinninghe-Damste J. *Structural Characterization, Occurrence and Fate of Archaeal Ether-Bound Acyclic and Cyclic Biphytanes and Corresponding Diols in Sediments*. Vol 29.; 1998.
172. Blumenberg M., Seifert R., Reitner J., Pape T., Michaelis W. Membrane lipid patterns typify distinct anaerobic methanotrophic consortia. 2004.
173. Niemann H., Elvert M., Hovland M., Orcutt B., Judd A., Suck I., Gutt J., Joye S., Damm E., Finster K., Boetius A. Methane emission and consumption at a North Sea gas seep (Tommeliten area). *Biogeosciences*. 2005; 2(4):335-351.
174. Niemann H., Elvert M. Diagnostic lipid biomarker and stable carbon isotope signatures of microbial communities mediating the anaerobic oxidation of methane with sulphate. *Organic Geochemistry*. 2008; 39(12):1668-1677.
175. Hinrichs K-U., Summons RE., Orphan V., Sylva SP., Hayes JM. Molecular and isotopic analysis of anaerobic methane- oxidizing communities in marine sediments. *Organic Geochemistry*. 2000; 31:1685-1701.

176. Pancost RD., Hopmans EC., Sinninghe Damsté JS. Archaeal lipids in mediterranean cold seeps: Molecular proxies for anaerobic methane oxidation. *Geochimica et Cosmochimica Acta*. 2001; 65(10):1611-1627.
177. Elvert M., Boetius A., Knittel K., Jørgensen BB. Characterization of Specific Membrane Fatty Acids as Chemotaxonomic Markers for Sulfate-Reducing Bacteria Involved in Anaerobic Oxidation of Methane. *Geomicrobiology Journal*. 2003; 20(4):403-419.
178. Hinrichs K-U., Boetius A. *The Anaerobic Oxidation of Methane: New Insights in Microbial Ecology and Biogeochemistry*.; 2002.
179. Elvert M., Hopmans EC., Treude T., Boetius A., Suess E. Spatial variations of methanotrophic consortia at cold methane seeps: Implications from a high-resolution molecular and isotopic approach. *Geobiology*. 2005; 3(3):195-209.
180. Camerlenghi A., Cita MB., Vedova B Della., Fusi N., Mirabile L., Pellis G. Geophysical Evidence of Mud Diapirism on the Mediterranean Ridge Accretionary Complex. 1994:115-141.
181. Cita MB., Erba E., Lucchi R., Pott M., Van Der Meer R., Nieto L. Stratigraphy and sedimentation in the Mediterranean Ridge diapiric belt. *Marine Geology*. 1996.
182. Mascle J., Huguen C., Benkhelil J., Chamot-Rooke N., Chaumillon E., Foucher JP., Griboulard R., Kopf A., Lamarche G., Volkonskaia A., Woodside J., Zitter T. Images may show start of European-African plate collision. *Eos*. 1999; 80(37):421-428.
183. Huguen C., Mascle J., Woodside J., Zitter T., Foucher JP. Mud volcanoes and mud domes of the Central Mediterranean Ridge: Near-bottom and in situ observations. *Deep-Sea Research Part I: Oceanographic Research Papers*. 2005; 52(10):1911-1931.
184. Limonov AF. Unesco reports in marine science 64 Mud volcanism in the Mediterranean and Black Seas and shallow structure of the Eratosthenes Seamount during the Third UNESCO-ESF. 1994; (July 1993).
185. Staffini F., Spezzaferri S., Aghib F. Mud diapirs of the Mediterranean ridge: sedimentological and micropaleontological study of the mud breccia. *Rivista Italiana di Paleontologia e Stratigrafia*. 1993; 99(2):225-254.
186. Robertson AHF., Kopf A. Tectonic setting and porcesses of mud volcanism in the Mediterranean Ridge accretionary complex: Evidence from Leg 160. 1998; 160.
187. Fusi N., Kenyon NH. Distribution of mud diapirism and other geological structures from long-range sidescan sonar (GLORIA) data, in the Eastern Mediterranean Sea. *Marine Geology*. 1996; 132(1-4):21-38.
188. Kopf A., Robertson AHF., Volkmann N. Origin of mud breccia from the Mediterranean Ridge accretionary complex based on evidence of the maturity of organic matter and related petrographic and regional tectonic evidence. *Marine Geology*. 2000; 166(1-4):65-82.
189. Robertson AHF., Party SS. Mud volcanism on the mdeiterranean Ridge. *Initial Reports*. 1996; 160.
190. Volgin A., Woodside JM. Sidescan sonar images of mud volcanoes from the Mediterranean Ridge: possible causes of variations in backscatter intensity. *Geology*. 1996.
191. Vrolijk P., Moore JC. Fluid flow in accretionary prisms Fluids in Accretionary Prisms. 1985; (January).
192. Robertson A. Mud volcanism on the Mediterranean Ridge: Initial results of Ocean Drilling Program Leg 160. *Geology*. 1996; 24(3).
193. Kastens KA., Breen NA., Cita MB. Progressive deformation of an evaporite-bearing accretionary complex: SeaMARC I, SeaBeam and piston-core observations from the Mediterranean Ridge. *Marine Geophysical Researches*.

1992; 14(4):249-298.
194. de Voogd B., Truffert C., Chamot-Rooke N., Huchon P., Lallemant S., Le Pichon X. Two-ship deep seismic soundings in the basins of the Eastern Mediterranean Sea (Pasiphae cruise). *Geophysical Journal International*. 1992; 109(3):536-552.
195. Dickman T., Reston T., Huene R. The structure of the Mediterranean Ridge near the deformation front; first results from the Imerse Project: Terra Abstracts. 1995.
196. Chaumillon E., Mascle J. Variation laterale des fronts de deformation de la Ride mediterraneenne (Mediterranee orientale). 1995; 166(5):463-478.
197. Chaumillon E., Mascle J., Hoffmann HJ. Deformation of the western Mediterranean Ridge: Importance of Messinian evaporitic formations. *Tectonophysics*. 1996; 263:163-190.
198. Huguen C., Mascle J., Chaumillon E., Kopf A., Woodside J., Zitter T. Structural setting and tectonic control of mud volcanoes from the Central Mediterranean Ridge (Eastern Mediterranean). *Marine Geology*. 2004; 209(1-4):245-263.
199. Huguen C., Mascle J., Chaumillon E., Woodside JM., Benkhelil J., Kopf A., Volkonskaïa A. Deformational styles of the Eastern Mediterranean ridge and surroundings from combined swath mapping and seismic reflection profiling. *Tectonophysics*. 2001; 343(1-2).
200. Akhmanov GG. Lithology of mud breccia clasts from the Mediterranean Ridge. *Marine Geology*. 1996; 132(1-4):151-164.
201. Premoli Silva I., Erba E., Spezzaferri S., Cita MB. Age variation in the source of the diapiric mud breccia along and across the axis of the Mediterranean Ridge Accretionary Complex. *Marine Geology*. 1996; 132(1-4):175-202.
202. Schulz H-M., Emeis K-C., Volkmann N. Organic carbon provenance and maturity in the mud breccia from the Napoli mud volcano: Indicators of origin and burial depth. *Earth and Planetary Science Letters*. 1997; 147(1):141-151.
203. Zitter TAC. Mud volcanism and fluid emissions in Eastern Mediterranean neotectonic zones. March 2004.
204. Slack JF., Turner RJW., Ware PLG. Boron-rich mud volcanoes of the Black Sea region: Modern analogues to ancient sea-floor tourmalinites associated with Sullivan-type Pb-Zn deposits? *Geology*. 1998; 26(5):439.
205. De Lange GJ., Brumsack H-J. Pore-water indications for the occurence of gas hydrates in eastern Mediterranean mud dome structures. 1998; 160.
206. Chaumillon E., Mascle J. GEOLOGY MARINE From foreland foreland to forearc forearc domains : domains : New New multichannel multichannel seismic reflection survey survey of of the the Mediterranean Mediterranean ridge ridge accretionary accretionary reflection complex (Eastern (. *Marine Geology*. 1997; 138(2):237-259.
207. Robertson AHF., Kopf A. Origin of clasts and matrix within the Milano and Napoli mud volcanoes, Mediterranean Ridge accretionary complex. *Proceedings of the Ocean Drilling Program: Scientific Results*. 1998; 160:575-596.
208. Rabaute A., Chamot-Rooke N. Quantitative mapping of active mud volcanism at the western Mediterranean Ridge-backstop contact.
209. Giresse P., Loncke L., Huguen C., Muller C., Mascle J. Nature and origin of sedimentary clasts associated with mud volcanoes in the Nile deep-sea fan. Relationships with fluid venting. 2010.
210. Emeis K., Robertson -C., Richter AHF. Paleoceanography and sapropel introduction. *Initial Reports*. 1996; 160.
211. Kopf A., Behrmann JH. Extrusion dynamics of mud volcanoes on the Mediterranean Ridge accretionary complex. *Geological Society, London, Special Publications*. 1999; 174(1).
212. Ryan WBF., Kastens KA., Cita MB. Geological evidence concerning

compressional tectonics in TImlF, eastern Mediterranean. 1982; 86:213-242.
213. Cita M., Camerlenghi A. The Mediterranean Ridge as an accretionary prism in collisional context. 1990.
214. Kopf A. The Mediterranean Ridge: A mass balance across the fastest growing accretionary complex on Earth. *Journal of Geophysical Research*. 2003; 108(B8):2372.
215. Planke S., Svensen H., Hovland M., Banks DA., Jamtveit B. Mud and fluid migration in active mud volcanoes in Azerbaijan. *Geo-Marine Letters*. 2003; 23(3-4):258-267.
216. Robertson AHF., Clennell MB., Flecker Casp R., Kopf A., Flecker · R. Mechanisms of mud extrusion on the Mediterranean Ridge Accretionary Complex. 1998; 18:97-114.
217. Pancost RD., Damsté J., Sinninghe S., Lint S De., Maarel MJEC Van Der., Gottschal JC. Biomarker Evidence for Widespread Anaerobic Methane Oxidation in Mediterranean Sediments by a Consortium of Methaogenic Archaea and Bacteria. *Applied and environmental microbiology*. 2000; 66(3):1126-1132.
218. Charlou JL., Donval JP., Zitter T., Roy N., Jean-Baptiste P., Foucher JP., Woodside J. Evidence of methane venting and geochemistry of brines on mud volcanoes of the eastern Mediterranean Sea. *Deep-Sea Research Part I: Oceanographic Research Papers*. 2003; 50(8):941-958.
219. Olu-Le Roy K., Sibuet M., Fiala-Meioni A., Gofas S., Salas C., Foucher J-P., Woodside J. Cold seep communities in the deep eastern Mediterranean Sea: composition, symbiosis and spatial distribution on mud volcanoes. *Deep-Sea Research I*. 2004; 51:1915-1936.
220. Fiala-Médioni A., Sibuet M., Gottschal J., Mariotti A. Chemosynthesis-based communities associated with fluids in deep mediterranean mud-volcanoes. *, CIESM Conference Monte ….* 2001.
221. Woodside JM., Volgin A. Brine pools associated with Mediterranean Ridge mud diapirs: an interpretation of echo-free patches in deep tow sidescan sonar data. 1996.
222. Gogou AI., Apostolaki M., Stephanou EG. Determination of organic molecular markers in marine aerosols and sediments: One-step flash chromatography compound class fractionation and capillary gas chromatographic analysis. *Journal of Chromatography A*. 1998; 799(1-2):215-231.
223. Gogou A., Bouloubassi I., Stephanou EG. Marine organic geochemistry of the Eastern Mediterranean:1. Aliphatic and polyaromatic hydrocarbons in Cretan Sea surficial sediments. *Marine Chemistry*. 2000; 68:265-282.
224. Gogou A., Bouloubassi I., Lykousis V., Arnaboldi M., Gaitani P., Meyers PA. Organic geochemical evidence of Late Glacial-Holocene climate instability in the North Aegean Sea. *Palaeogeography, Palaeoclimatology, Palaeoecology*. 2007; 256(1-2).
225. Blumer M., Guillard RRL., Chase T. Hydrocarbons of marine phytoplankton. *Marine Biology*. 1971; 8(3):183-189.
226. Bray EE., Evans D. Distribution of n-paraffins as a clue to recognition of source beds. 1961; 0(2).
227. Scalan E., Smith J. An improved measure of the odd-even predominance in the normal alkanes of sediment extracts and petroleum. *Geochimica et Cosmochimica Acta*. 1970; 34(5):611-620.
228. Volkman J. Biological marker compounds as indicators of the depositional environments of petroleum source rocks. 1988.
229. Brooks J., Hlitir AD. Morphology and chemistry of the organic insoluble matter from the onverwacht series precambrian chert and the Orgueil and Murray

carbonaceous meteorites. *Grana*. 1971; 11:9-14.
230. Powell TG. Geochemical studies related to the occurrence of oil and gas in the dampier sub-basin, Western Australia. *Journal of Geochemical Exploration*. 1975; 4(4):441-466.
231. Powell TG., Mckirdy DM. Pm. PrIntad in Northern Imlmd. 1971; 87:628-688.
232. Goossens H., de Leeuw JW., Schenck PA., Brassell SC. Tocopherols as likely precursors of pristane in ancient sediments and crude oils. *Nature*. 1984; 312(5993):440-442.
233. Chappe B., Albrecht P., Michaelis W. Polar lipids of archaebacteria in sediments and petroleums. 1982; 217(4554):65-66.
234. Kates M., Palameta B., Joo CN., Kushner DJ., Gibbons NE. Aliphatic Diether Analogs of Glyceride-Derived Lipids. IV. The Occurrence of Di-O-dihydrophytylglycerol Ether Containing Lipids in Extremely Halophilic Bacteria [*]. *Biochemistry*. 1966; 5(12):4092-4099.
235. Tissot B., Clifet-Debyse Y., Deroo G., Oudin J. *Origin and Evolution of Hydrocarbons in Early Toarcian Shales, Paris Basin, France*.; 1971.
236. Venkatesan MI. Tetrahymanol: Its widespread occurrence and geochemical significance. *Geochimica et Cosmochimica Acta*. 1989; 53(11):3095-3101.
237. Sinninghe Damste JS., Kenig F., Koopmans MP., Koster J., Schouten S., Hayes JM., de Leeuw JW. Evidence for gammacerane as an indicator of water column stratification. *Geochimica et cosmochimica acta*. 1995; 59(9):1895-1900.
238. A. L. Mann NSGSL. Geochemical Characteristics of Lacustrine Source Rocks: A Combined Palynological/Molecular Study of a Tertiary Sequence from Offshore China. 1987:241-258.
239. Chen J., Summons RE. Complex patterns of steroidal biomarkers in Tertiary lacustrine sediments of the Biyang Basin, China.
240. Volkman JK., Maxwell JR. *Acyclic Isoprenoids as Biological Markers*.; 1986.
241. Robson JN., Rowland SJ. Synthesis, chromatographic and spectral characterisation of 2,6,11,15-tetramethylhexadecane (crocetane) and 2,6,9,13-tetramethyltetradecane: reference acyclic isoprenoids for geochemical studies. *Org Geochem*. 1993; 20(7):1093-1098.
242. Kawka OE., Simoneit BRT. Polycyclic aromatic hydrocarbons in hydrothermal petroleums from the Guaymas Basin spreading center. *Applied Geochemistry*. 1990; 5:17-27.
243. Silliman JE., Meyers PA., Ostrom PH., Ostrom NE., Eadie BJ. Insights into the origin of perylene from isotopic analyses of sediments from Saanich Inlet, British Columbia.
244. Aizenshtat Z. Perylene and its geochemical significance. *Geochimica et Cosmochimica Acta*. 1973; 37(3):559-567.
245. Tisot., Welte. *Petroleum Formation and Occurrence*. Vol 66.; 1985.
246. Seifert WK., Moldowan JM. The effect of thermal stress on source-rock quality as measured by hopane stereochemistry.
247. Mackenzie AS., Patience RL., Maxwell JR., Vandenbroucke M., Durand B. Molecular parameters of maturation in the Toarcian shales, Paris Basin, France—I. Changes in the configurations of acyclic isoprenoid alkanes, steranes and triterpanes. *Geochimica et Cosmochimica Acta*. 1980; 44(11):1709-1721.
248. Farrimond P., Taylor A., Telnás N. Biomarker maturity parameters: the role of generation and thermal degradation.
249. Ensminger A., Dorsselaer A Van., Spyckerelle C., Albrecht G., Ourisson G. Pentacyclic triterpanes of the hopane type as ubiquitous geochemical markers. Origin and significance. *Advances in Organic Geochemistry*. 1974:245-260.
250. Zumberge JE. Prediction of source rock characteristics based on terpane

biomarkers in crude oils: A multivariate statistical approach. 51:1625-1637.
251. Seifert WK., Moldowan JM. Paleoreconstruction by biological markers. *Geochimica et Cosmochimica Acta*. 1981; 45(6):783-794.
252. Moldowan JM., Sundararaman P., Schoell M. Sensitivity of biomarker properties to depositional environment and/or source input in the Lower Toarcian of SW-Germany. *Organic Geochemistry*. 1986; 10(4-6):915-926.
253. Wakeham SG. Reduction of stenols to stanols in particulate matter at oxic–anoxic boundaries in sea water. *Nature*. 1989; 342(6251):787-790.
254. Seifert WK., Moldowan JM. *Use of Biological Markers in Petroleum Exploration*. Vol 24.; 1986.
255. Clayton JL., King JD. Effects of weathering on biological marker and aromatic hydrocarbon composition of organic matter in Phosphoria shale outcrop. 1987; 51:2153-2151.
256. McKirdy DM., Aldridge A., Ypma PJM. A geochemical comparison of some crude oils from pre-Ordovician carbonate rocks. *Advances in Organic Geochemistry*. 1981:99-107.
257. Meyers PA. Preservation of elemental and isotopic source identification of sedimentary organic matter. *Chemical Geology*. 1994; 114:289-302.
258. Werne JP., Baas M., Damsté JSS. Molecular isotopic tracing of carbon flow and trophic relationships in a methane-supported benthic microbial community. *Limnology and Oceanography*. 2002; 47(6):1694-1701.
259. Fang J., Barcelona MJ. Structural determination and quantitative analysis of bacterial phospholipids using liquid chromatography/electrospray ionization/mass spectrometry. *Journal of Microbiological Methods*. 1998; 33(1):23-35.
260. Elvert M., Whiticar M., Suess E. Diploptene in varved sediments of Saanich Inlet: indicator of increasing bacterial activity under anaerobic conditions during the Holocene. *Marine Geology*. 2001; 174(1):371-383.
261. Damste JSS., Muyzer G., Abbas B., Rampen SW., Massé G., Allard WG., Belt ST., Robert J-M., Rowland SJ., Moldowan JM., Barbanti SM., Fago FJ., Denisevich P., Dahl J., Trindade LAF., Schouten S. The Rise of the Rhizosolenid Diatoms. *Science*. 2004; 304(5670):584-587.
262. Blumenberg M., Kruger M., Nauhaus K., Talbot HM., Oppermann BI., Seifert R., Pape T., Michaelis W. Biosynthesis of hopanoids by sulfate-reducing bacteria (genus Desulfovibrio). *Environmental Microbiology*. 2006; 8(7):1220-1227.
263. Hartner T., Straub KL., Kannenberg E. Occurrence of hopanoid lipids in anaerobic Geobacter species. *FEMS Microbiology Letters*. 2005; 243(1):59-64.
264. Kastens K., Mascle J., Auroux C., Bonatti E., Broglia C., Channell J., Curzi P., Emeis K-C., Glacon G., Hasegawa S., Hieke W., Mascle G., McCoy F., Mckenzie J., Mendelson J., Muller C., Rehaut J-P., Robertson A., Sartori R., Sprovieri R., Torii M. ODP Leg 107 in the Tyrrhenian Sea: Insights into passive margin and back-arc basin evolution. *Geological Society of America Bulletin*. 1988; 100(7):1140-1156.
265. Duan Z., Wller N., Greenberg J., Weare JH. The prediction of methane solubility in natural waters to high ionic strength from 0 to 250°C and from 0 to 1600 bar. *Geochimico d Comochimrce Acm*. 56:1451-1460.
266. Yamamoto S., Alcauskas J., Crozier T. Table I. Experimental Bunsen Solubility Coefficients for Methane in Distilled Water and Seawater.